UNIVERSIDADE FEDERAL DO CEARÁ
CENTRO DE CIÊNCIAS
DEPARTAMENTO DE FÍSICA
PROGRAMA DE PÓS-GRADUAÇÃO EM FÍSICA

Levi Rodrigues Leite

Forças de depleção exercidas por matéria ativa e passiva em colóides passivos

---

Depletion forces exerted by active and passive matter on passive colloids

---

Fortaleza
2017

Levi Rodrigues Leite

Forças de depleção exercidas por matéria ativa e passiva em colóides passivos

---

Depletion forces exerted by active and passive matter on passive colloids

---

Tese apresentada ao Curso de Pós-graduação em Física da Universidade Federal do Ceará como parte dos requisitos necessários para a obtenção do título de Doutor em Física.

Orientador:
Prof. Dr. Wandemberg Paiva Ferreira

DOUTORADO EM FÍSICA
DEPARTAMENTO DE FÍSICA
PROGRAMA DE PÓS-GRADUAÇÃO EM FÍSICA
CENTRO DE CIÊNCIAS
UNIVERSIDADE FEDERAL DO CEARÁ

Fortaleza - CE
30 de março de 2017

Dados Internacionais de Catalogação na Publicação
Universidade Federal do Ceará
Biblioteca Universitária
Gerada automaticamente pelo módulo Catalog, mediante os dados fornecidos pelo(a) autor(a)

L554f Leite, Levi Rodrigues.
Forças de depleção exercidas por matéria ativa e passiva em colóides passivos / Levi Rodrigues Leite. – 2017.
133 f. : il. color.

Tese (doutorado) – Universidade Federal do Ceará, Centro de Ciências, Programa de Pós-Graduação em Física , Fortaleza, 2017.
Orientação: Prof. Dr. Wandemberg Paiva Ferreira.

1. Colóides . 2. Matéria ativa. 3. Força de depleção . I. Título.

CDD 530

LEVI RODRIGUES LEITE

Forças de depleção exercidas por matéria ativa e passiva em colóides passivos

---

Depletion forces exerted by passive and active matter on passive colloids

---

Tese de doutorado apresentada ao Curso de Pós-graduação em Física da Universidade Federal do Ceará como parte dos requisitos necessários para a obtenção do título de Doutor em Física.

Aprovada em: 30/03/2017.

BANCA EXAMINADORA

Prof. Dr. Wandemberg Paiva Ferreira (Orientador)
Departamento de Física – UFC

Prof. Dr. Fabrício Queiroz Potiguar
Instituto de Ciências Exatas e da Natureza – UFPA

Dr. Diego de Lucena Camarão
Departamento de Física – UFC

Prof. Dr. Aristeu Rosendo Pontes Lima
Instituto de Ciências Exatas e da Natureza – UNILAB

Prof. Dr. Gil de Aquino Farias
Departamento de Física – UFC

To my parents,
close relatives
and friends.

Acknowledgments

I would like to thank my advisor Prof. Dr. Wandemberg Paiva Ferreira, for trust in me as his student and for the support all these years, always being present when necessary and sharing his teachings.

I would like to thank Prof. Fabrício Queiroz Potiguar for all his support on the development of the works presented in this thesis, as well as the suggestions for personal improvements.

I also thank the other members of the jury: Dr. Diego de Lucena Camarão, Prof. Aristeu Rosendo and Prof. Gil de Aquino for all the help and suggestions gave on this thesis and for my personal career.

I would like to thank very much all my friends that were together with me in this journey: *Cesar Vieira*, *Daniel Gomes*, *Daniel Marchesi*, *Davi Dantas*, *Diego Lucena*, *Diego Ximenes*, *Heitor Credidio*, *Hygor Piaget*, *Leandro Jader*, *Rafael Alencar*, *Rilder de Sousa*, *Saulo Dantas*, *Vagner Bessa*, (...). To my colleagues of the GTMC group: *André Borba*, *Danilo Borges*, *David Figueiredo*, *Diego Frota*, *Felipe Munarin*, *Florêncio Batista*, *Jessé Pereira*, *João Cláudio* and *Jorge Capuan*.

A special thanks of course goes to my parents *Pedro Fausto Rodrigues Leite* and *Rosa Helena Rodrigues Leite*, as well as my brother *Pedro Fausto Rodrigues Leite Júnior*, for all the support in my career as a physicist. I also thank my wife *Tabata Vieira de Araujo* for understand and support my efforts as a doctorate student.

I would like to thank all professors of the physics department at UFC, specially Prof. Dr. *Valder Nogueira Freire*, who accepted me as his graduate student and Prof. Dr. *Gil de Aquino Farias*, who gave me the support for finding a research area for my master and doctor degrees.

I would like to thank the Brazilian agencies CNPq, CAPES and FUNCAP for all the financial support received along seven years.

Finally, I thank all those who helped me directly or indirectly, for the preparation and conclusion of this work.

"Let come what comes, let go what goes. See what remains."

Ramana Marhashi

Resumo

Nesta tese propõe-se o estudo da influência das forças de depleção induzidas em partículas passivas em função do meio (partículas) que as circundam.

Na primeira parte do trabalho, estudam-se as forças de depleção exercidas por partículas ativas (auto-propelidas) em objetos passivos circulares e elípticos através do cálculo numérico. Mostra-se que um banho de partículas ativas pode induzir forças repulsivas e atrativas que são sensíveis à forma e orientação dos objetos passivos. Em geral, a força resultante nos objetos passivos devido às partículas ativas são estudadas como função da forma e orientação dos objetos passivos, magnitude do ruído angular e distância entre os objetos passivos. No caso em que a separação entre objetos passivos é menor que um diâmetro de partícula ativa, o aumento desta separação resulta em um aumento da magnitude das forças de depleção, que são repulsivas neste caso. Para distâncias entre os objetos passivos maiores que um diâmentro da partícula ativa, a magnitude da força de depleção sempre decresce com o aumento da distância entre as partículas passivas. Observa-se também que a natureza da força de depleção (atrativa ou repulsiva) depende da forma e orientação relativa das partículas passivas. Observa-se que uma força de depleção atrativa ocorre quando objetos passivos de forma elíptica são dispostos lado a lado, mas de modo que os semi-eixos maiores estão paralelos e não alinhados. Isto ocorre para uma densidade suficientemente alta do banho de partículas ativas.

Na segunda parte do trabalho, estuda-se a dependência da força de depleção em relação a forma dos objetos que sofrem tal interação. Neste caso, os objetos passivos "grandes" (formas elíptica, triangular e semi-circular), que sofrem a interação de depleção, estão imersos em um solvente passivo (banho de partículas passivas com dimensões menores). Observa-se que as forças de depleção podem ser de natureza (atrativa ou repulsiva) distinta daquelas previstas por Asakura-Oosawa. O banho passivo induz forças de depleção de natureza distinta, dependendo da forma dos objetos passivos. Além disso, a intensidade das forças de depleção são também sensíveis à forma do obstáculo e à temperatura do banho de partículas passivas, bem como em relação ao tamanho dos objetos passivos que sofrem a interação de depleção, e à densidade das partículas do banho. Modificando-se a forma dos objetos passivos de elíptico para triangular, a magnitude das forças repulsivas de depleção aumentam em duas ordens de magnitude. Para o caso do objetos semi-circulares, uma oscilação fortemente amortecida é observada na força de depleção, ressaltando-se que a natureza dessa força é consideravelmente sensíveis à distância entre os objetos passivos. Para o caso de objetos triangulares, observa-se que as forças de depleção induzidas podem ser atrativas ou repulsivas dependendo do ângulo interno, tornando-se este um parâmetro de controle da força de depleção resultante.

Abstract

In this thesis it is proposed a study of the influence of the depletion forces induced by passive particles as a function of the medium (particles) that surrounds then.

In the first part of this thesis, the depletion forces exerted by active (self-propelled) particles on passive and elliptical passive objects are studied through numerical simulations. It is shown that a bath of active particles can induce repulsive and attractive forces that are sensitive to the shape and orientation of the passive objects. In general, the force resulting in passive objects due to the active particles is studied as a function of the shape and orientation of the passive objects, magnitude of the angular noise, and distance between passive objects. In the case where the separation between passive objects is less than an active particle diameter, the increase of this separation results in an increase of the magnitude of the depletion forces, which are repulsive in this case. For distances between passive objects larger than one diameter of the active particle, the magnitude of the depletion force always decreases with increasing distance between the passive particles. It is also observed that the nature of the depletion force (attractive or repulsive) depends on the shape and relative orientation of the passive particles. It is noted that an attractive depletion force occurs when elliptical passive objects are arranged side by side, but so that the semi-major axis are parallel and not aligned. This occurs for a sufficiently high concentration (or density) of active particles.

In the second part of the thesis, we study the dependence of the depletion force related to the shape of the objects that undergo such interactions. In this case, passive "large" objects (elliptic, triangular and semi-circular forms), which undergo the depletion interaction, are immersed in a passive solvent (bath of passive particles of smaller size). The depletion forces may present distinct nature (attractive or repulsive) from that predicted by Asakura-Oosawa. The passive bath always attractive or repulsive depletion forces depending on the shape of the passive objects. In addition, the intensity of the depletion forces are sensitive to the shape of the obstacle and the bath temperature of passive particles, as well as to the size of the passive objects suffering the depletion interaction and density of the bath particles. By modifying the shape of the passive objects from elliptical to triangular, the magnitude of the repulsive depletion forces increases by two orders of magnitude. In the case of semi-circular objects, a strong damped oscillation is observed in the depletion force, emphasizing that such forces are considerably sensitive to the distance between the passive objects. In the case of triangular objects, it is observed that the induced depletion forces can be attractive or repulsive depending on the internal angle, which becomes a parameter of control of the resulting depletion force.

Contents

List of Figures

1 Introduction

Soft matter comprises a set of states of matter which cannot be defined as purely solids or liquids. There are many examples of this states of matter that fit this characteristic: creams, styrofoam, pumice, fog, some types of sprays, milk, mayonnaise, jam, smoke, ink, blood, as well as much of the food we eat. All these examples are called colloidal systems, that is, a mixture of solid or liquid particles dispersed in another liquid medium. We can mention also polymers, large molecules built by small units (monomers) that repeat themselves, interconnected by covalent bonds. Examples of polymers are plastics in general, DNA, proteins of various types, rubber, polysaccharides, amber, wool, silk, cellulose, artificial polymers as well as synthetic rubber, nylon, PVC, polypropylene, silicone, etc.

There are some common features that describe soft matter systems. Its length scale abroad the intermediate range between macroscopic and nanometric scales. In the case of a colloidal particle, they are typically between $10^{-9}m$ and $10^{-5}m$ in size, which allows such particles to be easily visible with an optical microscope. It is precisely this characteristic that induces these systems to be "soft", because the elastic modulus for systems of this size are in order of k_BT/a^3, where k_B is Boltzmann's constant, T is the absolute temperature and a is the size of the objects the material is made from. In the case of soft matter, a is much greater than the spacing between the lattice in a crystalline solid, which culminates in a greater elasticity.

Another main feature of soft matter is that it undergoes Brownian motion. Although some times soft matter comprises big molecules such as proteins, they still small enough to feel the effect of temperature. Therefore soft matter is always in a constant random motion. Brownian motion is explained in detail in section 2.1.

Soft matter also have an interesting property which is called self-assembly. Pursuing the equilibrium, soft matter systems can self-assembly and form clusters of particles and/or molecules. However, because of the thermal influence, by equilibrium we mean a dynamical equilibrium and consequently exhibiting a rich phase behavior and many spontaneously complex structures. If equilibrium phase is not attained, in general non-equilibrium self-assembled structures undergoes a phase transition, a very recurrent phenomenon in soft matter systems.

One of the main factors in soft matter systems is the different types of interaction between its components, as well as the magnitude of these interactions. In a liquid, molecules are also held together by intermolecular forces in a state of high density, but in contrast to a solid the molecules are not locked rigidly into well-defined positions on a lattice.

To form such aggregates, intermolecular forces needs to be short-range repulsive and long-range attractive, in order to have a interaction potential with a clear minimum, as shown in Fig. 1.1. Pauli exclusion principle explains repulsive curve for these systems. Attractive forces can have different influences, depending on the system. In general, we can mention van der Waals forces, ionic, covalent, metallic and hydrogen bonds, as well as hydrophobic interactions.

When the attractive force is stronger than the repulsive one, there is a low temperature situation and the system goes packing until the minimum interparticle distance is attained, and the system is frozen. For higher temperatures, particles energy becomes almost kinetic and the system goes in the opposite direction towards ideal gas conditions.

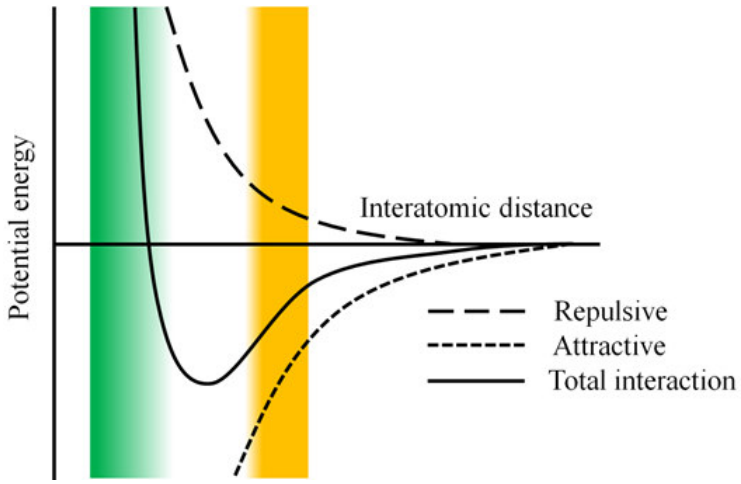

Figure 1.1: Illustration of the potential energy curve as a function of the interatomic distance. The total interaction is a combination of a short-range repulsion and a long-range attraction.

There is also a type of soft matter that deserves a special attention, which is living systems. Although having a individual own trajectory, these systems rely heavily on the medium in which they are immersed, and on surrounding particles, living or not living particles, which interacts with. Therefore, these systems are thus able to be modeled in the exact science frame, more specifically the out-of-equilibrium physics, because this system are kept far from the equilibrium by a constant input of energy.

To maintain order, life depends of a constant consumption of energy and is itself based on well ordered structure. The whole narrative is that the existence of life is necessarily related to the self-organized emergence of order. In nature, self organization of order manifests itself in a large variety of different processes, and examples are detailed on

section 1.1.

However, on the same way that interatomic interactions does not interact on a simple and easy way, also living systems interactions and behavior cannot be generalized in a just one simple model. Therefore, still open some fundamental questions such as if it is possible to find a model which describes with accuracy all living systems motions and interactions, or at least divide them in few classes. This problem is not so simple specially when we remember that this living particles inludes physical, chemical and biological systems, which gives an amazing variety of systems with different length scales.

One of the most common and interesting manifestation behavior in nature is what we call collective motion. For collective motion we understand the phenomenon occurring by similar interacting units in collections which moves with the same velocity. The source of energy which produces collective motion are not relevant. Collective motion seems to appear in almost every living system consisting of dozens of units. In such small systems, we associate with "flocking"a state of the group in which assume an approximately common direction (or orientation) developing through local communications among the entities. In last decade, many papers were published showing that depending on the interaction of particles, different patterns can emerge, in a large variety of systems following the above characteristics with many different sizes. So, we can observe that this interesting feature appears in purely physical, chemical as well as biological systems [1].

This kind of "matter", called *active matter*, is in focus of this work and it will be covered in details on section 1.1.

1.1 Active Matter

Active matter refers to a variety of systems which take energy from an internal source of energy or ambient medium and transform it into useful work performed on the environment. These individual units may interact both directly as well as through the medium in which they are immersed.

The difference between active systems from other classes of driven systems (sheared fluids, sedimenting colloids, driven vortex lattices etc.) is that the energy input is related to the environment such a way that is located on each unit, and does not act at the boundaries or via external fields. Furthermore, the direction in which each unit moves is dictated by the state of the particle and not by the direction imposed by an external field. The direction of movement is therefore not determined by outside forces. On the other hand, passive systems depends on the external force to determine the direction of motion.

A theory for this new type of condensed matter should yield to interesting properties, such as non-equilibrium phases and phase transitions, the nature of correlations and response, and characteristic instabilities. This properties of active matter theory must arise *in vivo*, which is why biologists are so interested in this type of particles. Besides that,

understanding active matter, perhaps we can develop artificial biological components. We should note that the theories of active matter were formulated not in response to a specific problem emerged by experiments but rather to incorporate living, metabolizing, spontaneously moving matter into the condensed-matter fold. This was done through minimal models whose consequences are relatively easy for theoreticians to work out. However natural realizations of living matter are far from minimal; thus, comparisons of active-matter theory with experiment are likely to be qualitative until well-controlled model systems are elaborated.

Active systems span an enormous range of length scales, examples are cell cytoskeleton [2, 3, 4] with their microtubules [5] , bacterial colonies [6, 7, 8, 9], animal groups [10, 11, 12, 13, 14, 15] and catalytically activated colloidal particles [16, 17, 18, 19]. These disparate systems exhibit mesoscopic to large-scale phenomena, including bacterial turbulence [20], swarming [21], active clustering [22, 23], rectification of motion [24, 25, 26, 27], phase separations [28, 29, 30, 31, 32, 33, 34], phase transition type behavior in several growth processes [35, 36, 37, 38], spontaneous self-assembly and pattern formation [39, 40], giant density fluctuations [20, 41, 42], surprising mechanical properties [21, 40], "random organization" of sheared colloidal suspensions [43] and rods [44], dynamical self-regulation [45], unusual rheological behavior [46, 47, 48], and ability to power microscopic motors [25, 49]. There are also non-clear topics in which an effort has been made in order to have a better understanding, such as spontaneous flow [50] and phase equilibrium in active matter [51, 52, 53, 54, 55], but as for now there is no definite thermodynamic framework for these systems. Biological [12, 56, 57] and artificial active particles [58, 59, 60, 61] also exhibit swarm patterns that result from their interactions [21, 42, 62, 63].

When active systems exhibit directed motion along an axis, the terminology "swimmers" or "self-propelled particles (SPP)" is often used, while the terms "active nematic" or "living liquid crystals" appear in the discussion of the orientationally ordered collective states of active particles. In conclusion, SPP refers to a particular case of active matter systems.

SPP refers to a class of particles that have the elementary ability of self-propulsion. The consequence is the resulting many interesting properties which can be very different from properties of particles in a heat bath, for example. Therefore it is clear that SPP behave as an out-of-equilibrium system. It is important to note that self-propulsion is an essential feature of most living systems. The motion of the organisms is usually controlled not only by some external fields, but also by interactions with other organisms in their neighborhood. Active particles are generally elongated and can order in states with either polar or apolar (nematic) orientational order.

There is a specific type of SPP that emerges when, by its micro- or nanometric size, effects caused by thermal fluctuations become relevant in its position. Such effects, when combined with the self-propulsion of the particle, generate a particular type of active matter, called active brownian particles (ABP). Such particles swim at roughly constant

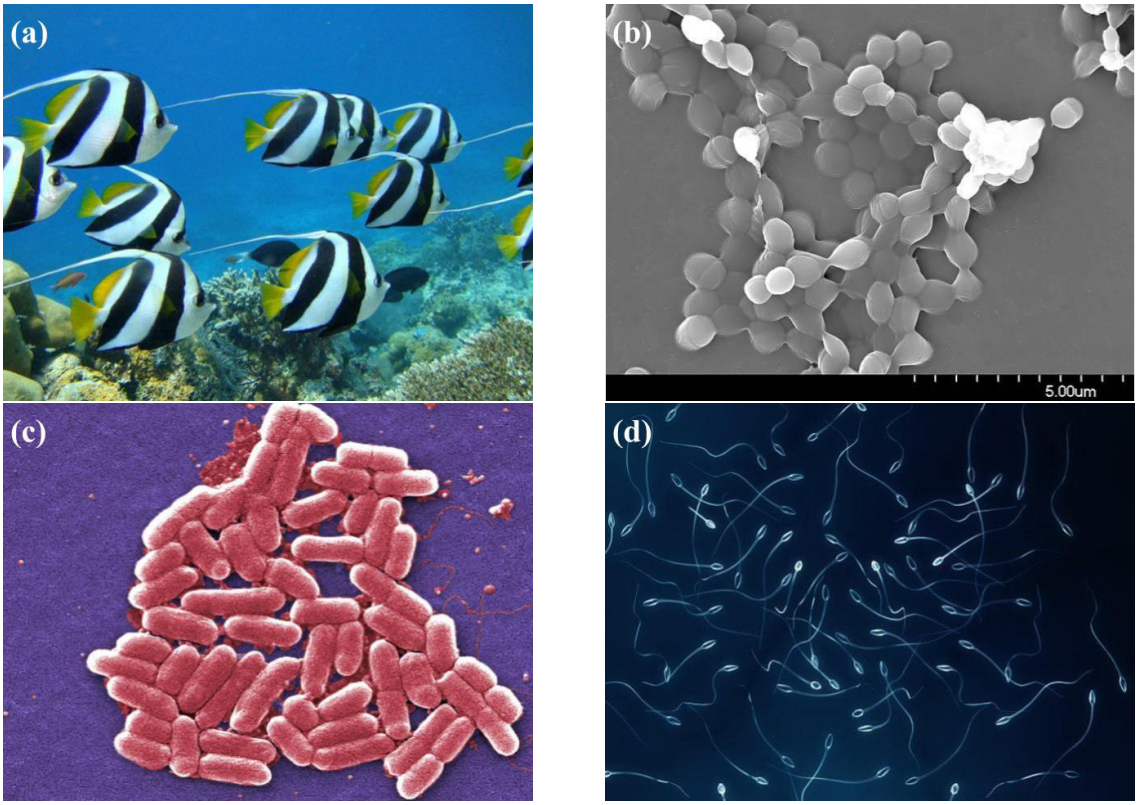

Figure 1.2: Examples of active matter systems which form agglomerate and present collective behaviour: (a) fishes; (b) bacterial colony; (c) *Escherichia coli* and (d) Spermatozoa.

speed, with a swimming direction that relaxes continuously by rotational diffusion. The ABP model is the most used model to describe living systems, because it takes into account the effect of temperature on the self-propulsion of particles. Some examples of living active brownian particles are *E. Coli* and spermatozoa. Other natural active brownian particles are magnetic colloidal particles [58], paramagnetic colloidal particles [64] and catalytic microjets [65]. However, artificial active brownian particles have been fabricated and we can cite Janus rods [59], Janus spheres [60, 66], chiral particles [67] and Au/Pt rod-shaped particles [68] as recent examples.

1.1.1 Applications

Because of the interesting properties listed above, active matter studies can reveal new properties in physics, as well as new techniques of device and material fabrication. Though in principle focused in animals collective behavior [69], soon the SPP study widened and is now applied in many other different areas of knowledge, such as biology, medicine, soft matter, statistical physics, social transport, biophysics, sustainability and social security [39, 50, 68, 70, 71, 72, 73, 74, 75]. Examples of applications are transport phenomena, sensing, imaging, artificial microswimmers device fabrication, drug delivery and water decontamination [58, 76, 77, 78, 79], which are detailed below.

The evolution of nanotechnology has allowed us to develop synthetic self-propelled entities for various tasks and diverse applications. One important area is nano-medicine where therapeutic diagnosis and site-specific drug delivery are of key importance. The current research on drug delivery focuses on specific problems like targeted delivery [80], solubility issues of drugs [81], protecting drugs from biochemical degradation and controlling the therapeutic payload [82, 83]. In the past few decades, nanoscale vectors e.g. nanoparticles [84], emulsions [85], micelles [86] and liposomes [87] have been constructed for drug delivery.

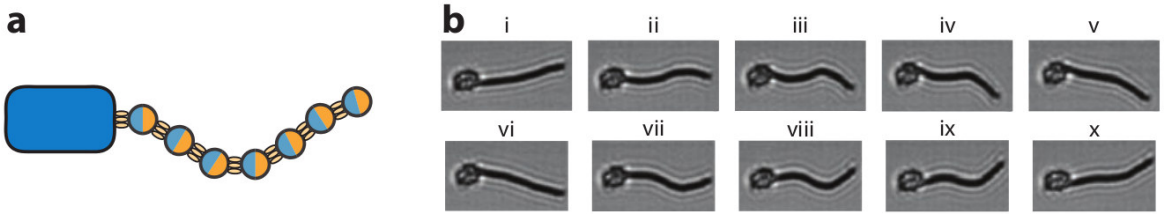

Figure 1.3: An example of microscopic artificial swimmer. (a) A chain of paramagnetic beads linked by DNA can be used as a propeller. (b) Experimental motion sequence of such a propeller pulling a red blood cell. Image extracted from ref. [75].

Cargo and Delivery: We start first mentioning self-powered micro- and nanodevices made of inorganic particles focusing on cargo and delivery applications. There are transporters developed using micro-/nanorods, by asymmetric electrocatalytic decomposition of H_2O_2. Application on cargo transportation and delivery are also wide: Wang's group reported also the transport of cargo bound to Au-Ni-Au-Pt-CNT nanorods and their controlled release in the microfluidic channel [88]. In this system, the nanorods transport their respective cargoes at high speeds. Spherical colloidal particles are found to be attractive candidates for cargo delivery applications as they are cost effective, easy to synthesize and have great potential in immunoassay as well as cancer therapy [89].

It is possible to rectify the flux of active particles for rigid obstacles with asymmetric characteristics. Galadja *et al.* showed that when a population of bacteria is exposed to microfabricated wall of funnel-shaped openings, bacteria random motion gets rectified by trapping the swimming bacteria through the funnel [24]. The funnel can be arranged for different shapes and hence bacteria moves in well-defined patterns, improving active transport through irregular confined environments. Asymmetric environments can also produce a spontaneous rotation of nano-objects immersed in active bacterial baths [25, 49]. Random walks with finite persistence length can be observed in passive colloids suspended in a bath of swimming bacteria [90, 91], where steric interactions due to collision are found to be one important feature in determining collective motion of the bacterial bath [92]. Active baths can mediate effective interactions between suspended bodies: swimming bacterias that give rise to short range attractions by a combination of non-equilibrium dynamics and excluded volume effects [93]. Similar phenomena were found by Buttinoni *et al*, where carbon-coated Janus particles in low densities form small clusters, induced by

a short-range attraction, even if reduced by carbon coating material. At higher densities, the suspension undergoes a phase separation into large clusters and a dilute gas phase [34]. Liquid-vapor transition are also observed induced by short-range attractions [94]. Lu *et al* also obtained gelation of particles with short-range attraction by spherical particles, initiated by spinodal decomposition [95].

Studies have been conducted to incorporate motor proteins into synthetic systems to create function-specific hybrid bio-synthetic nanomotors using microtubules, myosins and kinesins. Applications of molecular shuttles can be envisioned, e.g. in the field of nano-electro-mechanical systems (NEMS), where scaling laws favor active transport over fluid flow and the bottom-up assembly of novel materials [96]. Moreover, controlled loading, active concentration and unloading of cargo can be achieved by instructions encoded into DNA sequences [97]. Berg et al. demonstrated that flagellated bacteria when adsorbed at a solid-liquid interface can create motion in the surrounding fluid with potential applications in fluid pumping [98].

There is also what is called rolled-up nanotubes, a new class of nanostructured materials. They have potential applications due to easy motion control, high speeds, integration of various functions and straight trajectories compared to traditional self-propelled micromotors [99]. These microjet-like structures can be propelled in biological and high ionic-strength fluids [100, 101]. The first real biological cargo was found by Sanchez *et al.* using Pt/Ti/Fe microtubes. They reported the loading, carrying and release of CAD (cathecolaminergic cell line from the central nervous system cells) using these micromachine transporters [101].

Sensing, Isolation and Imaging: Sensing is another application for active matter. Wang *et al.* have also designed a sensing tool for biodetection of nucleic acids in function of Au-Pt micromotors speed [102]. Further improving ultrasensitive DNA biosensors have been designed, with detection limits in the zeptomolar range [103]. On-chip biosensing were also developed [104]. For sensing and isolation of cells, micro- and nano-motors rely on electrostatic [105] or magnetic [88] interactions with the cargo in order to deliver it.

Isolation, capturance and imaging of particles is very important to biochemical and medicinal applications. Campuzano *et al.* using lectin functionalized microtubes isolates pathogenic bacteria from peroxide-fuel. The captured bacteria were selectively released from the micromotor, breaking lectin-bacteria conjugate [106]. Following a similar strategy, tubular nanorods were used for isolate target proteins from complex biological samples based on an aptamer-modified self-propelled microtube engine. This technique represents a new approach in bioanalytical chemistry based on active transport of proteins and diagnostic applications [107]. Also another fascinating work in this matter is the design of microengines for cancer cells, where antibody functionalized microengines showed preferential binding for antigenic surface proteins expressed on cancer cells, which lead to imagine its potential application on early cancer diagnostic [100]. Tubular microjets have a special feature because of their different functionalities [108, 109]. For example, Kagan

et al. present a highly efficient microscale propulsion technique that utilizes ultrasound (US) to vaporize biocompatible fuel (i.e., perfluorocarbon PFC emulsions) bound within the interior of a micromachine for high velocity, bullet-like propulsion [108].

Imaging can be focused thanks to the micro- and nanomotors sensitivity to pathological factors such as hydrogen peroxide, temperature and water content [110]. NCS particles can produce a signal when injected in the vicinity of a bacterial abscess [111]. Micromotors can be also applied in magnetic resonance imaging. Polar magnetostatic bacterial nanorobots can load cargo, while nanodevices can provide detailed information about the microvascular system diameter [112].

Environment depolution: Water depolution applications are possible by nanosensors and reactive nanomaterials and can facilitate the detection of major pollutants [113] or prevent contamination [114, 115, 116]. Its amazing properties such as high surface area, catalytic activity and surface chemistry, allowed different environmental applications such as decontamination processes [117, 118], water-quality screening [119] to the removal of oil spills [120].

On-site and real-time analytical measurements can address the limitations of a discrete sample collection for laboratory analysis [121]. Also identification of target analytes are extremely important for meeting environmental monitoring requirements [122]. Self-propelled functionalized nanomachines here can be applied in order to direct selective isolation of target analytes from untreated environmental samples [123].

Rapid nanomachine-based target isolation directly from raw samples is another technique for molecular biological techniques relevant to environmental water quality [124]. Enzymatic-powered asymmetric hybrid silica nanomotors can facilitate the identification of aquatic microbes and on-site microbiological water quality testing [125].

The removal and destruction of pollutants from contaminated media is an important focus of environmental sustainability [126]. Reactive nanomaterials enables the efficient transformation of toxic pollutants [115, 116].

Molecularly imprinted polymers (MIPs) offer another promising route for removal of target pollutants. MIPs have been shown particularly attractive as selective binding medium for the removal of highly toxic micropollutants [127]. MIPs represent a possible choice for creating of specific recognition sites in synthetic self-propelled nanomachines [128, 129].

Some studies with active particles conclude that they have water purification applications. It is possible to use catalytically self-propelled microjets (dubbed micromotors) for degrading organic pollutants in water. The ability of these catalytically self-propelled micromotors to improve intermixing in liquids results in the removal of organic pollutants twelve times faster than catalytically active micromotors, holding considering promise for the remediation of contaminated water [118]. Were also developed in recent years new micromotors toxicity testing concept mimics live-fish water testing and relies on the toxin-induced inhibition of the enzyme catalase, responsible for the biocatalytic bubble

propulsion of tubular microengines. Such artificial microfish offers an attractive alternative to the common use of aquatic organisms for water-quality testing, by exposure to a broad range of contaminants, that lead to distinct time-dependent irreversible losses in the catalase activity, and hence of the propulsion behavior [119].

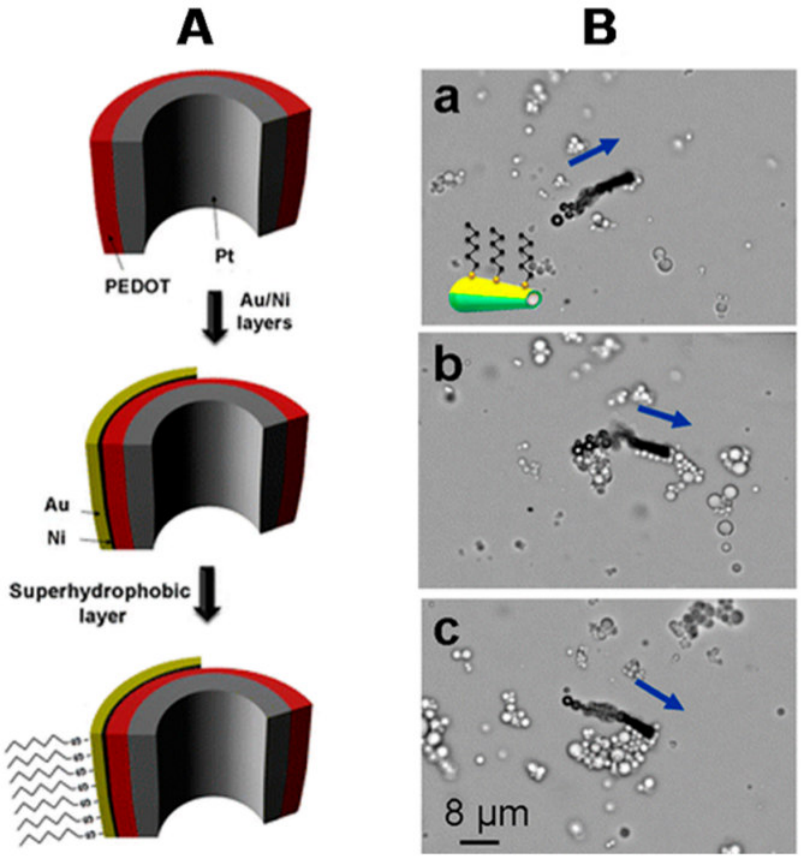

Figure 1.4: An example of a self-propelled micromachine for the removal of oil droplets. (a) Cross-section of a superhydrophobic SAM-modified Au/Ni/PEDOT/Pt tubular microengine. (b) Hexanethiol-modified microsubmarine transporting a payload of multiple oil droplets. Image extracted from ref.[120].

Nano-medicine: In medicine, micro- and nano propelled particles also have a huge application areas. The tiny advances reached until today is enough to show that nanomedicine will be an very important area of driven active matter. We can start mentioning that we already have a significant progress in robot-assisted colonoscopy [130]. We can mention either that cancer cells eject drugs as a defense mechanism, thus hindering the treatment of certain diseases. An important application is the fabrication of transport efflux inhibitors. Detailed information is required for the development of new antibiotics which turns traditional antibiotics to be effective [131, 132, 133, 134].

We start with targeted therapy, where active self-propelled systems can help the placement of a radioactive source in the selected cells, or with local delivery of heat energy to destroy such unwanted cells, generating advances on brachytherapy [135], hyperthermia and thermoablation [136].

Microrobots can act as simple static structures whose positions are controllable. The microrobot itself can act as the scaffold, or the microrobot can deploy microscopic building blocks that act as scaffolding [137].

The central nervous system can be explored. Therefore, it may be possible to insert a microrobot at that site and navigate to the brain for intervention, leaving the skull intact. This principle of using percutaneous intraspinal navigation was recently applied in brain surgery through the use of catheters [138].

A great deal of research has dealt with wireless manipulation of magnetic seeds in the brain for the purpose of hyperthermia with the fabrication of many prototype systems [139, 140, 141]. Kosa *et al.* propose a swimming microrobot for endoscopic procedures in the subarachnoid space of the spine [142].

Edd et al. propose a microrobot that would swim up the ureter to destroy kidney stones in a process whose potential benefits would include less overall harm to the kidney and increased choice over the mechanism of stone destruction [143].

Microrobots can also provide an alternative approach to retinal procedures. The most promising application are therapies for retinal vein occlusions, detached retinas, and epiretinal membranes, as well as the diagnosis of retinal health. Trocars can be used in the pars plana region with only topical anesthesia and with no suture requirement [144]. Yesin et al. propose a microrobot for intraocular procedures, controlled wirelessly with magnetic fields and tracked visually through the pupil [145]. Also another proposes emerged with an optical oxygen sensor for diagnosis of retinal health based on luminescence quenching, targeted retinal drug delivery based on diffusion from a surface-coated microrobot docked to a blood vessel with a microneedle and controlling a group of magnetic particles collectively to act as a tamponading agent in retinal therapy [146, 147, 148].

Finally, microrobots may hold the key to the future of fetal surgery. Researchers have proposed a number of procedures that could be performed by a microrobot that enters the uterus through the cervix [149, 150].

There are a lot of possible applications which promiss to be extremely important in the future. We can cite microrobots used to remove material by mechanical means. It is so well suited for utilizing rotary motion to perform ablation tasks, such as the removal of fatty deposits from the internal walls of blood vessels and ultrasound ablation, in which a microrobot uses a resonating mechanical structure to emit ultrasonic pressure waves to destroy an object. Occlusions can be introduced to intentionally block a passageway, either temporarily or permanently, with microrobots. Implants/electrodes can be introduced by microrobots which can act as a temporary or permanent implant. Microrobots can be used to transmit information that would otherwise be difficult or impossible to obtain. Telemetry applications can emerge including remote sensing and marking. Some of the most promising applications for microrobots is in the circulatory system, performing targeted drug delivery, removing plaque (rotational atherectomy), destroying blood clots (thrombolysis), acting as stents to maintain blood flow, acting as occlusions to intention-

ally starve a region of nutrition, and administering therapy for aneurysms. Microrobots could also carry electrodes for electrophysiology. Microrobots also offer minimally invasive access to the prostate through the urethra. They could improve the effectiveness of prostate procedures and reduce the chances of nerve damage. At least, it may be possible to improve cochlear implant procedures with wireless microrobotic techniques for ear healthy [75].

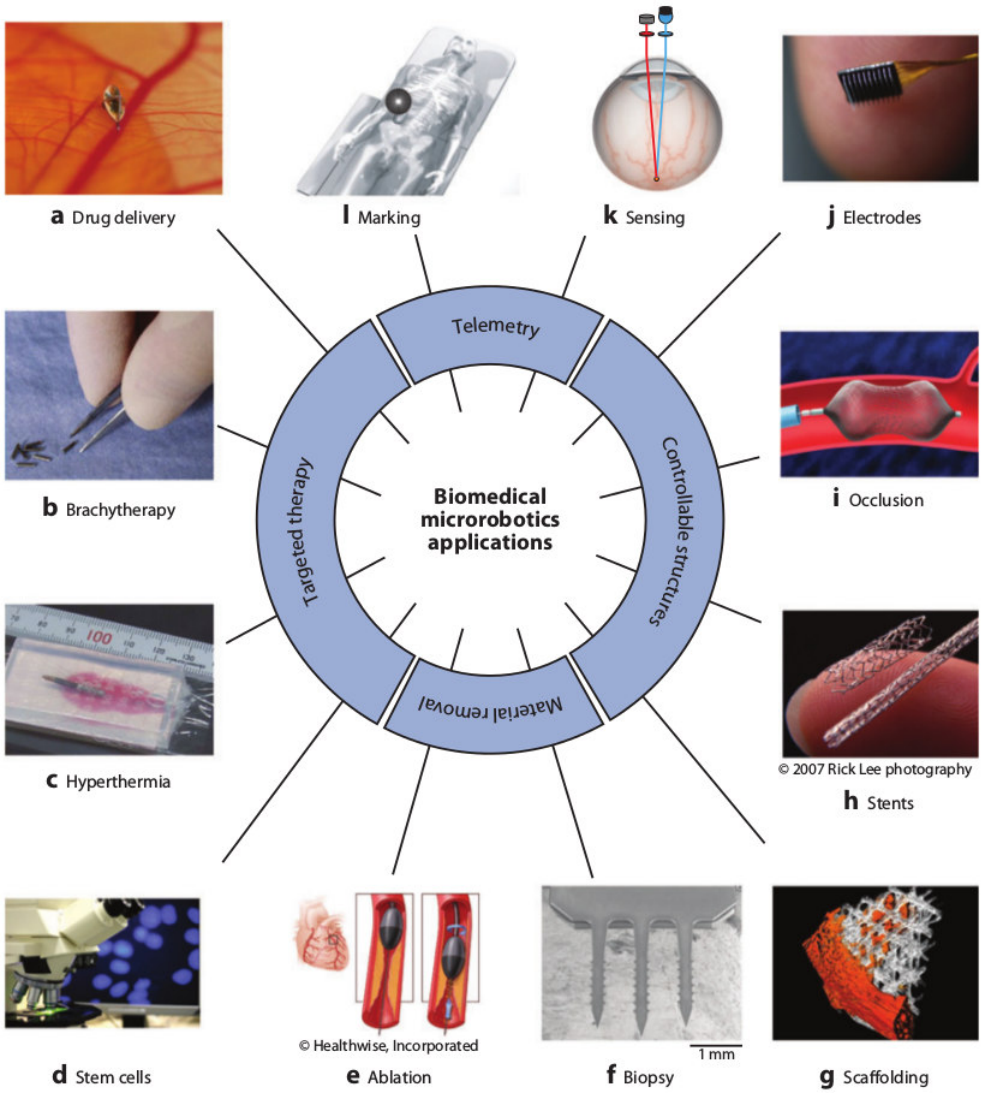

Figure 1.5: Biomedical microrobots applications, relating with its fundamentals branches: telemetry, targeted therapy, controllable structures and material removal. Image extracted from ref.[75].

1.2 Active Particles Motion with Obstacles

In general real active systems motion are restricted by some type of boundary or obstacles in particles path. The simplest case is of a particle that is obstructed by a

flat obstacle. When this happens, due to their self-propelling force, particles tend to accumulate on the walls for a certain time, until a tangential component on the particle velocity lead it to unattach of the wall and continue its trajectory. For simulation purposes, the particle-wall interaction can be modeled in three steps: (i) checking if the particle is inside the obstacle; (ii) approximate the boundary of the obstacle to a flat surface and (iii) refresh particle position reflecting its coordinates according to the reflecting line (see Fig. 1.6). In the case of a system of passive particles in equilibrium, it requires a very strong attractive force between particles, but for active systems this is not necessary. This accumulation effect has been observed in several works, for different types of particles and walls [22, 151, 152, 153, 154]. It is noteworthy that in case of particles with chiral motion, the constant torque of this type of particles facilitates the detachment of the walls once it slides along the obstacle and continues its trajectory [155, 156].

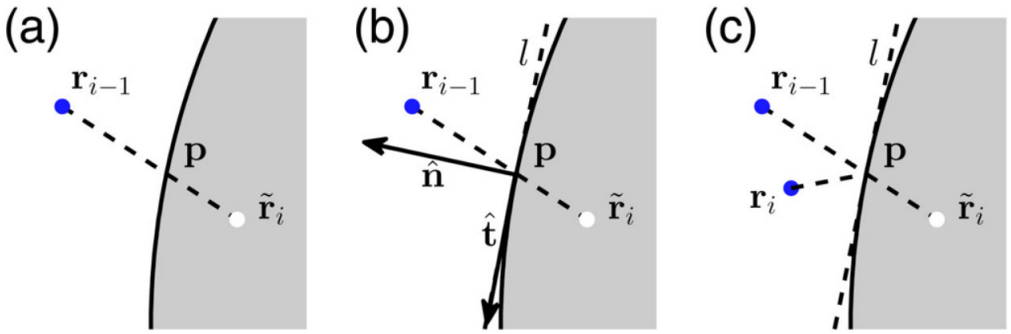

Figure 1.6: Illustrative scheme for particle-wall interaction. (a) Checks if particles is inside the obstacle; (b) the boundary of the obstacle is approximated by its tangent l at the point p where the particle entered the obstacle and (c) particle change its position according to the reflecting line. Picture extracted from reference [151].

It is interesting to note that for confined out-of-equilibrium systems there is no stationary probability distribution that characterizes all types of active particles. It is possible, however, under certain conditions, to find some analytical solutions and generate a Boltzmann state equation [51, 157, 158, 159, 160]. This leads us to ask the question whether it would not be possible to find a equation of state for active systems, even if at first only under specific conditions. In this sense, Mallory *et al.* performed numerical studies with the purpose of deducing a state equation for self-propelling repulsive interaction disks in two-dimensional and three-dimensional systems [161]. The result was a non-monotonic dependence of pressure and temperature. Solon *et al.* studied the pressure produced for active particles. Notice that in this case, the pressure depends on the nature of the interaction between the active particles and the confinement. The conclusion is that it is not possible to find a generic state equation for active fluids [162]. It is also observed that, depending on the confinement geometry, collective motions, such as vortices [163, 164], may be observed for different types of particles, such as bacteria [165, 166], colloidal rollers [167] and vibrated granular disks and rods [168, 169].

These grouping properties, collective behaviors, and complexity which arises when there is a particle interaction with some type of confinement, opens space to use the medium in which the particles are immersed to induce active matter separation. For example, one can perform a particle capture by placing obstacles in the form of wedges. Kaiser *et al.* considered active self-propelled rods interacting with stationary wedges as a function of the wedge angle, where the angle variation can lead to total particle capture for situations where no particle capturance were possible before [170]. In a later work Kaiser et al. found enhanced trapping when the wedge is moved in certain orientations [171]. This trapping behavior can be enhanced employing a system of multi-layered asymmetric barriers [172]. The self-trapping behavior of active rods was also confirmed on artificial rod-like swimmers [173] and sperm cells [174].

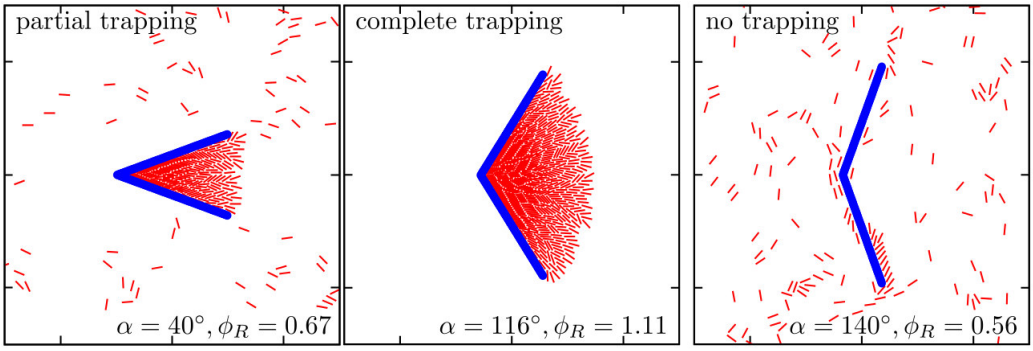

Figure 1.7: Snapshots showing wedges capturance in function of the inner angle ϕ. Picture extracted from reference [170].

It is also possible to observe the so called ratchet effect, which has a consequence, e.g., a continuous net drift of particles through funnel shapes [24], or on systems with long run lengths, such as run-and-tumble particles [175]. It is also possible to eliminate ratchet effects [158]. It is interesting to note that such an effect is also observed in colloidal systems, as shown by Koumakis *et al.* when active swimmers push colloids into asymmetric obstacles [78]. In addition, it is convenient to emphasize that active particles when in contact with asymmetric obstacles possess a property of do not have spontaneous motion in only one direction [176, 177, 178, 179]. This effect has also been observed in numerous recent works under various conditions, e.g., by applying a continuous external *dc* drive force on particles [180], circular motion when particles are under the influence of an environment with chiral patterns, coupled with asymmetry in the proper particles motion [181, 182], in Janus particles [179] and a reversible ratchet effect of active flocking particles in motion through a series of funnel-shaped obstacles [183].

Rectification is another interesting property of active systems in contact with boundaries. When a group of active particles is funneled by a channel, the rectification of the particles motion is observed (see Fig. 1.9). This effect was found to be correlated with many different parameters and patterns such as velocity and particles size dependence [181, 184], moving edges [171], pedestrian flows [185], asymmetric energy barriers [78] and

Janus particles [186].

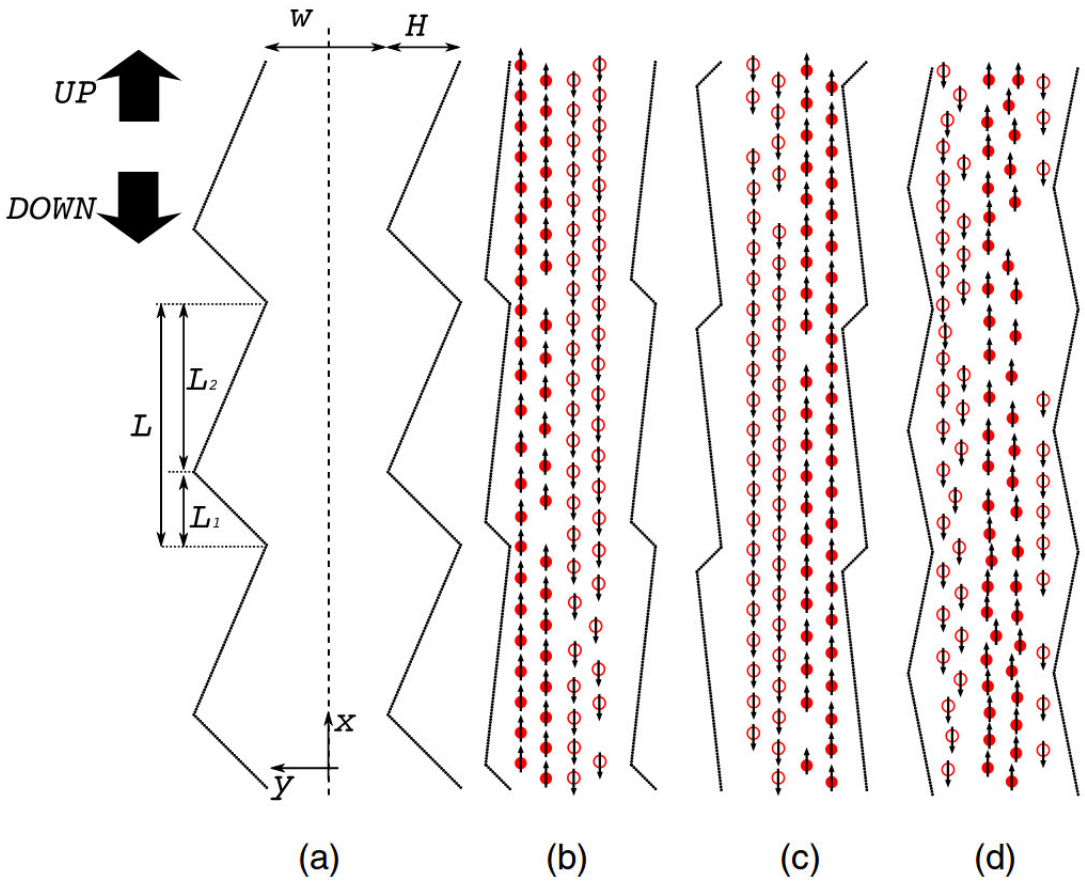

Figure 1.8: Different rectification patterns of pedestrian flows for (a) a channel of depth H and width W; (b-d) Typical snapshots for rectified motion induced by different patterns of channel boundaries. Picture extracted from reference [185].

Different types of phase transitions are also seen in systems involving self-propelled particles and obstacles. In 2014 Reichhardt *et al.* observed in repulsive disks of run-and-tumble type that for high densities of active matter it was possible to the particles become trapped in a single large clump [187].

Another type of phase transition observed is when particles - moving according to the Vicsek model - go from an ordered motion to a disordered motion. This happens through increasing the noise intensity. Interestingly, Chepizhko *et al.* observed that when obstacles are present in the system, disordered motion occurs for small values of the noise, and when noise is increased, the system transits into a state with quasi-long-range order [188]. Only after increasing even more the noise intensity does the system start to have disordered motion again. This work is important to show that when an active particle is in contact with obstacles, the increase of the noise intensity reduces the effect of the quenched disorder array and make the particle density more homogeneous, which contributes to the ordering of the system.

Finally, another interesting phenomena occurs when transitions in the diffusive regime

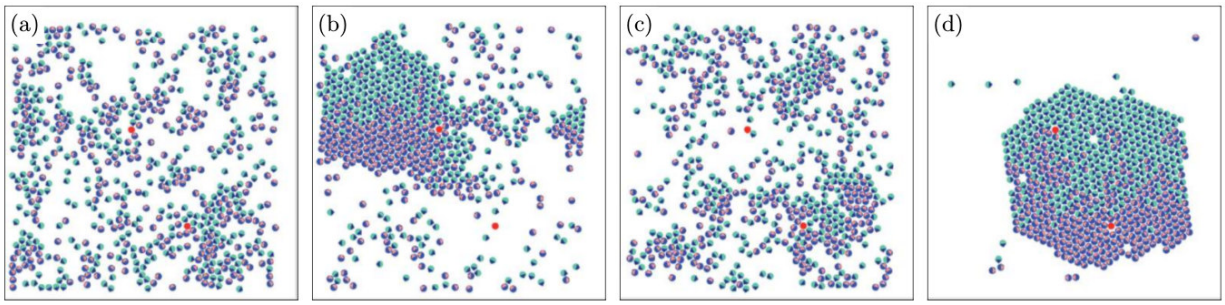

Figure 1.9: Cluster formation induced by immovable red disks. (a-d) As time evolves, particles goes from an initial fluctuating state to a dynamically frozen steady state around the obstacles. Picture extracted from reference [187].

of self-propelled particles are observed, for particles moving at constant speed in an heterogeneous two-dimensional space, with random-distributed obstacles. There may be a change in the mobility of the particles so that they change from a normal diffusion regime to a sub-diffusive regime, induced by when the turning speed reach relatively high values, combined with a low density of obstacles [189]. The turning speed is defined as the avoidance contribution of the obstacles that are randomly presented in the system.

1.3 Colloidal Suspensions

On this thesis colloidal suspensions are studied in active and passive media. Therefore its fundamental properties needs to be understood and it is explained below.

A colloidal dispersion is a heterogeneous system in which particles of solid or dorplets of liquid with dimensions of order $10m$ or less are dispersed in a liquid medium. A colloid is, by definition, a system with a large amount of surface. They consists of at least two phases and the dimension of the dispersed phase traditionally been considered to be in the submicroscopic region but greater than the atomic size range. The particle size is similar to the range of the forces that exists between the particles and the timescale of the diffusive motion of the particles is similar to that at which we are aware of changes. Typically the range of interparticles forces is 0.1 to $0.5m$ wheter they are forces of attraction between the particles of forces of repulsion.

A very attractive feature is that the colloidal forces can be readily manipulated by changes in the chemical environment of the colloidal particles. When colloidal particles are able to come into contact they will stick together irreversibly; as time goes on larger and larger assemblies of particles will be formed in a process known as *aggregation*. If we are to render a colloidal dispersion stable against aggregation, we must modify the forces acting between the colloidal particles, which are normally attractive, to make particles repel each other. This can be done by exploiting electrostatic forces, in charge stabilization, or by modifying the interfaces by attaching polymer chains to them, in steric stabilization. For example, aggregates of surfactant molecules can form nematic (when the aggregates

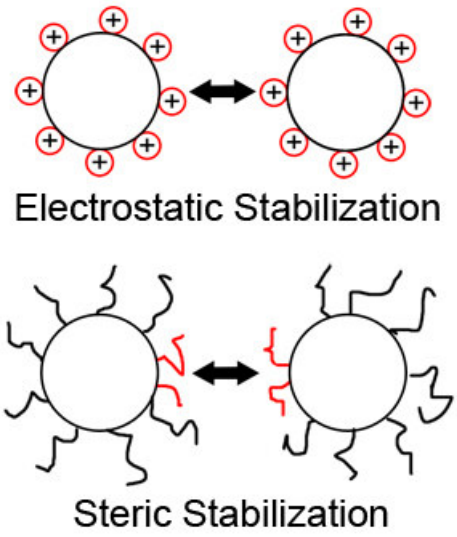

Figure 1.10: Illustration of two different forms of colloidal stabilization. On the top, stabilization is performed by electrostatic contributions induced by added ions; on the bottom, colloidal stabilization by steric contributions induced by added polymers, causing repulsion due to the unfavorable decrease in entropy.

are ellipsoidal micelles), columnar (when the aggregates are cylindrical micelles), lamellar (when the aggregates are continuous bilayers), and other phases. The intermolecular and interaggregate forces are of various origins: electrostatic, dipolar, van der Waals, entropic due to the presence of large fluctuations of the membranes (an effect not present in particulate colloidal solutions), and repulsive solvent-mediated complex forces, called solvation forces (or hydration forces when water is the solvent).

Another interesting feature is that colloidal particles are sufficiently large enough that they are easily viewed with optical microscopy. For this reason, microscopy has become an important tool for studying the structure of these types of samples. Along with the spatial scales, the temporal scales of these soft systems are often compatible with conventional video microscopy [190].

1.4 Passive and Active Depletion Overview

Although dating to 1954, for many years the model of Asakura and Oosawa (AO) remained without some attention of the scientific community of that time. However, especially in the 90's and driven mainly by the advances of experimental area, the model began to receive attention and today the article "On interaction between two bodies immersed in the solution of macromolecules" already has more than two thousand citations.

In the field of theoretical and experimental physics, interesting results may be highlighted to the study of the depletion forces exerted on suspended particles by fluids. In this section we will show some of the main recent contributions on this field.

In a system of large spheres (radius R) in a dilute solution of small particles (diameter a) that repel each other, not only the attraction already known among the particles suspended in the range of 0 to a, but also it was found a repulsive barrier for even greater separations, being considered then as a second minimum of distances for which a peak in the intensity of the force is obtained, but now in the opposite direction. This result is interesting because, with attractive and repulsive minima, it is possible to obtain stable structures with purely entropic forces. The key idea is that when the distance has a value multiple to the diameter of the particle, the repulsion between mutual repulsion of spheres within the gap is substantially reduced. At this limit, the spheres become practically non-interacting [191].

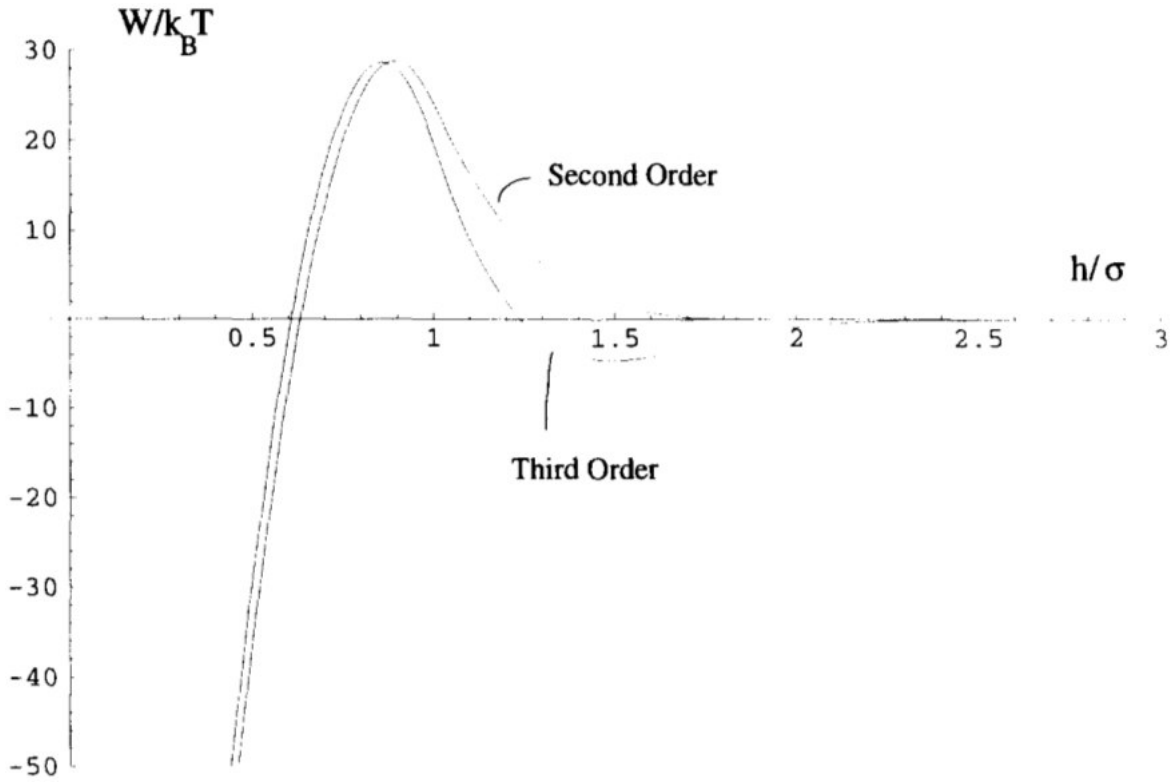

Figure 1.11: Interaction energy curve $W(h)/k_BT$ versus h/σ separation between suspended large spheres, where the attraction and repulsion are evident. Image extracted from reference [191].

Two years later, Dickman *et al.* performed extensive Monte Carlo simulations of binary hard-sphere mixtures, to determine the entropic force between a macrosphere and a hard wall, and between a pair of macrospheres, obtaining similar results i.e., showing that the entropic force can be repulsive as well as attractive. The force profiles exhibit a repulsive peak at a separation of about one microsphere diameter, and show strongly damped oscillations at larger separations. This analysis entirely absent from the AO theory, which predicts a purely attractive potential with a range of one microsphere diameter. This result leads to the conclusion that the entropic force grows faster than

the bulk fluid density and that the entropic force should be repulsive when bigger particle diameter becomes ≈ 2 times the smaller particle radius [192]. Further analytic work appeared studying the entropic depletion force that arises between two big hard spheres. By the framework of the Derjaguin approximation, it was obtained an exact expression for the depletion force and showing that the Asakura-Oosawa result emerges as the low density ideal gas approximation for the density profile of the fluid at contact [193]. Also Castañeda-Priego *et al.* studied analytically this problem in more detail, relating depletion interaction and the surfaces of suspended particles. Among many other results, it was shown that convex regions of the wall are found to interact weakly with the particles, while the concave regions become very attractive. The crossover from a convex to a concave region were found to induce a depletion force parallel to the wall [194]. Later this attractive behavior were observed in cellular structures, ranging from the cytoskeleton to chromatin loops and whole chromosomes. Dependence on entropic depletion on the size and shape of this cellular structures were found, such as the larger the overlap volume, the larger the attraction induced by the solute [195].

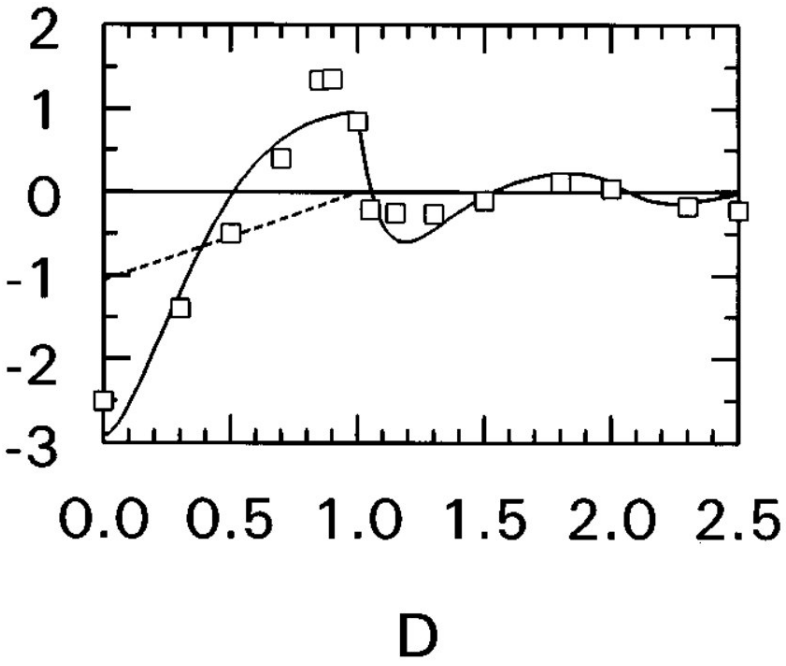

Figure 1.12: Entropic force profile between a pair of hard macrospheres in a fluid composed of microspheres with a diameter five times smaller. Image extracted from reference [192].

In 2010 Buzzaccaro *et al.* have shown that depletion interactions and fluctuation induced forces near a critical point have a common physical origin. This effect, called critical Casimir effect, is regarded as a kind of depletion of long–wavelength fluctuations in the volume comprised by two colloidal particles [196].

The dynamics of passive colloids in a bath of self-propelled particles were receiving a lot of attention in the context of non-equilibrium statistical mechanics. Hence some works starts to emerge considering passive suspended particles and active solutes. In particular,

Angelani *et al.* demonstrate that a bath of swimming bacteria gives rise to a short range attraction similar to depletion forces in equilibrium colloidal suspensions. With a bath of *E. Coli* cells, the emergence of an "effective" attraction between beads becomes evident. It was concluded that the origin of attraction mainly relies on the off-equilibrium dynamics, which provides strong fluctuating forces acting on colloidal particles, opening the way to new investigations on self-assembly phenomena mediated by active particles [93]. Combining the two previous ideas, we have in 2014 a work by Ray *et al.* where it was shown that the Casimir effect can emerge in microswimmer suspensions, for low Reynold numbers [197].

When we have a similar system with run-and-tumble particles in the Casimir-like geometry, then that there is an attractive force between the two walls of a magnitude that increases with increasing run length. This attraction depends on the distance between walls, arising by the swimmers in the regions between the plates. This results shows that active matter systems can exhibit a rich variety of fluctuation-induced forces between objects, which may be useful for applications such as self-assembly or particle transport [198].

On the same year a system composed of a solution of small active disks interacting with large passive colloids were performed. Results indicate that while colloidal rods experience a long-ranged predominantly attractive interaction, colloidal disks feel a repulsive force that is short-ranged in nature and grows in strength with the size ratio between the colloids and active depletants. In this paper, it is also important to note that the sign, and the range of the effective interaction was found to be controlled by tuning the geometry of the passive bodies. They concluded that crucial to the depletion intensity is the role of curvature, which determines whether passive bodies act as traps or as efficient scatterers of active particles. Therefore it becomes clear that active depletion can have dramatic consequences on both the phase behavior and the self-assembly of differently shaped colloids, with possible applications in material engineering and particle sorting [199].

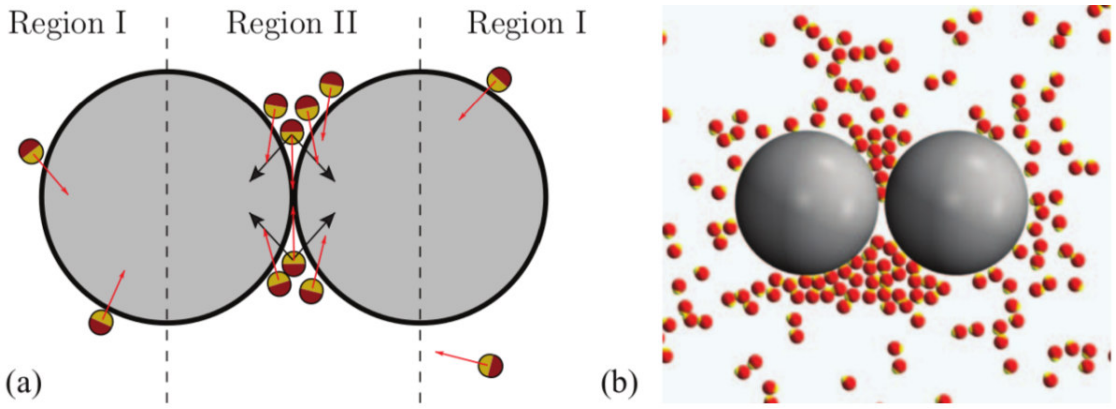

Figure 1.13: (a) Sketch explaining how repulsion arises on spherical particles induced by self-propelled particles (b) Typical snapshot for the two colloidal disks in an active bath. Image extracted from reference [199].

Now the control of short- and long-range forces are in focus by Ni *et al.*, where using Brownian dynamics simulations they study the effective interaction between two parallel hard walls in a 2D suspension of self-propelled (active) colloidal hard spheres. It was found that the effective force between two hard walls can be tuned from a long range repulsion into a long range attraction by changing the density of active particles. Also a strong oscillating long range dynamic wetting repulsion between walls were obtained, due to a crystallization in the region between plates. By decreasing density of particles, particles crystallization starts to vanish and then an attractive behavior emerge. Therefore a interesting result is that the sign of interaction can be tuned from long range repulsive to long range attractive by changing the density of particles. Also it was shown that the range of interaction can be controlled by varying the magnitude of self-propulsion on the particles [200].

Elucidations on this matter were also done experimentally, where depletion interaction potentials between micron-sized colloidal particles were induced by nanometer-scale surfactant micelles, and measured by video microscopy. The strength and range of the depletion interaction is revealed to arise from variations in shape anisotropy of the surfactant micelles. Thus shape anisotropy is now identified as a tool for interparticle control interactions in colloidal suspensions. The depletion potentials were revealed to vary substantially in magnitude and range with temperature [201].

2 Fundamentals

2.1 Brownian Motion

Brownian motion (BM) plays a key role on soft matter physics due to the mesoscopic scale which soft matter ranges, causing it to be always under the influence of thermal motion. In the case of suspended particles, due to endless colisions, its motion exhibit a brownian-like trajectory, with the seven characteristics listed on the below paragraph and illustrated on Fig. 2.1. Therefore, to understand soft matter and suspended particles, we must understand brownian motion.

In 1828 the Scottish botanist Robert Brown observed that little particles immersed in a fluid presented a random motion. After, this motion received in his honor the name Brownian Motion (BM). After many experiments, it was observed many characteristics among which we can highlight: (i) the motion observed was extremely irregular, with translational and rotational motions, and that particles trajectory had no tangent; (ii) two particles seems to move independently one another, even if they are very close (diameter magnitude order); (iii) the smaller the brownian particle the greater its motion; (iv) the composition and density of particles appeared to exert no influence; (v) the less viscous the fluid, the greater the motion of the particle; (vi) the higher the temperature, the greater is the motion of the particle and (vii) the motion never ceases.

In 1905 Einstein proposed the first mathematical model to describe BM. In his approach, it is necessary first to consider that suspended particles have an independent motion from the other particles. This can be considered for times not so small, which we will call by τ.

Lets consider N particles in suspension in a liquid. These particles will, in a time interval between τ and $t+\tau$, undergo a displacement along the x axis such that $\Delta x = \mu$, where μ is a variable which can assume different values for each particle. With the different values that μ can assume we can associate to it a probability distribution such that we can consider that the particle fraction that undergo a displacement between x and $x+\mu$,

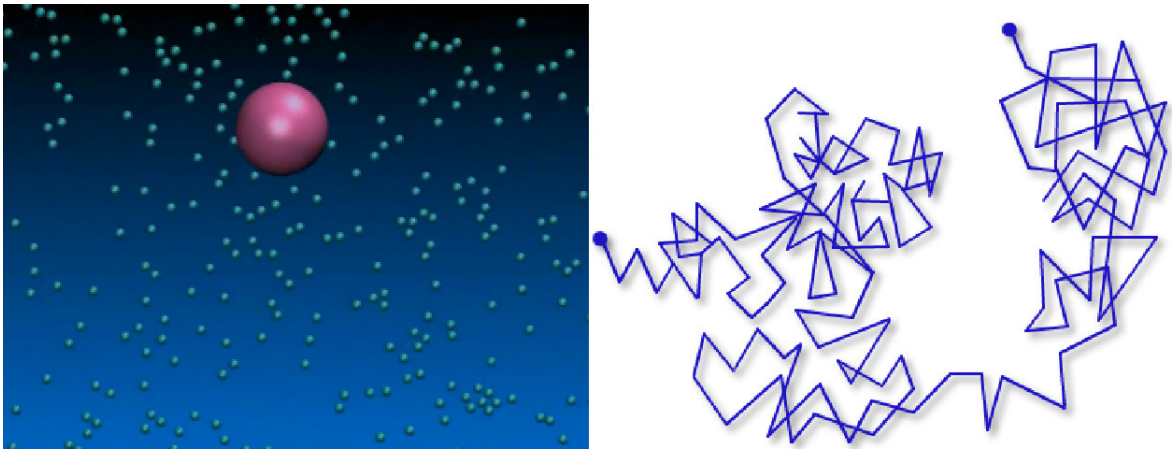

Figure 2.1: Illustration of brownian motion. Small particles collide with big particles inducing an random trajectory.

in a time interval τ, can be expressed by:

$$\frac{dN}{N} = \xi(\mu)d\mu \tag{2.1}$$

where $\xi(\mu)$ satisfies the normalization condition

$$\int_{-\infty}^{+\infty} \xi(\mu)d\mu = 1. \tag{2.2}$$

Calling $\eta(x,t)$ the number of particles per unit length, and considering that time t has passed, the number of particles on instant $t+\tau$ that are between x and $x+\mu$ is:

$$\eta(x,t+\tau)dx = dx\int_{\mu=-\infty}^{\mu=+\infty} \eta(x+\mu,t)\xi(\mu)d\mu \tag{2.3}$$

where τ is very small. Making a second-order Taylor series expansion:

$$\eta(x,t+\tau) \cong \eta(x,t) + \tau\frac{\partial\eta(x,t)}{\partial t} + \frac{\tau^2}{2}\frac{\partial^2\eta(x,t)}{\partial t^2} + ... \tag{2.4}$$

μ is also very small, so we repeat the procedure for $\eta(x+\mu,t)$ in second order power for μ:

$$\eta(x+\mu,t) \cong \eta(x,t) + \mu\frac{\partial\eta(x,t)}{\partial x} + \frac{\mu^2}{2}\frac{\partial^2\eta(x,t)}{\partial x^2} + ... \tag{2.5}$$

Substituting these two expansions above on Eq.(2.3), simplifying for $\eta(x,t) = \eta$:

$$\eta + \tau\frac{\partial\eta}{\partial t} + \frac{\tau^2}{2}\frac{\partial\eta^2}{\partial t^2} = \eta\int_{-\infty}^{+\infty}\xi(\mu)d\mu + \frac{\partial\eta}{\partial x}\int_{-\infty}^{+\infty}\mu\xi(\mu)d\mu + \frac{\partial^2\eta}{\partial x^2}\int_{-\infty}^{+\infty}\frac{\mu^2}{2}\xi(\mu)d\mu... \tag{2.6}$$

We should observe that are no preference to particles motion on x axis, so the probability distribution associated to μ variable is symmetric in y axis. We can conclude that function $\xi\mu$ is a even function, i.e., that $\xi(\mu) = \xi(-\mu)$. So we can solve the integrals of previous equation. The first one η multiplied by normalization condition, which is equal

to 1. The second term on right side is an integral of a even function multiplied by an odd function. The result of a even function multiplied by a odd function is an odd function. Because interval integration varies from $-\infty$ two $+\infty$, the second term vanishes. Substituting these results and dividing then by τ, we obtain:

$$\frac{\tau}{2}\frac{\partial^2\eta}{\partial t^2} + \frac{\partial\eta}{\partial t} = D\frac{\partial^2\eta}{\partial x^2} \tag{2.7}$$

where

$$D = \frac{1}{\tau}\int_{-\infty}^{+\infty}\frac{\mu^2}{2}\xi(\mu)d\mu \tag{2.8}$$

We call D the *diffusion coefficient*. If we take the limit

$$\tau\frac{\partial^2\eta}{\partial t2} \ll \frac{\partial\eta}{\partial t} \tag{2.9}$$

Then Eq.(2.7) becomes

$$\frac{\partial\eta}{\partial t} = D\frac{\partial^2\eta}{\partial x^2} \tag{2.10}$$

This is the standard form for diffusion equation.

In order to calculate D coefficient, suppose a set of particles in suspension on a fluid in dynamic equilibrium. We shall assume that these particles are under influence of a K force which depends on distance, but not time. Einstein obtained that the condition for equilibrium can be expressed by the following equation:

$$-K\eta + \frac{RT}{N}\frac{\partial\eta}{\partial x} = 0 \tag{2.11}$$

where η is the number of particles in suspension. This equation shows that these equilibrium state under influence of K force is reached with the influence of osmotic pressure. Dividing the equilibrium condition in two opposite motions, we have: (i) the motion of the substance in suspension, which undergo the K force influence acting on each particles and (ii) a diffusion process that appears due to particles random motion (induced by thermal effects). Particles in suspension are considered as spherical with radius and the liquid with k viscosity. So the K force induce the particle to move with velocity $\frac{K}{6k\pi\rho}$, where passes $\frac{K\eta}{6k\pi\rho}$ particles by area unit and by time unit. Calling m particle mass, diffusion leads to $-D\frac{\partial\eta}{\partial x}$ particles crossing by area and time unit. To keep equilibrium dynamics situation we shall have

$$\frac{K\eta}{6k\pi\rho} - D\frac{\partial\eta}{\partial x} = 0 \tag{2.12}$$

From Eq.(2.11) we obtain

$$-K\eta + \frac{RT}{N}\frac{\partial\eta}{\partial x} = 0 \longrightarrow \frac{\partial\eta}{\partial x} = \frac{K\eta}{6Dk\pi\rho} \tag{2.13}$$

and from equation

$$\frac{K\eta}{6k\pi\rho} - D\frac{\partial\eta}{\partial x} = 0 \longrightarrow \frac{\partial\eta}{\partial x} = \frac{KN\eta}{RT} \tag{2.14}$$

Equating Eq.(2.13) and (2.14), we have

$$\frac{K\eta}{6Dk\pi\rho} = \frac{KN\eta}{RT} \tag{2.15}$$

and D:

$$D = \frac{RT}{N}\frac{1}{6k\rho\pi} \tag{2.16}$$

This equation shows that diffusion coefficient depends only on the liquid viscosity, particles size and the Avogadro's number [202].

2.2 Active Matter

Since scientific interest grows about active matter, different models were elaborated in recent years [69, 203, 204, 205, 206, 207, 208, 209, 210, 211, 212, 213]. In this section we present some of the main and simple active particle models.

2.2.1 Non-interacting Particles

We know that a passive brownian particle have only diffusive motion, with the translational diffusion coefficient given by (in 3D)

$$D_T = \frac{k_B T}{6\pi\eta R} \tag{2.17}$$

and with rotational diffusion coefficient given by

$$D_R = \tau_R^{-1} = \frac{k_B T}{8\pi\eta R^3} \tag{2.18}$$

where the coefficients are, in a homogeneous medium, independent of each other. However, in a case of a active brownian particle, there is a constant self-propulsion velocity v. Thereby, the particles trajectory depends now on its rotation and consequently emerges a correlation between rotation and translation. Therefore, the velocity of an active brownian particle consists on the sum of the thermal contribution and the self-propulsion contribution, that is for convenience written below on bi-dimensional case [214]

$$\begin{cases} dx/dt = v\cos\theta + \sqrt{2D_T}\eta_x \\ dy/dt = v\sin\theta + \sqrt{2D_T}\eta_y \\ d\theta/dt = \sqrt{2D_R}\eta_\theta \end{cases} \tag{2.19}$$

where D_T is the translational diffusion coefficient, D_R is the rotational diffusion coefficient, η_x, η_y and η_0 are the independent white noise therms with zero mean and unitary variance, along x, y and θ direction, respectively. To calculate the average position of particles, all is needed is to understand that, as a consequence of the self-propulsion, the direction of

motion is itself subject to rotational diffusion, as shown on Eq.(2.19). Therefore, from random-walk one-dimensional theory, it is known that $\langle x(t)\rangle = x_0 + v_0(1/\gamma)/(1 - e^{-\gamma t})$ is the average position of the particle in the x-axis. Applying this equation in our case, following substitutions are performed: (i) $v_0 = v$; (ii) $x_0 = 0$ and (iii) $\gamma = D_R$, i.e., the viscosity of the medium now is taked into account by the rotational diffusion. Thus leads to

$$\langle x(t)\rangle = \frac{v}{D_R}[1 - \exp(-D_R t)] = v\tau_R\left[1 - \exp\left(-\frac{t}{\tau_R}\right)\right] \tag{2.20}$$

where $\tau_R = 1/D_R$, and remembering that $\langle y(t) = 0\rangle$ by symmetry arguments. We note that the position of the particle is directly proportional to the coefficient $v/D_R = v\tau_R$, so it is convenient to define a new physical quantity, called *persistence length*, as

$$L = \frac{v}{D_R} = v\tau_R \tag{2.21}$$

This quantity plays a quite important role on self-propelled particles motion, because it determines the average displacement that the SPP will move before its direction is randomized. In order to relativize this quantity with SPP translational diffusion, i.e., due to competition between self-propulsion and brownian motion, it is also convenient to define a physical quantity which simplifies the information about which of these two forces is the most relevant in a given set of particles. Therefore, this physical quantity, called the *Péclet Number*, is defined as

$$Pe = \frac{v}{\sqrt{D_T D_R}} \tag{2.22}$$

It is important to note that the higher the Péclet number, the greater the influence of self-propulsion on particles trajectory. The lower the Péclet number, the greater the influence of brownian motion in particles trajectory.

These Self-propelled systems can be modelled simply adding on particles equation of motion a constant internal force $F = \gamma v$. In the case of known external forces that are responsible for particles self-propulsion, just simply adding the known term togheter with γv on the expression of the force is enough. That is why this model is very simple to be applied and it is used in several recent works [20, 22, 23, 31, 55, 155, 170, 171, 180, 181, 215, 216, 217, 218, 219, 220, 221, 222, 223, 224, 225, 226]. Note that in this case it is considered that the forces and torques arising as a consequence of an external field or interaction between particles does not affect the mechanism of self-propulsion of the particle.

Another simple model for SPP is the so called run-and-tumble dynamics, which is very common in nature. First detected on *E.Coli* bacteria, this motion consists on the combination of a step in a straight line, and after the step a random rotation, and then another step in straight line, and then another rotation, and so on. Bacteria in a fluid generally follow this type of motion, but due to its small size, small steps lead necessarily to a motion very similar to the active brownian motion. Therefore, both models are equivalent in this limit [52].

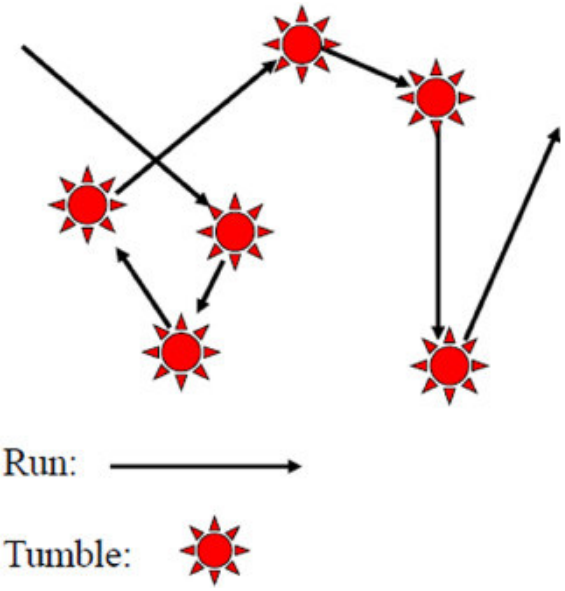

Figure 2.2: Illustration of the run-and-tumble motion, exerted by bacteria such as *E. Coli*. Picture extracted from reference [227]

2.2.2 Interacting Particles

On this section we present two of the most used self-propelled particles model. The first one, without alignment rules, is called Angular Brownian Motion (ABM) model [54]. The alignment rule consists of a condition imposed by the model such a way that particles acquire an ordered collective motion. The second one, having an alignment rule between particles and is called *Vicsek Model* [21] and are detailed below.

No-aligning models

Angular Brownian Motion (ABM) model refers to a model for SPP introduced by Fily and Marchetti [54] with *no alignment rule*. As a result, particles, although self-propelled, do not order in a moving state at any density. The particles are soft repulsive disks of radius a with a polarity defined by an axis $\vec{v}_i = v_0 \cos\theta_i(t)\hat{i} + v_0 \sin\theta_i(t)\hat{j}$ where i labels the particles. The dynamics is governed by the equations

$$\frac{\partial \vec{r}_i}{\partial t} = \vec{v}_i + \mu \vec{F}_i + \eta_i^T(t), \frac{\partial \theta_i}{\partial t} = \eta_i^R(t) \tag{2.23}$$

with v_0 the self-propulsion speed and μ the mobility. The translational and rotational noise terms, $\eta_i^T(t)$ and $\eta_i^R(t)$, are Gaussian and white, with zero mean and correlation $\langle \eta_{i\alpha}^T(t)\eta_{j\beta}^T(t')\rangle = 2D\delta_{ij}\delta_{\alpha\beta}\delta(t-t')$ and $\langle \eta_i^R(t)\eta_j^R(t')\rangle = 2\nu_r\delta_{ij}\delta(t-t')$ with $D = k_BT\mu$ the Brownian diffusion coefficient and ν_r the rotational diffusion rate (Greek labels represents Cartesian coordinates). Although self-propulsion speed v_0 is fixed, the instantaneous speed of each particle is determined by the forces due to neighbors, in contrast to Vicsek-type models. It is interesting to note that this model allows particles to aggregate, as shown on Fig. 2.3.

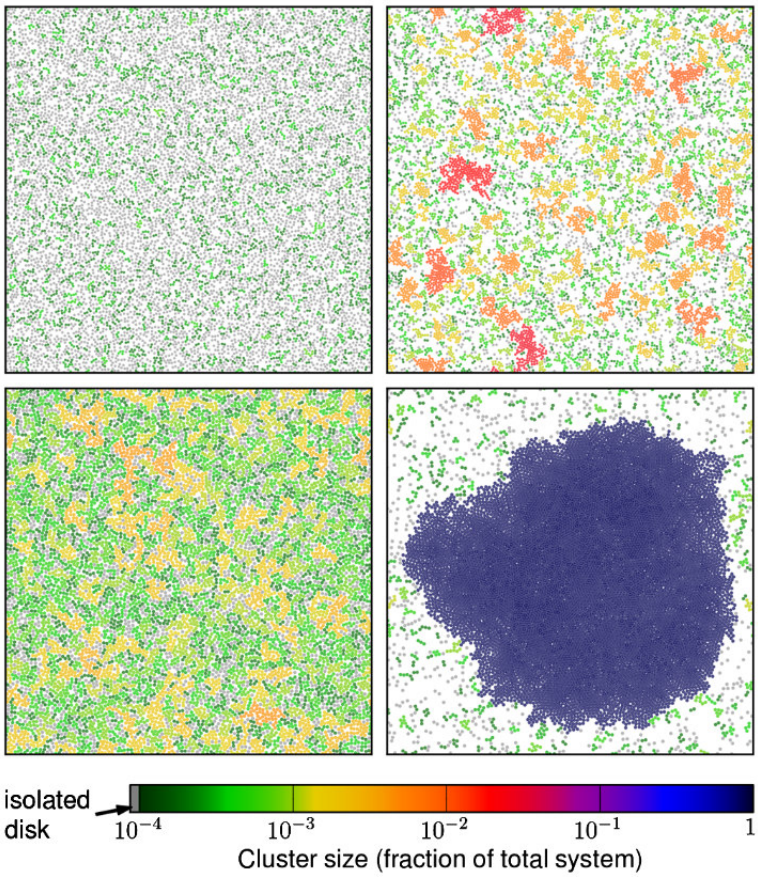

Figure 2.3: Snapshots of 10^4 disks, showing different clusters size for different densities and self-propulsion velocities. Image extracted from reference [54].

Aligning models

In 1995 Tamás Vicsek *et al* introduced [21] a simple model to SPP which still widely used nowadays due to its simplicity and capacity. In this model there is a collection of particles moving independently of the others, but with the same rules which governs its motion. Particles are driven with a constant absolute velocity and at each time step assume the average direction of motion of the particles in their neighborhood with some random perturbation added. This model results in a kinetic phase transition from no transport to finite net transport through spontaneous symmetry breaking of the rotational symmetry, with a continuous transition. Equations of motion can be written as

$$\vec{v}_i(t+1) = v_0 \frac{\langle \vec{v}_j(t) \rangle_R}{|\langle \vec{v}_j(t) \rangle_R|} + perturbation \tag{2.24}$$

$$\vec{x}_i(t+1) = \vec{x}_i(t) + \vec{v}_i(t+1) \tag{2.25}$$

where $\langle \dots \rangle$ denotes averaging (or summation) of the velocities within a circle of radius R surrounding particle i. Angular noise are accounted by equation

$$\theta_i(t+1) = \theta_i(t) + \Delta_i(t) \tag{2.26}$$

where perturbations are represented by letter $\Delta_i(t)$, which is a random number taken from a uniform distribution in the interval $[-\eta\pi, \eta\pi]$. The only parameters of the model are the density ρ, the velocity v_0 and the level of perturbations with $\eta < 1$. By varying some parameters, initial conditions and settings, the simulations exhibit a rich variety of collective motion patterns, such as moving groups, mills, rotating, chains, bands, etc. According to the studies, noise, density, the type of interaction and the boundary conditions all proved to play an important role in the formation of certain patterns.

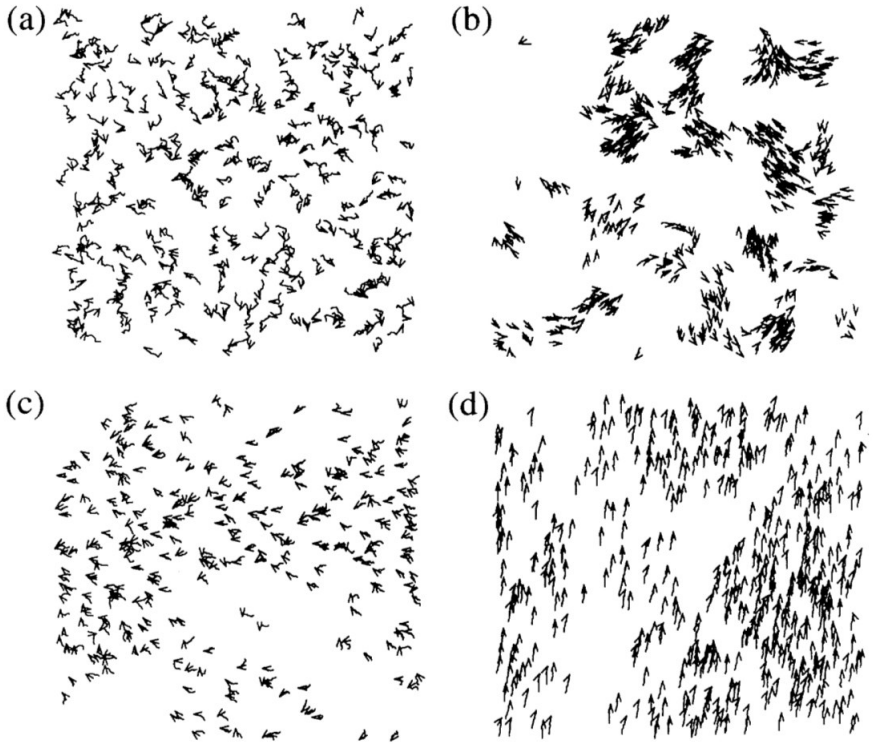

Figure 2.4: (a-d) Examples of pattern formation for different densities and noise values, for constant self-propulsion velocity. Image extracted from reference [21].

2.3 Depletion Forces Fundamentals

One of equilibrium statistical mechanics results is the well known depletion force between two large particles (macromolecules) when immersed in a bath of hard-spheres (solute). This force consists in an effective attraction due to the excluded volume effect between two large particles when they come close enough so that they expel (deplete) the region between them of small particles. This produces an unbalance of forces between the large and small particles in a way that there are interactions only outside the region and, given that they are repulsive, the small ones push the large ones towards one another such that the net result is an effective attraction between the first. Such attraction can also be explained in terms of increase of entropy of the solute, once the total volume available to the solute is the difference between the total sample volume and the volume occupied

by the large particles plus the excluded volume around each of those. When the large ones approach each other, the excluded volume increases, which makes the total entropy increase and the system to stay in this larger entropy state.

2.3.1 Asakura-Oosawa Model

In 1954 Asakura and Oosawa proposed an analytical model pointing out that between two bodies immersed in a solution of macromolecules, an interaction appears owing to characteristics of the medium.

Let us consider two spherical bodies of diameter D immersed in a solution of rigid spherical macromolecules. If the distance a between these bodies is smaller than the diameter of the solute molecules d, a force equivalent to the osmotic pressure of the solution of macromolecules acts inwards on each big particle. From statistical mechanics, it is known that, for a very dilute and monodisperse solution, the force between the two bodies in it, can be given by the generalized force equation

$$F = -\frac{\partial A}{\partial a} \tag{2.27}$$

where A is the Helmholtz's free energy

$$A = -k_B T \ln Z \tag{2.28}$$

and Z is the canonical partition function, given by

$$Z = \frac{1}{N! a^{3N}} \int \exp(-\beta E) d\Gamma = \frac{1}{N! a^{3N}} \int \exp\left(\frac{-\beta \vec{p}^2}{2m}\right) d^3p d^3q \tag{2.29}$$

where particles are considered to be non-interacting, because the model intends to show that depletion forces emerges uniquely by medium properties. N is the number of particles, $\vec{p}$ is the particle's momentum and m is particle's mass. Now remembering that

$$\int \exp(-\alpha x^2 dx) = \sqrt{\frac{\pi}{\alpha}} \tag{2.30}$$

and that $\int d^3q = V_A$, then partition function becomes

$$Z = \frac{V_A}{N! h^3} \left(\sqrt{2\pi m k_B T}\right)^3 \tag{2.31}$$

where V_A is the accessible volume for smaller particles. In therms of the de Broglie thermal wavelength $\lambda = \sqrt{\frac{h^2}{2\pi m k_B T}}$:

$$Z = \frac{V_A^N}{N! \lambda^{3N}} \tag{2.32}$$

and then Helmholtz's free energy can be written as

$$A = -k_B T \ln\left(\frac{V_A^N}{N! \lambda^3}\right) \tag{2.33}$$

Using Stirling's approximation $\ln n! = n \ln n - n$, we have that

$$A = -Nk_BT(\ln V_A - \ln \lambda^3 - \ln N + 1) \tag{2.34}$$

Observe that we can rewrite the above expression isolating therms that are independent of distance a between particles. To do this, it is convenient to create a new variable (F_{ia}) which includes all these therms $F_{ia} = N(1 - \ln N + \ln V - \ln \lambda^3)$. So A can be rewritten as

$$A = F_{ia} - Nk_BT \ln\left(\frac{V_A}{V}\right) \tag{2.35}$$

In this point we need to consider the two situation pointed out by Asakura and Oosawa, which is (i) big particles are far away one another and then small particles can pass between then, i.e., $a \geq D + d$ or (ii) big particles are too close one each other and small particles cannot pass between then, i.e., $a < D + d$. Analyzing first case (i), the accessible volume V_A for small particles are just the volume of the box V minus the volume of big particles V_P, so $V_A = V - V_P$, where $V_P = \pi(D + d)^3/6$. Analyzing case (ii), it is important to observe (see Fig. 2.5) that V_A now is lower than in case (i), because together with the volume of large particles V_P, now also the volume between large particles is inaccessible. Lets call this volume the inaccessible volume V_I and note that V_I is the volume of two spherical caps, so

$$V_I = \frac{2\pi l^2}{3}\left[\frac{3(D + d)}{2} - l\right] \tag{2.36}$$

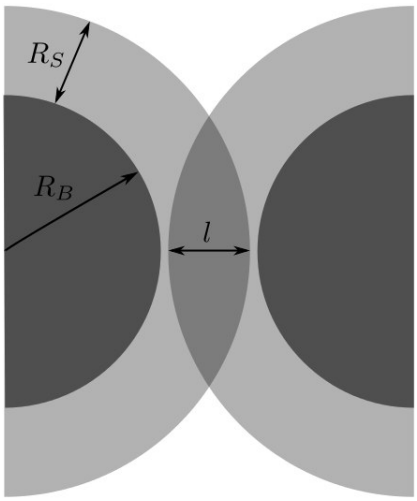

Figure 2.5: Illustration of a two-dimensional cross section of the overlapping volume between hard spheres. R_S is the smaller particle diameter, R_B is the big particle diameter and l is the width of a lens formed by spherical caps.

We are interested in study the influence of distance a between big particles to the depletion forces. It is important to write l and a relation that is $l = (D + d)/2 - a/2$, and then, in therms of a, V_I becomes

$$V_I = \frac{\pi}{6}(D + d - a)^2\left(D + d + \frac{a}{2}\right) \tag{2.37}$$

Finally, V_A for case (ii) can be expressed as

$$V_A = V - V_P + \frac{\pi}{6}(D + d - a)^2 \left(D + d + \frac{a}{2}\right) \tag{2.38}$$

and

$$\ln\left(\frac{V_A}{V}\right) = \ln\left[1 - V_P + \frac{\pi}{6}(D + d - a)^2 \left(D + d + \frac{a}{2}\right)\right] \tag{2.39}$$

For a very dilute system, we have $V >> V_A$, and hence using taylor expansion $\ln(1 + x) = x - x^2/2 + x^3/3 - ...$, considering first order therm, we can approximate to

$$\ln\left(\frac{V_A}{V}\right) \approx -\frac{V_P}{V} + \frac{\pi}{6}(D + d - a)^2 \left(D + d + \frac{a}{2}\right) \tag{2.40}$$

and finally, we find the force by Eq.(2.27) for both cases, that is

$$\begin{cases} F = 0, a \geq D + d \\ F = \frac{-\pi N k_B T}{4V}(D + d - a)(D + d + a), a < D + d \end{cases} \tag{2.41}$$

It is important lay emphasis on the negative sign of the force for $a < D + d$, which means that big particles tends to attract one each other, i.e., depletion forces is always attractive.

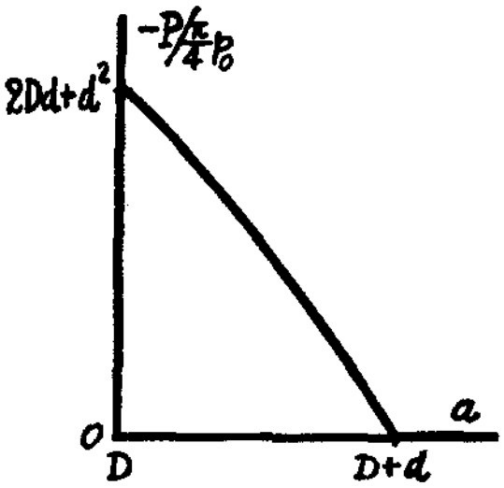

Figure 2.6: The force between two spherical bodies in a solution of spherical macromolecules. Figure extracted from reference [228].

2.3.2 More Accurate Models

On Asakura-Oosawa model, we assumed that the local density of small particles changes only when $h < D + d$. In reality, near confining walls, inhomegeneties appear, by the effect of excluded volume of the small spheres. In order to incorporate such effects, we need more accurate models, which includes a spatially varying external field on potential energy of interaction between small particles and the large spheres, separated by distance h. Some of the main theories are presented below.

Density Functional Theory

The density functional theory consists on the information that for any fluid exposed to an arbitrary external potential, the intrinsic free energy is a unique functional of equilibrium single-particle density $\rho(\mathbf{r})$. Thus any quantity dependent on free energy is also a unique quantity of $\rho(\mathbf{r})$, meaning that all measurable equilibrium quantities are unique functionals of the number density $\rho(\mathbf{r})$. So it is natural that the first step on this approach is to define the local particle density, by

$$\rho(\mathbf{r}) = \left\langle \sum_{\mathbf{i=1}}^{\mathbf{N}} \delta(\mathbf{r} - \mathbf{r_i}) \right\rangle \tag{2.42}$$

where angular brackets means average in the grand canonical ensemble, in a system which allows exchange of particles with a reservoir. In the case of inhomogeneities on depletants particles, the local density $\rho(\mathbf{r})$ becomes non-uniform. Considering the model shown on Fig. 2.7, the external potential acting upon the small particles can be written as

$$V(\mathbf{r};\mathbf{h}) = \mathbf{V_1}(\mathbf{r}) + \mathbf{V_2}(\mathbf{r} - (\mathbf{2R_b} + \mathbf{h})\mathbf{e_z}), \mathbf{h} > \mathbf{0} \tag{2.43}$$

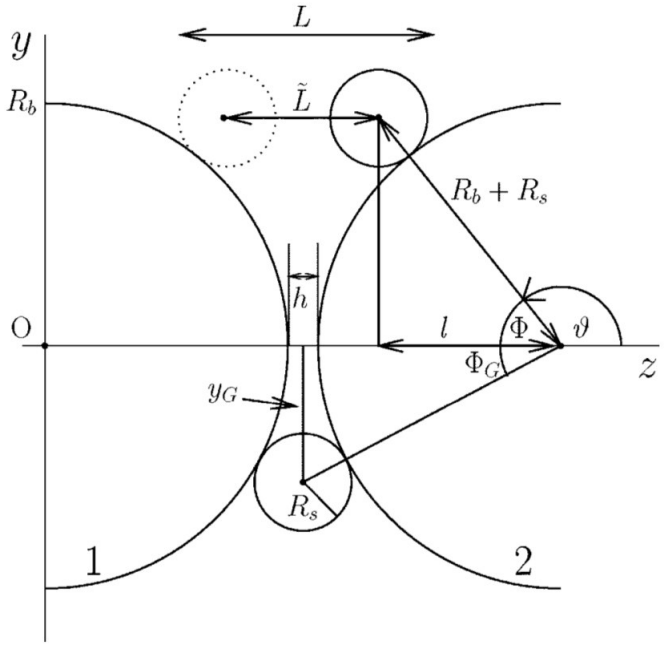

Figure 2.7: Two fixed hard spheres of radius R_b. denoted as 1 and 2, in a fluid of smaller hard spheres of radius R_s. Picture extracted from reference [193].

where V_1 and V_2 is a hard-sphere potential. The second term in Eq.(2.43) is the potential due to a big hard sphere of radius R_b. Then the exact result within density functional theory for the depletion force in the presence of potential is

$$\beta\mathbf{F} = -\int_{\mathbf{S}} \rho(\mathbf{r})\mathbf{n}\mathbf{dA} \tag{2.44}$$

where $\beta = 1/kT$, $\mathbf{F}$ is the force exerted by the fluid on the big sphere 2, S is the surface of a sphere of radius $R_b + R_s$ and $\mathbf{n}$ is the unit normal vector pointing outwards from this sphere. Calculating details can be seen on Ref. [193].

If we consider a radially symmetric external potential, then the local density have the same symmetry and

$$\beta F_z(h) = \pi\epsilon \int_h^\infty [(R_b + R_s) - \epsilon(L - h)]\Delta\rho(L)dL \tag{2.45}$$

for $\Delta\rho(\mathbf{r})$ being the difference of the contact densities between the left and the right hemisphere of sphere 2. ϵ is a geometrical factor in which is equal to 1 for spheres and 2 for plates.

In order to calculate the contact density numerically by molecular dynamics simulations, some approximations are needed. One of these is performed considering that $\Delta\rho(L)$ quickly decaying function of L. Then Eq.(2.45) becomes

$$\beta F_z(h) = \pi\epsilon(R_b + R_s) \int_h^\infty \Delta\rho(L)dL \tag{2.46}$$

This approximation is called the projection approximation, because the projection onto z axis were not taken into account. Now, if we remember that in Asakura-Oosawa model we have

$$\Delta\rho(L) = \begin{cases} 0, & \text{if } L \geq 2R_s \\ -\rho_s, & \text{if } L < 2R_s \end{cases} \tag{2.47}$$

then substituting Eq.(2.47) on Eq.(2.45), we obtain

$$\beta F_z(h) = \pi\epsilon\rho_s\theta(2R_s - h)(R_b + R_s)(2R_s - h) \tag{2.48}$$

For small size ratios $s = R_s/R_b$, the ratio of forces given by Eq.(2.48) and Eq.(2.41) approaches 1, i.e., we recover Asakura-Oosawa model.

Derjaguin Approximation

The Derjaguin approximation consists in the proposal that the interaction energy between two planar surfaces can be related to the force between two curved surfaces, for example, spherical bodies. In this case we will consider a system composed of two spheres of radii R_1 and R_2 with centers lying on z axis at distance $h + R_1 + R_2$ one each other. If we consider that $R_1 >> D$ and $R_2 >> D$, then the force between the two spheres can be obtained by integrating the force between small circular regions of area $2\pi xdx$ on one surface and the opposite surface. Observing that $Z = D + z_1 + z_2$, then the net force between the two spheres in z direction is

$$F(D) = \int_{z=D}^{z=\infty} 2\pi x dx f(z) \tag{2.49}$$

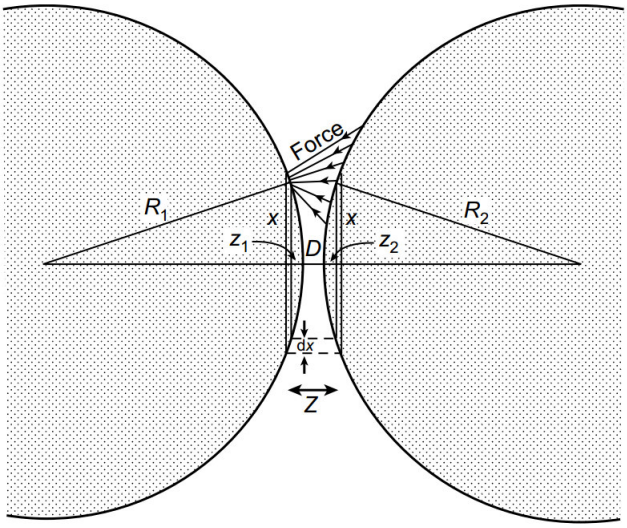

Figure 2.8: Illustration of the Derjaguin model for two spherical particles relating it to two flat surfaces distant apart by z. Extracted from reference [229]

where $f(z)$ is the normal force per unit area between two flat surfaces. Applying Chord theorem $x^2 \approx 2R_1z_1 = 2R_2z_2$ then

$$z = D + z_1 + z_2 = D + \frac{x^2}{2}\left(\frac{1}{R_1} + \frac{1}{R_2}\right) \tag{2.50}$$

and

$$dz = \left(\frac{1}{R_1} + \frac{1}{R_2}\right) xdx \tag{2.51}$$

and then Eq.(2.49) becomes

$$F(D) = \int_D^\infty 2\pi \left(\frac{R_1R_2}{R_1 + R_2}\right) f(z)dz = 2\pi \left(\frac{R_1R_2}{R_1 + R_2}\right) W(D) \tag{2.52}$$

which gives the force between two spheres in terms of the energy per unit area of two flat surfaces at the same separation D. This equation is the Derjaguin approximation, where

$$W(D) = \int_D^\infty f(z)dz \tag{2.53}$$

with D being the distance between the two planar surfaces, and $f(z)$ the normal force per unit area between two flat surfaces at distance z apart (see Fig. 2.8).

When $0 < D < 2R_S$ all small spheres are squeezed out of the slit and the contact density in the slit is 0. The force is then given by the bulk pressure $p(\rho) = -k_BT\Delta\rho(D)$. Calling $\gamma(\rho, h)$ the contribution to the grand potential defined by $-p(\rho) = -\partial\gamma(\rho, D)/\partial D$, and applying on Eq. (2.45) and Eq.(2.46), then

$$F(D) = -\pi\epsilon(R_B + R_S)[p(\rho)(2R_S - D) + \gamma(\rho, \infty)], 0 < D < 2R_S \tag{2.54}$$

The last term is repulsive, in contrast to Asakura-Oosawa model. This model thus explains why numerical simulations can obtain negative values of depletion forces on suspended particles in a bath of small particles.

Integral Equations Theory

Integral equation theory consists in a more powerful theory, which establishes that the depletion potential is a part of potential of mean force $V(r)$ between a pair of large particles in the presence of small particles. The theory proposes that the mean force $V(r)$ can be calculated by the radial distribution function $g(r)$ by the following equation:

$$V(r) = -k_B T \ln g(r) \tag{2.55}$$

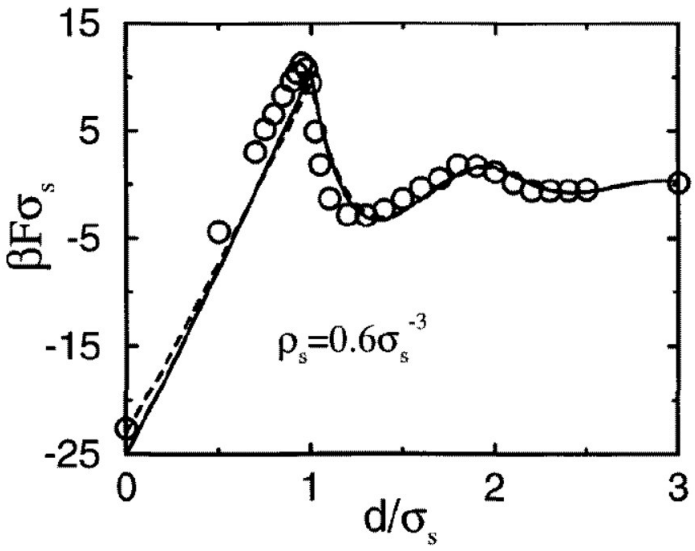

Figure 2.9: The depletion force between two large spheres in a fluid of small spheres as measured by molecular dynamics simulation (empty circles). Image extracted from reference [230].

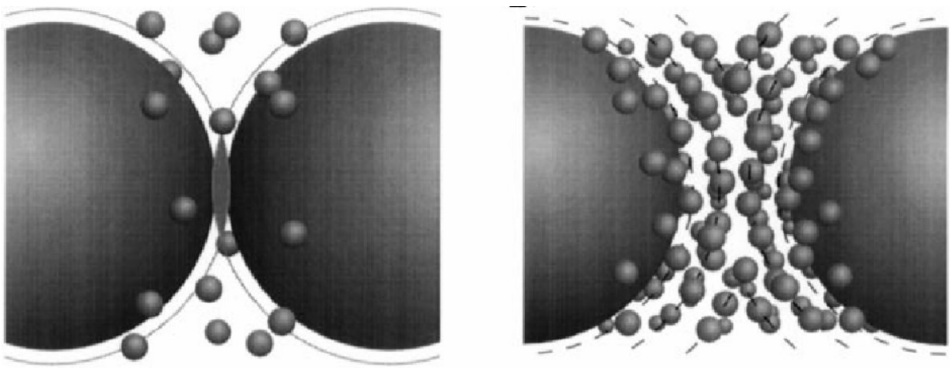

Figure 2.10: At high densities small particles forms layers around big particles. If the gap between the plates is commensurate to the diameter of small sphere, the free energy is smaller than at separations incommensurate with the small sphere diameter. This causes the depletion force to oscillate. Image extracted from reference [232].

To calculate $g(r)$, we use the fact that it is related to the total correlation function $h(r)$ by [230, 231]

$$h(r) = g(r) - 1 \tag{2.56}$$

In order to obtain $h(r)$ for particle 1 and 2, we use the Ornstein-Zernike equation and then Eq.(2.56) becomes

$$h_{ij}(r_{12}) = c_{ij}(r_{12}) + \sum_{k=1}^{N} \rho_k h_{jk}(r_{13}) c_{kj}(r_{32}) dr_3 \tag{2.57}$$

where N is the number of different types of particles in a system and ρ_k is the number density of particle of type k. To solve Eq.(2.57) we need to apply a closure relation between $h(r)$ and $c(r)$, which in this case it is the Percus-Yevick relation:

$$h_{12}(r) + 1 = \exp -\beta V_{12}(r)[1 + h_{12}(r) - c_{12}(r)] \tag{2.58}$$

where V_{12} is the pair potential between particle 1 and particle 2 (interparticle potential).

Numerical solution of Eq.(2.58) leads to an oscillatory behavior of the depletion force (Fig. 2.9), which were not detected by previous theories [230]. Oscillations appears because at large densities, small spheres tend to form layers around the large objects as shown in Fig. 2.10.

2.3.3 Measuring and Calculating Depletion Forces

Experimental measure of depletion forces requires very accurate experimental setup, because this force is usually very weak and are mixed with other forces like van der Waals, double layer electric repulsion and hydrodynamic effects. So such experimental setup needs to be capable to filter such forces and measure only the depletion one.

There are different methods to measure depletion forces. First, we can mention using a line optical tweezer which uses optical gradient forces to trap a pair of large spheres [232]. The spheres becomes constrained to a frictionless rod of light, executing Brownian diffusion. Then a digital video microscopy is used to measure the probability of finding the two spheres at a given separation.

Another measure experimental setup is by laser radiation pressure measurement. Here the pressure of laser beam is exerted on a polystyrene latex colloid particle near a hard wall in a suspension of non-adsorbing polymers. The schematic representation of experiment is shown in Fig. 2.11. The minimum laser intensity that is required to blow the particle away from the wall is then measured [233].

An third option for depletion forces measurements is by atomic force microscopy (AFM). With colloidal probes, a micrometer-sized colloidal particle is attached to an AFM cantilever. The procedure consists in measure the force which drags a cantilever with a colloidal probe to a silica surface immersed in a fluid (see Fig. 2.12). The deflection of the cantilever is then measured with laser reflection on it and because the spring constant of the cantilever is known, force can be computed [234].

For numerical calculation of depletion forces, there are two applicable methods: Monte-Carlo and molecular dynamics simulation, where equilibrium properties are then obtained

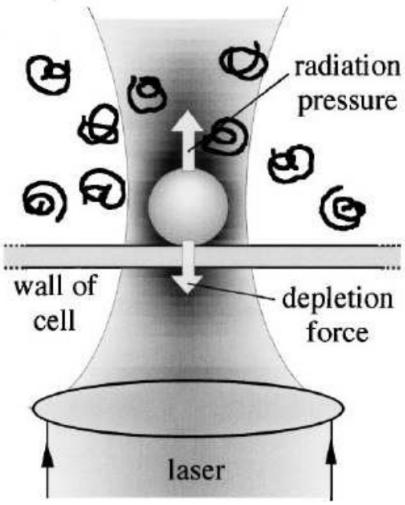

Figure 2.11: A scheme of laser radiation experiment, where the depletion attraction between a colloidal sphere and a plate was measured. Image extracted from reference [233].

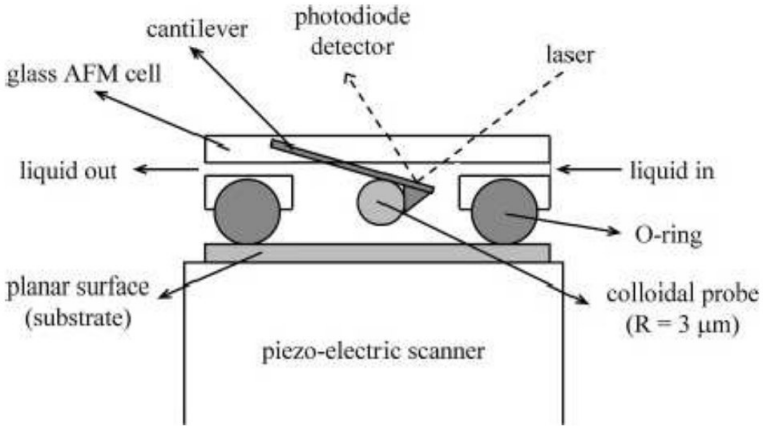

Figure 2.12: A scheme of atomic force microscope with colloidal probe where the depletion force between the colloidal particle on a probe and the planar surface was measured. Image extracted from reference [234].

by the time-averaging over the dynamical history of the system. On this thesis molecular dynamics is used, and it is explained in details on section 3.1, on the following chapter.

3 Numerical Methods

3.1 Molecular Dynamics

The history of molecular dynamics (MD) starts in the 50s with the work of Alder and Wainwright [235] in 1957 and subsequently and independently with Rahman in 1964, where he studied a system of liquid argon, with potential Lennard-Jones interaction type [236].

The motivation for developing such methods is basically to understand the properties of interaction between the particles of a system, taking into account interactions on the microscopic level. This study serves as a complement to conventional experiments, opening new ways to understand particles interaction. Basically molecular dynamics (MD) consists of a computational technique to calculate structural and transport properties in classic systems of many bodies. This means that, in this method, particles obey classical mechanics laws. It is a deterministic method since the trajectory of the particles in this case is not stochastic, but the nearest to the real motion that it would do in an experiment. This not only allows study of properties and configurations after equilibration, but also its properties and how system behaves as time evolves. MD allows the calculation of the macroscopic properties such as temperature, pressure, kinetic energy, potential energy, etc.

Starting with the theoretical physics this method has gained popularity in approximately 1970. Currently there are numerous areas in which MD is widely used, such as kinetic theory, diffusion, transport properties, phase transitions, order parameters, critical phenomena, collective behavior of particles, coupling of rotational and translational motions, vibration, resonance spectrum, dielectric properties, complex fluids, formation of chains, rings and other patterns between interacting particles, fractures, grain dynamic, elastic properties and plastic, molecular crystals, structure and dynamics of proteins, protein folding, fluid dynamics, among others.

3.2 MD method description

The structure of the method can be divided into a few main points:

Initialization: Consists to specify the initial program parameters such as the initial position and particles velocities, initial temperature, particles number, density, step size, etc. The position of particles should be assigned according to the system under study. Obviously, it is not recommended initial positions such that particles overlap one each other, because this can lead to a considerable gain in speed by these particles, leading to numerical errors. In atomic systems, the most commonly used geometries are the FCC and cubic type for three-dimensional case and square and triangular networks for the two-dimensional case. It may also be convenient to distribute initial velocities according to *Maxwellian* distribution.

Force calculation: This step consists in calculate the force acting on each particle in the system. We must consider the contribution to the force exerted on the particle index i with all neighboring particles that interact with it. It is convenient to introduce the concept of *cutoff radius*. The cutoff radius assumes that a relatively large number of particles have negligible interactions. Considering cubic boundary conditions (or squares in 2D case) the distance between the particle i and the nearest particle j will always be lower than half the width of the simulation box. Thus, cutting radius is used such that if the distance between the particle i and j is greater than cutoff radius, the interaction between them is not taken into account, therefore accelerating the speed of simulation. However, if the pair of particles are close enough to interact, the force exerted between them is calculated. Assuming the one-dimensional case, then

$$f_x(r) = -\frac{\partial u(r)}{\partial x} = -\frac{x}{r}\frac{\partial u(r)}{\partial r} \tag{3.1}$$

where $u(r)$ represents the interaction potential between particles.

Integration of Equations of Motion: Once obtained all forces between particles, it is necessary perform calculation in order to integrate equations of motion. Numerous algorithms have been developed to perform this calculation. Undoubtedly, the simplest among these methods is the *Euler method*. It is a first order approximation around a point such that given a function $f(x)$, we expand it around the point $\Delta x : f(x + \Delta x) = f(x) + f'(x)\Delta x$. However, other methods are more used due to greater accuracy of its results. A widely used method is the *Second-order Runge-Kutta method*, which is explained in detail on section 3.2.2.

3.2.1 Euler Method

Euler method is the simplest method to solve ordinary differential equations. In order to understand it lets suppose a function such that $dy/dx = f(x, y)$. Looking at Fig. 3.2, we can note that y_{n+1} in $x = x_{n+1}$ is given by

$$y_{n+1} = y_n + \Delta y \tag{3.2}$$

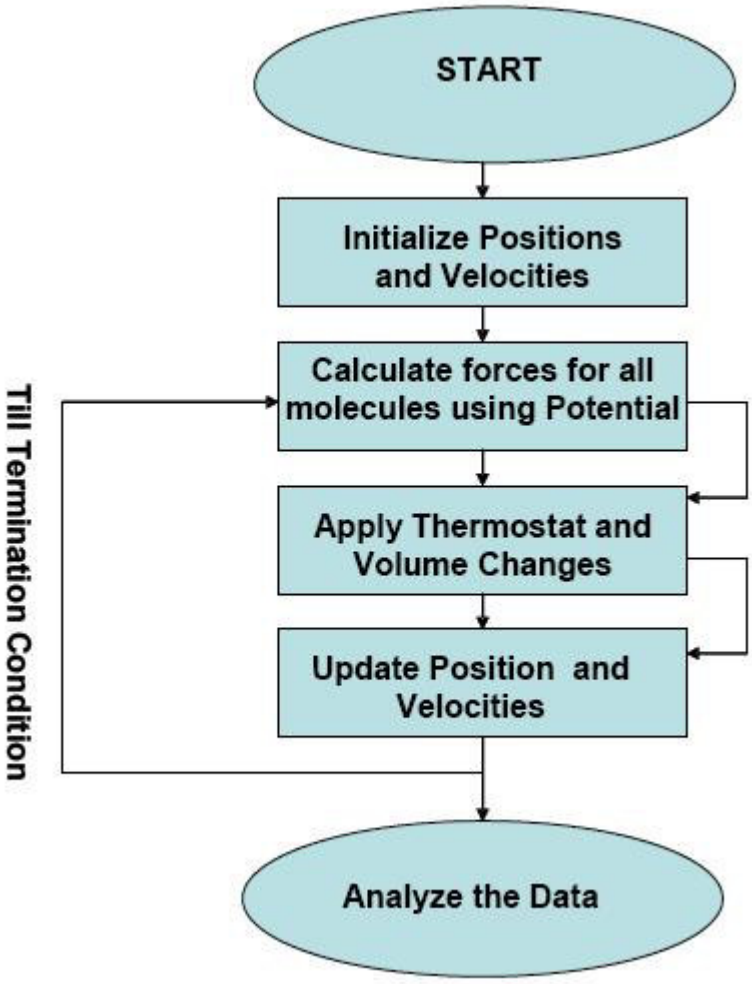

Figure 3.1: Molecular dynamics algorithm fluxogram.

From calculus, we can write

$$dy = \frac{dy}{dx}dx \tag{3.3}$$

and from Eq.(3.3), there is an approximation for Δ_y:

$$\Delta y \approx \frac{dy}{dx}\Delta x \tag{3.4}$$

and from Eq.(3.2) and Eq.(3.4) we have

$$y_{n+1} = y_n + (x_{n+1} - x_n)f(x_n, y_n) \tag{3.5}$$

On Fig. 3.2, we note that the less the difference between x_{n+1} and x_n, the less the error for y_{n+1} evaluation. However, the calculation process raises as difference between x_{n+1} and x_n reduces. Defining the step

$$x_{n+1} = x_n + h \tag{3.6}$$

and applying it in Eq.(3.5) we have

$$y_{n+1} = y_n + hf(x_n, y_n) \tag{3.7}$$

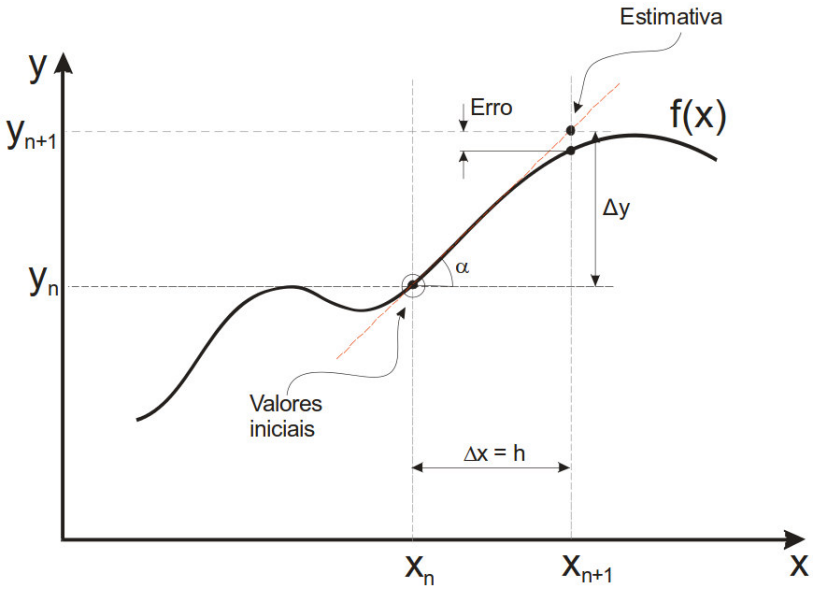

Figure 3.2: Illustrative graph for Euler method.

Equation (3.7) is known as Euler equation. The solution of such equation is obtained by applying Eq.(3.6) and Eq.(3.7) in a recursive manner, using boundary condition x_0 and y_0. Euler method have an error on $O(h^2)$.

3.2.2 Second-Order Runge-Kutta Method

The Runge-Kutta method can be seen as an improvement of the Euler method with a better estimative of the derivative of the function. In Euler's method to estimate the value of y_{n+1} we need y_n and the derivative on x_n point. On Runge-Kutta method we aim to get a better estimate of the derivative by evaluating the function at more points in the range $[x_n, x_{n+1}]$. A second-order Runge-Kutta (RK2) method has an error of $O(H^3)$ order.

On RK2 method y_{n+1} value is calculated using y_n and with the estimate of the derivative at a point closer x_{n+1}, in $x_{n+\frac{h}{2}}$:

$$y_{n+1} = y_n + hf(x_{n+\frac{h}{2}}, y_{n+\frac{1}{2}}) \tag{3.8}$$

On Eq.(3.8), $y_{n+\frac{1}{2}}$ is the y value on $x_n + \frac{h}{2}$. An estimate of $y_{n+\frac{1}{2}}$ is found with Euler's method:

$$y_{n+\frac{1}{2}} = y_n + \frac{h}{2} f(x_n, y_n) \tag{3.9}$$

Defining

$$k_1 = hf(x_n, y_n) \tag{3.10}$$

and

$$k_2 = hf(x_{n+\frac{1}{2}}h, y_{n+\frac{k_1}{2}}) \tag{3.11}$$

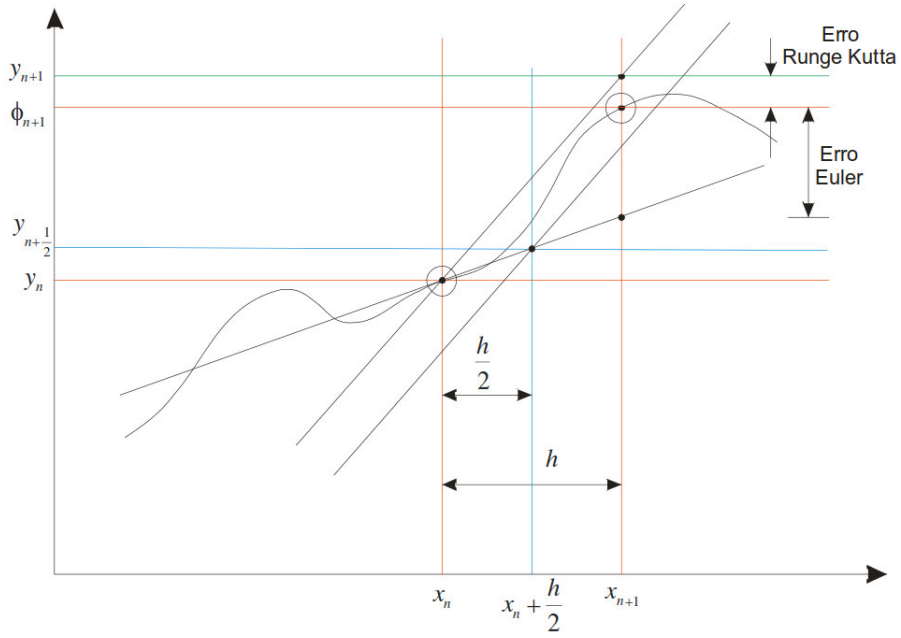

Figure 3.3: Illustrative graph for second-order Runge-Kutta method.

then Eq.(3.8) can be rewritten as

$$y_{n+1} = y_n + k_2 \tag{3.12}$$

On RK2 method calculations are performed on Eq.(3.10), Eq.(3.11) and Eq.(3.12).

3.2.3 Boundary Conditions

Boundary conditions are used to solve the problem of simulating an infinite system using a finite number of particles. It considerably minimize edge effects considering that these edges are not rigid. This is possible considering that system is surrounded by identical copies of the simulation box. In this case, when a particle leaves the box on one side, it immediately appears on the other side of the box. Another important point is that a particle in a simulation box can interact with particles of another box, since the cutting radius permits. This should be taken into account when calculating the forces between particles. After the coordinates each time step should be examined, and if a particle is found out of the box, its coordinates should be adjusted so that it re-enter the box. For example, if a particle is located between $-\frac{L_x}{2}$ and $\frac{L_x}{2}$ where L_x is the width of the box in x direction, it must follow some steps:

1 - If $r_{ix} \geq \frac{L_x}{2}$, assign it the value $r_{ix} - L_x$;

2 - Else, if $r_{ix} < -\frac{L_x}{2}$, assign it the value $r_{ix} + L_x$.

Even with boundary conditions, edge effects are still present in the simulation. So, yet the size of the simulation box should be chosen carefully. The box should have a minimum size such that its width is greater than the distance between particles where interactions are relevant.

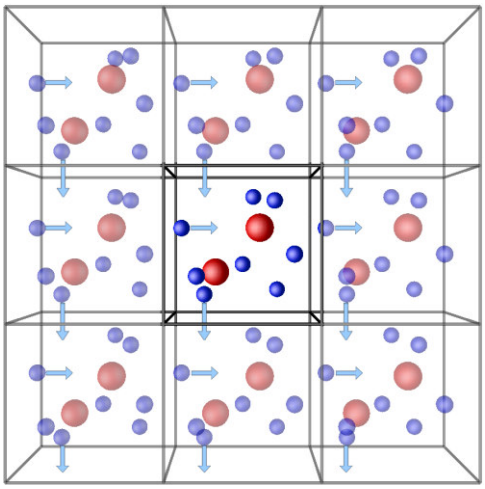

Figure 3.4: Illustration of boundary conditions. Simulation box is surrounded by identical boxes.

4 Depletion forces on elliptical colloids induced by active matter

4.1 Motivation

Active matter or self-propelled particles (SPP) refers to systems in which its entities convert internal energy into motion, being therefore out of equilibrium [39, 54]. Typical examples of these systems are biological systems [227], where microorganisms such as bacteria and eukaryote cells propel themselves with hair-like structures known as flagella. These microorganisms exhibit a variety of structural and dynamical patterns [58, 237, 238, 239, 240, 241, 242]. Recent studies showed that colloidal particles can also behave as self-propelled particles [237, 243]. Active colloids can be induced using photoactive materials [244]. Partially coated colloidal particles with platinum and dispersed in H_2O_2 solution are often used as model of self-propelled colloids [245]. The motion of an artificial micro-swimmer that uses chemical reaction catalyzed on its own surface to achieve autonomous propulsion is also experimentally possible [60]. Erbe *et al.* showed [246] that it is possible to induce active colloids with three different driving mechanisms: by gravity, by a gradient in a magnetic field, and by a local chemical reaction. Catalytically active Janus micro-spheres are capable of autonomous motion and can potentially act as carriers for transportation [89].

When hard colloidal particles are held in suspension, in a bath of smaller passive colloids under Brownian motion, attractive interactions between the large colloidal particles arises by means of depletion forces. This attraction emerges when particles are close to each other. The overlap of the excluded volume around the large particles increases the volume available to the small ones. Hence, the total entropy increases, as shown in the pioneering paper of Asakura and Oosawa [228] almost fifty years ago. However, the excluded volume effect observed in equilibrium systems can not be the sole cause for the effective interaction between passive colloids in a bath of active particles [93]. Instead, this effect, added to the peculiar non-equilibrium features of the dynamics of the self-propelled particles, generates an effective attractive or repulsive interaction which depends, *e.g.* on the shape of the passive particles, magnitude of the velocity of the active particles, ratio

size between the passive colloids and active particles, and density [198, 199, 200]. In spite of its distinct nature, we follow the literature and still name here the effective interaction between passive objects in a bath of active particles as depletion interaction, and also name the force on the passive objects due to the active particles as depletion force. It is worth to mention that the shape of passive objects is indeed a relevant feature that induce modifications in the depletion interaction, as demonstrated very recently on a experimental study of colloidal particles in a passive bath [201].

In this work, we analyze the effects of the shape and relative orientation of passive elliptical colloids (PEC) in a bath of active particles in order to determine the effective interaction between such passive particles. We systematically study how the depletion interaction between two passive elliptical colloids behaves in a 2D (two-dimensional) bath of active particles. In most of the cases we find that the depletion interaction is repulsive, even for very short distances between the passive objects. This is very surprising, and opposite to what has been recently observed for the interaction between parallel hard-walls [200], also in a bath of SPP. As will be discussed along the manuscript, the clustering of SPP on the surface of passive objects is the reason for the depletion interaction in a bath of SPP [176]. The clustering of SPP was well described by an athermal model system [54], the same considered in the present work.

In Sect. 5.2 we introduce the model system and define the key quantities used to characterize the system. In Sect. 4.3, we present and discuss the numerical results.

4.2 Model System

4.2.1 Details of the numerical simulations

Our system consists of two passive elliptical colloids (PEC) in a 2D bath of $N = 1270$ active particles (or SPP). The SPP are modeled as soft disks of diameter σ which interact with each other and with the PEC through spring-like forces of stiffness κ_{SPP} and κ_{PEC}, respectively, with $\kappa_{\mathrm{PEC}} \gg \kappa_{\mathrm{SPP}}$. Each SPP moves with velocity $\vec{v}_i = v_0 \cos\theta_i(t)\hat{i} + v_0 \sin\theta_i(t)\hat{j}$, where v_0 is the magnitude of the self-propulsion velocity. In every timestep Δt, the velocity $\vec{v}_i$ is subjected to random fluctuations in the direction $\theta_i(t)$ which is proportional to a Gaussian white noise ($G_i(t)$) satisfying $\langle G_i(t)\rangle = 0$ and $\langle G_i(t)G_j(t')\rangle = 2\eta\delta_{ij}\delta(t-t')$, where η is the angular noise intensity. Similarly, $\langle \xi_i(t)\rangle = 0$ and $\langle \xi_i(t)\xi_j(t')\rangle = 2\xi\delta_{ij}\delta(t-t')$, where ξ is the translational noise intensity. Therefore the equations of motion for the ith active particle are written as

$$\frac{\partial \vec{r}_i}{\partial t} = \vec{v}_i + \mu\vec{F}_i + \xi_i(t), \qquad \frac{\partial \theta_i}{\partial t} = G_i(t), \tag{4.1}$$

where μ is the SPP motility, $\vec{F}_i = \sum_j \vec{F}_{ij}$ is the total force on particle i and the sum is over $j \neq i$ SPP and/or PEC, where $\hat{\mathbf{r}}_{ij}$ is the unitary vector with the direction pointing

from the contact point at the surface of the PEC to the center of the SPP, i.e., from j to i. The force on the PEC is the negative of this force, i.e., $\mathbf{F}_{ij} = -\kappa\alpha_{ij}\hat{\mathbf{r}}_{ij}$, where α_{ij} is the SPP-PEC overlap. When $\alpha_{ij} > 0$ then ($\mathbf{F}_{ij} = 0$ otherwise). For interaction between SPP $\alpha_{ij} = \sigma - r_{ij}$, where σ is the diameter of a single SPP. For SPP-PEC interaction $\alpha_{ij} = R_{ij} - 2z$, where $z = a$ (if $a > b$) and $z = b$ (if $b > a$), and $R_{ij} = r_{ij}^{(1)} + r_{ij}^{(2)}$, where $r_{ij}^{(1)}$ ($r_{ij}^{(2)}$) is the distance between the ith SPP and the first (second) focus of the jth ellipse (Fig. 5.1).

For horizontal (semi-major axis along the x-axis) PEC, $r_{ij}^{(1)}$ and $r_{ij}^{(2)}$ equations are given by

$$r_{ij}^{(1)} = \sqrt{\left(x_i - \left(x_j - \sqrt{\left(a+\frac{\sigma}{2}\right)^2 - \left(b+\frac{\sigma}{2}\right)^2}\right)\right)^2 + y_i^2}, \tag{4.2}$$

$$r_{ij}^{(2)} = \sqrt{\left(x_i - \left(x_j + \sqrt{\left(a+\frac{\sigma}{2}\right)^2 - \left(b+\frac{\sigma}{2}\right)^2}\right)\right)^2 + y_i^2}. \tag{4.3}$$

where x_i and y_i are the coordinates of the ith SPP, and x_j is the coordinate of the jth PEC. The PEC are assumed to be always along the x-axis ($y_j = 0$). For vertical (semi-major axis along the y-axis) PEC, $r_{ij}^{(1)}$ and $r_{ij}^{(2)}$ are given by

$$r_{ij}^{(1)} = \sqrt{x_i^2 + \left(y_i + \sqrt{\left(a-\frac{\sigma}{2}\right)^2 - \left(b+\frac{\sigma}{2}\right)^2}\right)^2}, \tag{4.4}$$

$$r_{ij}^{(2)} = \sqrt{x_i^2 + \left(y_i + \sqrt{\left(a+\frac{\sigma}{2}\right)^2 - \left(b+\frac{\sigma}{2}\right)^2}\right)^2}. \tag{4.5}$$

In the present work we consider $\xi_i(t) = 0$, which means that the SPP are not submitted to translational thermal fluctuations, and the detailed balance is not obeyed in this system. Recently, such a model system has been called an athermal model system [54, 176].

In all simulations we employed periodic boundary conditions in both $x-$ and $y-$directions. The equations of motion are integrated using a second order stochastic Runge-Kutta algorithm [247]. Lengths are given in units of σ, and the unit of force F_0 is such that $\kappa_{\mathrm{SPP}} = \tilde{\kappa}(\sigma/F_0)$ where $\tilde{\kappa}$ has units of force per distance. The unit of time is $t_0 = \sigma/\mu F_0$. Henceforth, all quantities are dimensionless, unless stated otherwise. We consider $v_0 = 1$, $\kappa_{SPP} = 50$, $\kappa_{PEC} = 1000$ and $\mu = 1$. The equations of motion are integrated using a time step $\Delta t = 10^{-3}$. In all simulations, we run 5×10^6 thermalisation time steps and calculated averages from $5 - 15 \times 10^6$ time steps.

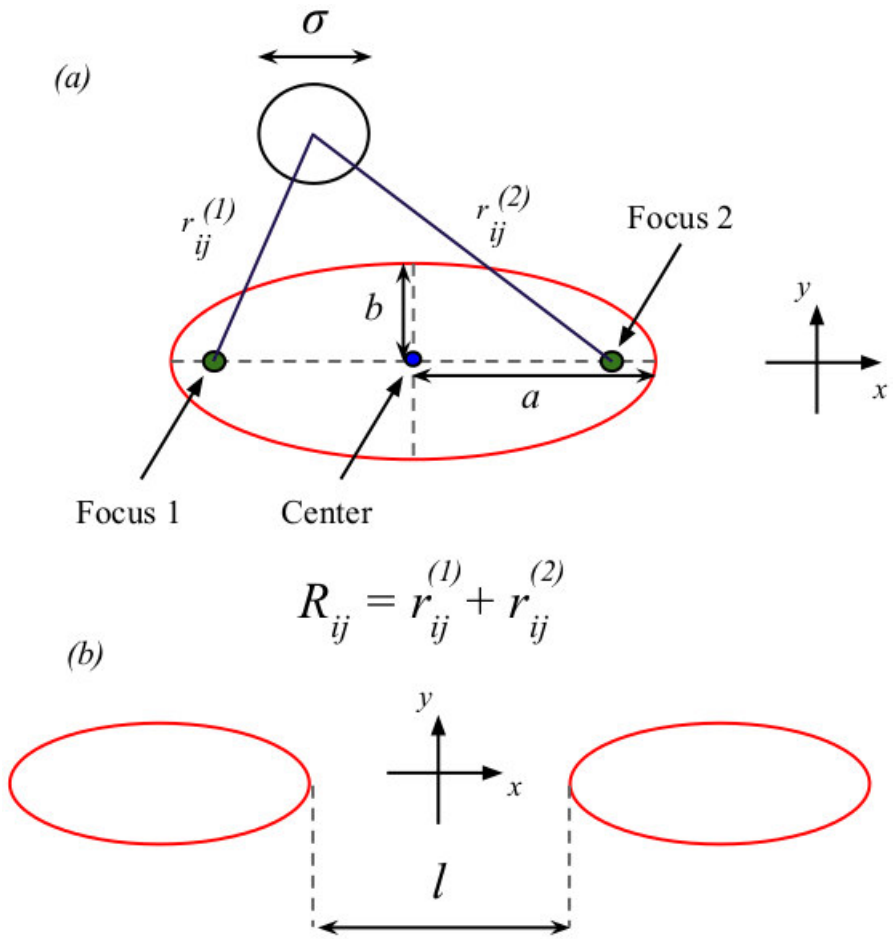

Figure 4.1: (a) The schematic representation of model system. The black circle represents the SPP of diameter σ and red ellipse represents the obstacle. $r_{ij}^{(1)}$ ($r_{ij}^{(2)}$) is the distance between the SPP and the Focus 1 (Focus 2) of the obstacle. a is the size of the horizontal semi-axis and b is the size of the vertical semi-axis. (b) indication of the distance l between the closest points of the passive elliptical colloids.

4.3 Results and Discussions

4.3.1 Interaction between the passive colloids

We are interested in the force between PEC in a bath of active particles. We proceed in this way by considering two PEC at fixed separation and by calculating their interaction with the active particles. Specifically, we calculate the average force $\langle F_x \rangle$, along the x-direction, exerted on the left ellipse (Fig. 5.1) by the bath of active particles, which is the same in magnitude to the average force exerted on the right ellipse. We define l as the distance between the closest points of the two passive elliptical colloids (Fig. 5.1).

It is convenient to define a dimensionless parameter $\lambda = b/a$. For the case $\lambda = 1$, the PEC are circles. For $\lambda > 1$ the ellipses have their major axis along the y-direction (vertical ellipses), while for $\lambda < 1$ the ellipses have their major axis along the x-direction (horizontal ellipses). We always consider the minor axis of the PEC equal to 5. In this

way, for $\lambda \geq 1$, $a = 5$ and $5 \leq b \leq 10$. For $\lambda \leq 1$, $b = 5$ and $5 \leq a \leq 10$.

The magnitude of the interaction between the PEC is studied as a function of the dimensionless parameter λ, the distance between the PEC, l, the angular noise intensity η and the area fraction ϕ, with the later defined as $\phi = \frac{N\pi}{4(L^2 - S_T)}$, where N is the number of SPP, L is the size of the 2D squared simulation box and S_T is the total area occupied by the PEC. Note that ϕ is related to the density n of SPP, i.e. $\phi = \pi n/4$, where n is the SPP density.

In order to present how the SPP are distributed over the simulation box over time, it is convenient to introduce the reduced area fraction distribution, defined as $log_{10}[\phi_i/\phi_{bulk}]$, where ϕ_i is the time average area fraction in the i-th sub-box (the total simulation box is split in small sub-boxes) and ϕ_{bulk} is the time average area fraction calculated far from the PEC. ϕ_{bulk} is the average area fraction of the four sub-box located in the corners of the simulation box, which are far enough from the PEC in order to "feel" their presence.

4.3.2 Influence of the shape and orientation of the obstacles

In this section we analyze the influence of the shape and orientation of the PEC on the depletion interaction in the active bath. For this, we study how $\langle F_x \rangle$ depends on the separation l (Fig. 5.1) between the PEC along the x-axis. The shape and orientation of the PEC are controlled by the parameter λ which is considered in the interval $0.5 \leq \lambda \leq 2$. The other relevant parameters of the model, namely, the area fraction and noise intensity are kept constant as $\phi = 0.1$ and $\eta = 10^{-4}$, respectively. The average force $\langle F_x \rangle$ on the left PEC as a function of l for different values of λ, is shown in Fig. 4.2. $\langle F_x \rangle$ exhibits negative values for any λ, indicating that the left PEC is pushed away from the right PEC. The explanation for this behavior consists of two arguments, based on what we observed in our simulations: the first one is based on the aggregation of the SPPs in between the PEC (which is the main reason for the repulsive character of this force); as a consequence of the fact that the SPPs do not collide in the usual sense, but stick to surfaces upon contact. The second argument is stated mainly to explain the general shape of the curves seen in Fig. 2. Therefore, the effective interaction between the PEC is repulsive, which is opposite to the result obtained by Asakura and Oosawa [228] for a bath of passive particles. Recently, Ni *et al.* showed that the repulsive interaction is not the only one observed in a 2D bath of active particles. In the low density case, it was observed a long-range attraction between parallel hard-wall plates [200]. Similar results were also obtained by D. Ray *et al* [198] but there they found regimes in which there is a crossover from attraction to repulsion between the walls as a function of wall separation and wall length and by Stenhammar *et al* [248], where it was found that in a mixture of active and passive particles motility of the active component triggers active-passive segregation, which illustrates the attraction between passive particles.

For $l \leq 0.9$ the magnitude of $\langle F_x \rangle$ increases monotonically with increasing l in both cases $\lambda < 1$ and $\lambda > 1$. $\langle F_x \rangle$ drops considerably as the separation between the obstacles

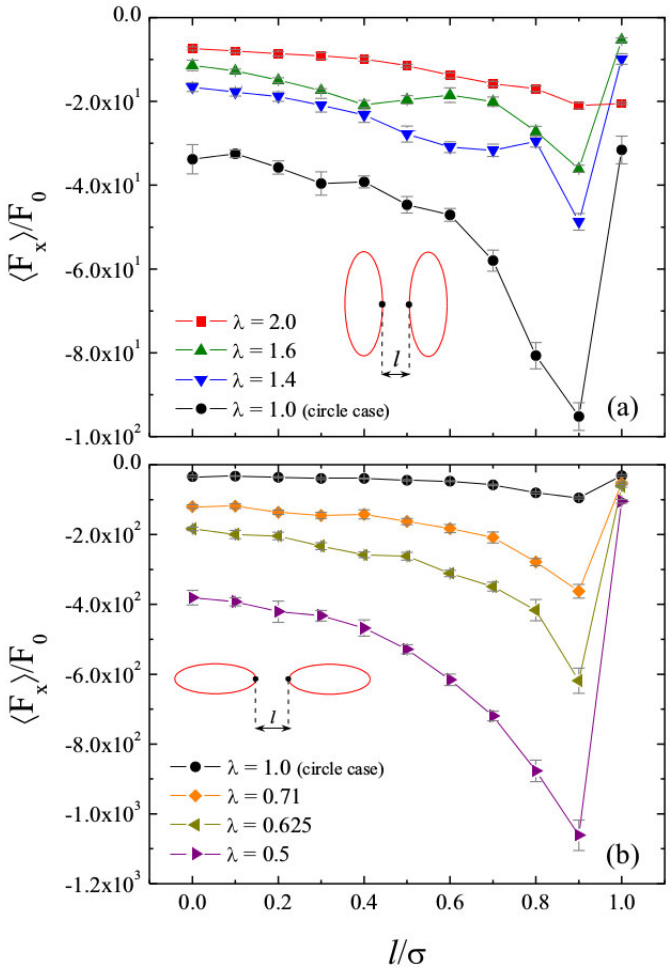

Figure 4.2: The average force $\langle F_x \rangle$ as a function of the distance between the PEC (l), for different values of λ. (a) Vertical PEC ($\lambda > 1$); (b) Horizontal PEC ($\lambda < 1$). In both cases, the area fraction of the active bath is $\phi = 0.1$ and the angular noise is $\eta = 10^{-4}$. The force is calculated on the left PEC. Note that Fig.2(a) and Fig.2(b) have different scales, with $\lambda = 1$ curve plotted in both figures.

approach the diameter of a single SPP. This happens because the SPP becomes able to pass between the obstacles, reducing drastically the pressure on them. It is also interesting to observe that the depletion forces on horizontal PECs are one order of magnitude higher than those on vertical PECs.

In order to complement and have a better understanding of the previous results, the reduced area fraction distribution for $l = 0, 0.5, 0.9$ and $l = 1$ is presented in Fig. 4.3. The concentration of SPP is larger in the region between the PEC compared to the aggregation around them. This creates an unbalance on the SPP concentration between PEC such that induces forces on both PEC in opposite directions. In addition, the concentrations of SPP in cases with $\lambda < 1$ are larger than the ones found in cases with $\lambda > 1$. This is one of the reasons for the difference in magnitude of $\langle F_x \rangle$ as a function of λ observed in Fig. 4.2. In addition, the closer the SPP are from the line joining the center of the PEC, the more intense is the x-component of the depletion force. Figs. 4.3(a), (d), (g), and (j) indicate

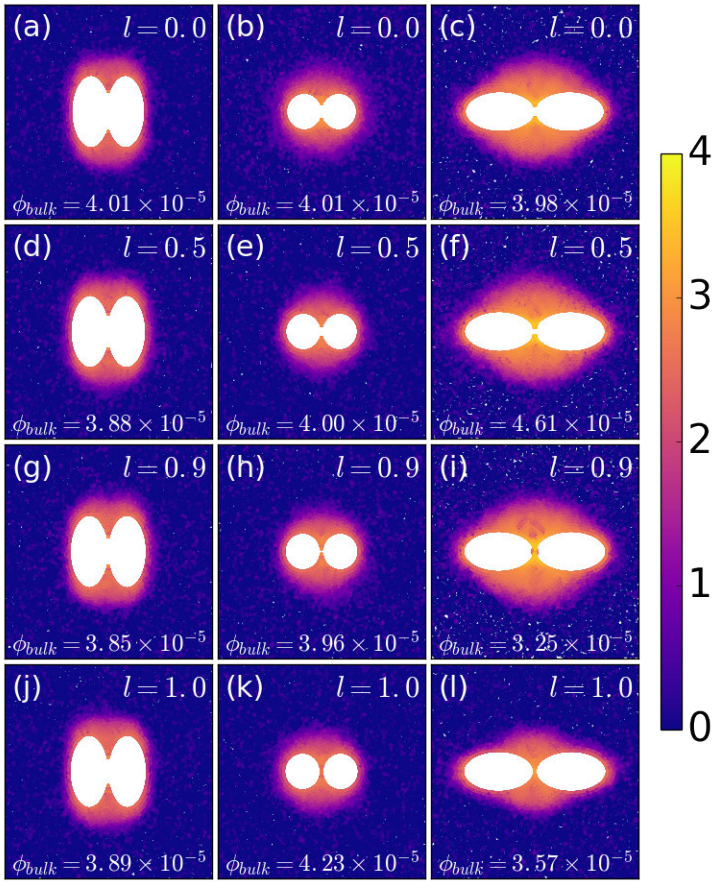

Figure 4.3: The reduced area fraction distribution for $l = 0$ and (a)$\lambda = 2$, (b)$\lambda = 1$, (c)$\lambda = 0.5$, $l = 0.5$ and (d)$\lambda = 2$, (e)$\lambda = 1$, (f)$\lambda = 0.5$, $l = 0.9$ and (g)$\lambda = 2$, (h)$\lambda = 1$, (i)$\lambda = 0.5$ and $l = 1$ and (j)$\lambda = 2$, (k)$\lambda = 1$ and (l)$\lambda = 0.5$, for $\phi = 0.1$. We consider a logarithmic plasma color code.

that the accumulation of SPP around the vertical PEC is higher in the region around $x = 0$, $y \pm a$, while from Figs. 4.3(c), (f), (i), and (l) the aggregation of SPP around horizontal PEC is higher around the point $x = 0$, $y = 0$. Therefore, the distribution of SPP around the PEC indicates that the force exerted by the SPP on vertical PEC, is smaller than that exerted on horizontal PEC.

Regarding the dependence of $\langle F_x \rangle$ on the separation l between the PEC (Fig. 1), we may understand this result qualitatively as follows. When the PEC are at $l = \sigma$, a single particle (we consider it to have very low rotational noise) can fit through them with no overlap, and hence the force is zero. When $l < \sigma$, a particle may still pass between them, but with some overlap (due to the soft-core elastic interaction). Therefore, the repulsive force should increase. This will occur up to a point in which the maximum compression balance the intrinsic force of the SPP, and it gets trapped in between the obstacles. As we lower l, the horizontal (x-axis) projection of the trapping force decreases, for the SPP will be trapped at a point further away in y from the line joining the PECs; therefore, we should expect a lower repulsion for closer l. The active particles get trapped in a similar

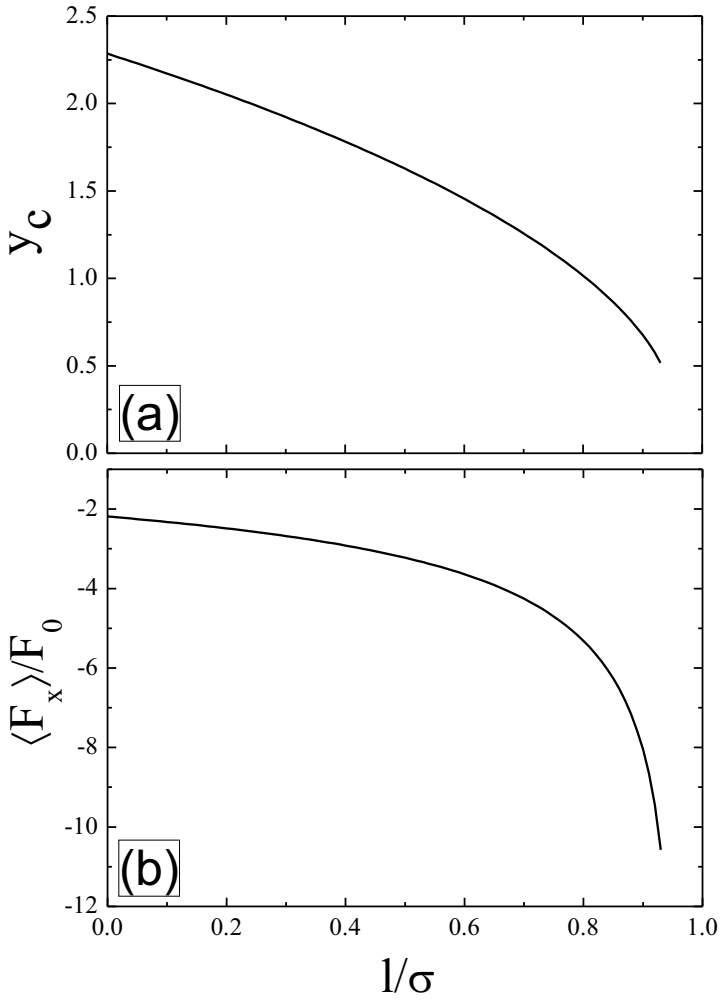

Figure 4.4: (a) Maximum approach distance, y_c, as given by the solution of Eq. (6) and (b) depletion force calculated from the compression of a single particle due to the right PEC.

mechanism as found by Kaiser *et al* [170]. In our case, vertical PEC, because of the more narrow inner space (compared to that of horizontal PEC), accumulates fewer particles than horizontal PEC, which has a larger inner space.

Moreover remember that we considered very low rotational noise ($\eta = 10^{-4}$) and its variation would only change the magnitude of the force (as detailed in Sect. 4.3.3), but not its general dependence on l.

Quantitatively, we can frame this discussion by considering a circular PEC ($\lambda = 1.0$), in which an active particle moves in the direction perpendicular to the line joining the obstacles and through the middle point of such line. When it is compressed by the PEC, it experiences a force with a magnitude of $F = \kappa_{\mathrm{PEC}}(\frac{D+\sigma}{2} - r)$, where D is the circular PEC diameter and $r = \sqrt{(D+l)^2/4 + y^2}$ is the SPP-PEC distance. The vertical force on the active particle due to the compression with the PEC is $F_y = Fy/r$, and, in general, we have $F_y \leq v_0\gamma$. When the equality holds, the particle gets trapped in between the

PEC. Hence, we can calculate the y_i in which this will occur, for a definite l, by solving the following equation:

$$v_0\gamma = \kappa_{\text{PEC}} \left(\frac{D+\sigma}{2} - r \right) \frac{y}{r} \tag{4.6}$$

The repulsive force in each PEC due to this passage of the small particle is simply $F_x = F(D+l)/2r$; then, by calculating y, and r, we can calculate F_x . In Fig. 5.4 we present this force and the corresponding solution to Eq. 4.6, with the parameters used in our simulations. Note that for $l/\sigma > 0.93$, there is no curve because the particle is able to cross the line joining the PEC, resulting that there is no solution to Eq. 4.6. The curve we obtained has the the features of those seen in Fig. 4.2, it has a minimum (maximum force) and decreases up to the point in which the PEC touch each other, and the behavior with l is non-linear. The depletion force evaluated above is lower, compared to the numerical results, by, approximately, one order of magnitude.

These differences between our simulation results and the single particle compression argument we drew are due to the aggregates between the obstacles. This phenomenon will clearly increase the depletion force because more particles will interact with the PEC.

To make sure the results found in Fig. 2 are induced by the active behavior of the SPP, we made simulations switching off the self-propulsion with non-zero translational noise (results not shown). The expected attractive interaction between the colloids in a bath of passive particles is indeed observed for $\lambda = 1$ and $\lambda = 2$. On the other hand, for $\lambda = 0.5$ the depletion force was found to be repulsive, contrary to the well known result of Asakura-Oosawa. The magnitude of this repulsive force is of the order of those we show in Fig. 2(b) ($\langle F_x/F_0 \rangle = -250$ for a thermal noise intersity of 100). We leave the investigation of this result for future work.

4.3.3 Influence of the angular noise η

Recent studies have shown that the noise intensity plays an important role in active matter systems [21, 176]. Therefore it is interesting to consider its influence on the depletion interaction in the present model. We study the noise dependence of $\langle F_x \rangle$ for $\lambda = 0.5$ (horizontal ellipse), $\lambda = 1.0$ (circle) and $\lambda = 2.0$ (vertical ellipse). The area fraction is $\phi = 0.1$. The PEC are placed in contact with each other, i.e., $l = 0$.

The results are presented in Fig. 5.5. In general, the repulsive force vanishes for a large enough noise intensity. As shown previously [176], the dynamics of SSP around rigid obstacles is based on the sliding of the particles over the PEC surface. Large noise intensity results in large fluctuations in the direction of the SPP velocity which allows the SPP to leave the PEC surface, reducing the pressure, and consequently, reducing the repulsive depletion force between the PEC.

We also found that with decreasing η, the magnitude of the force increases much faster

for $\lambda = 0.5$ than in the other two cases. This is a consequence of the mechanism explained in the Sect. 5.3.1. By decreasing the noise intensity large clusters are allowed to form, and these clusters contribute more to the repulsive force in the horizontal case.

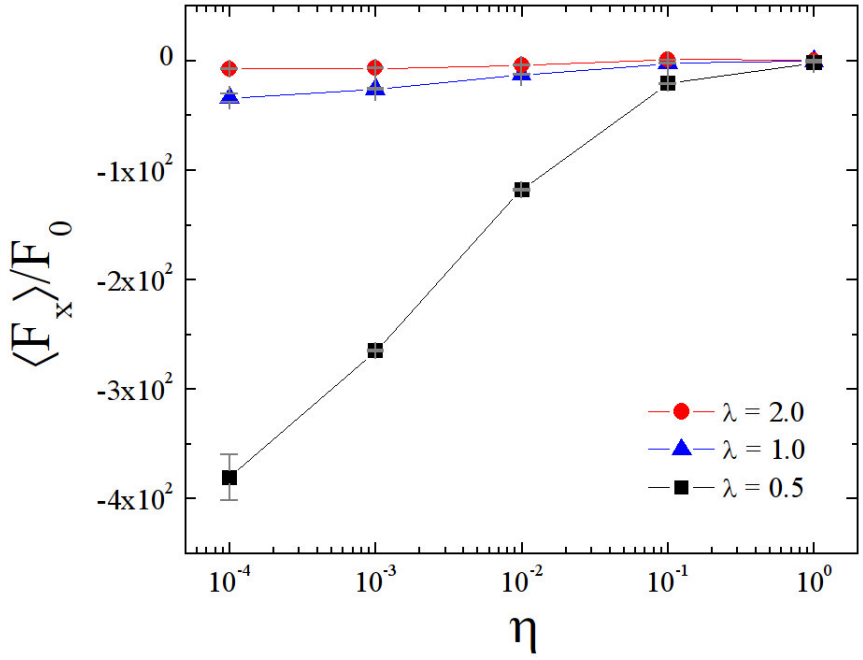

Figure 4.5: The average force $\langle F_x \rangle$ as a function of the noise, η for $\phi = 0.1$. Black squares indicates $\lambda = 0.5$, blue triangles indicates $\lambda = 1.0$ and red circles indicates $\lambda = 2.0$. The obstacles are in contact ($l/\sigma = 0.0$).

4.3.4 Influence of the area fraction

In this section we study the dependence of the average force $\langle F_x \rangle$ on the area fraction ϕ of the active particles. The results, for the same three λ values presented in Sect. 4.3.3, are shown in Fig. 5.6 for the case in which the PEC are in contact ($l/\sigma = 0$). The angular noise is $\eta = 10^{-4}$, which corresponds to the largest magnitude of $\langle F_x \rangle$ for both horizontal and vertical PEC (see Fig. 6). Beyond the difference of one order of magnitude between the force observed in the cases with vertical and horizontal PEC, the resultant interaction presents a clear qualitative distinction with respect to the shape and orientation of the PEC. For horizontal PEC ($\lambda = 0.5$) the depletion force is always repulsive and increases in magnitude with increasing ϕ. On the other hand, for vertical PEC ($\lambda = 2$), the depletion force is repulsive for low ϕ, and becomes attractive for $\phi \gtrsim 0.2$. A similar qualitative behavior seems to be followed by circular PEC ($\lambda = 1$), but we did not found any change from repulsion to attraction in the ϕ-interval considered in our study ($\phi < 0.4$). Our results are different from the ones found by Ni *et al* [200], in which attractive forces are induced in the low density case in a system of hardwall bars in an active bath. In the present system, we observe only repulsive forces in the low area fraction limit.

Qualitatively, our results can be understood by observing how the SPP are distributed around the PEC. In this case, we resort again on the reduced area fraction distribution, presented in Fig. 4.7 for $\lambda = 2.0$, $\lambda = 1.0$, and $\lambda = 0.5$. The shape and orientation of the PEC is important concerning the accumulation of particles around them. It is remarkable that for any ϕ presented in Fig. 4.7 the concentration of SPP around the central region (where the PEC touch each other) is higher in the case of horizontal PEC when compared to the cases of vertical and circular PEC. As a consequence, there is a larger pressure in the central region, explaining the higher repulsive depletion force observed on the horizontal PEC. When the PEC are vertical, the SPP become more spread around the PEC (and less in the central region) as ϕ increases, reducing in this way the pressure in the central region of the PEC and consequently the magnitude of the repulsive force on the PEC. The accumulation of SPP out of the central region between the PEC eventually change the character of the force on the PEC repulsive to attractive.

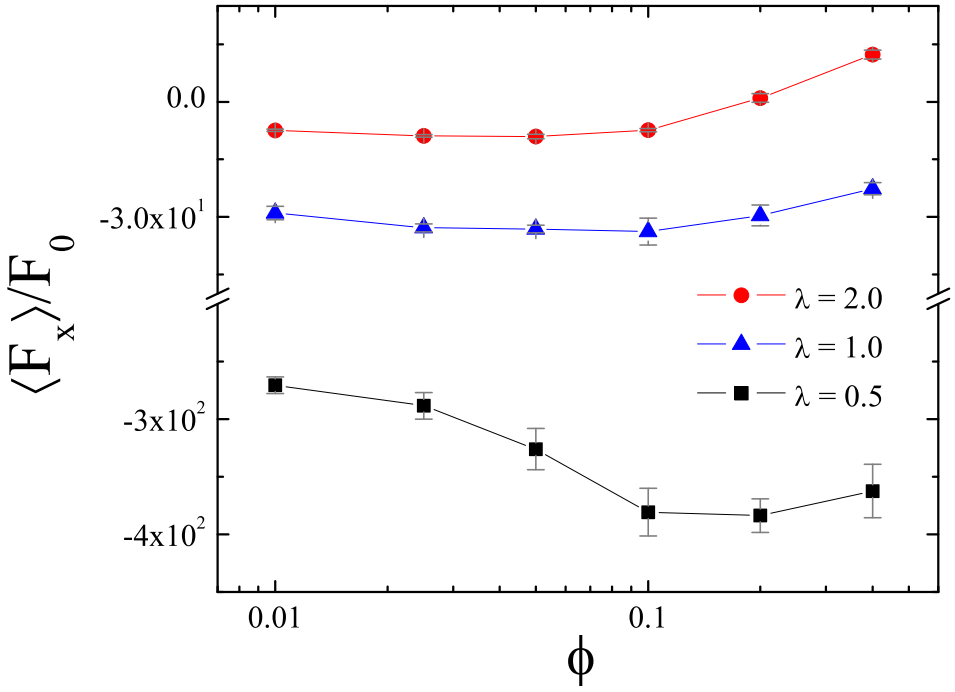

Figure 4.6: The average force $\langle F_x \rangle$ on the left PEC as a function of the area fraction ϕ for $\eta = 10^{-4}$. Black squares indicate $\lambda = 0.5$, blue triangles indicate $\lambda = 1.0$ and red circles indicate $\lambda = 2.0$. The obstacles are in contact ($l/\sigma = 0.0$). For $\lambda = 2.0$ the error bars are smaller than the symbols.

4.3.5 Depletion forces for $l/\sigma > 1$

In this section, the depletion forces are analyzed as a function of separation l between the PEC, but, for $l/\sigma > 1$. The results are shown in Fig. 4.8. For circular PEC ($\lambda = 1$) the depletion forces do not vanish up to $l/\sigma = 2$, differently from the analytical prediction by Asakura and Oosawa considering a bath of passive particles [228]. Null forces were

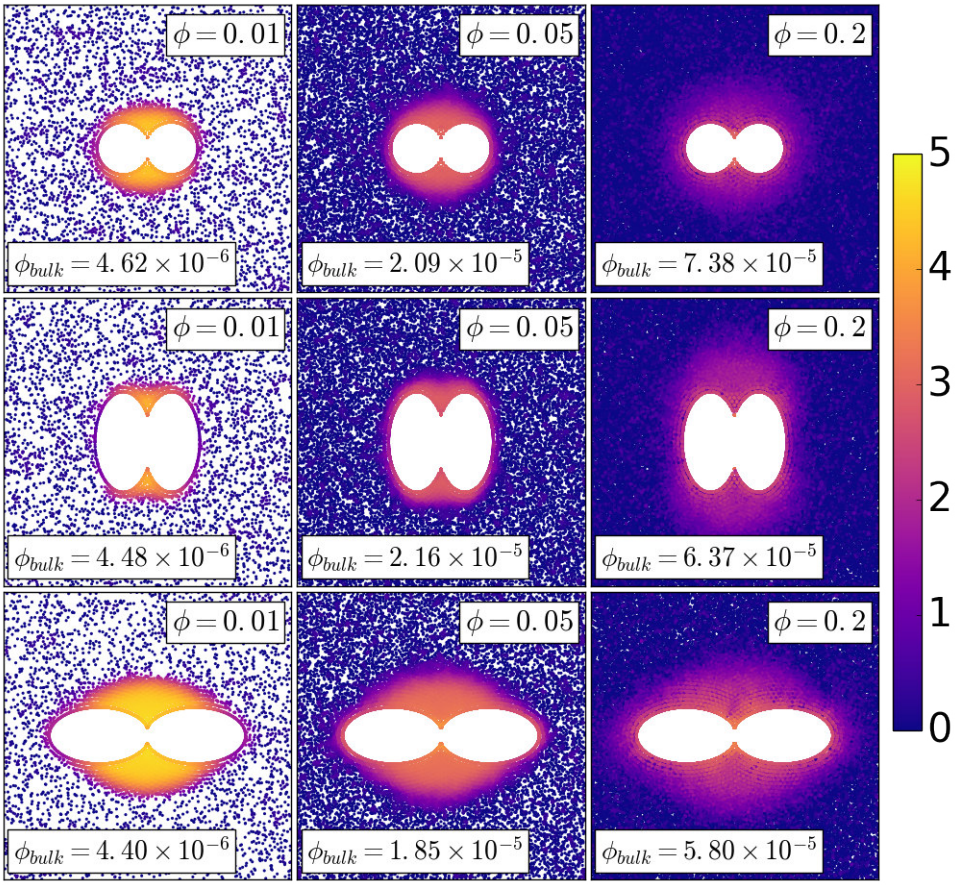

Figure 4.7: The reduced area fraction distributions for different area fractions and $\lambda = 1$ (three top panels), $\lambda = 2$ (three middle panels) and $\lambda = 0.5$ (three bottom panels). The angular noise is $\eta = 10^{-4}$. We consider a logarithmic plasma color code.

observed only for larger distances ($l/\sigma \geq 10$ independent of λ). For the cases shown in Fig. 4.8 $\langle F_x \rangle$ decreases, but falls more rapidly for horizontal PEC. For $\lambda = 0.5$, $\langle F_x \rangle$ takes a longer distance to vanish ($l/\sigma = 10$). In Fig. 5.7, we show the reduced area fraction distribution for $\lambda = 2$, $\lambda = 1$ and $\lambda = 0.5$, and $l/\sigma = 0$ and 5. For $\lambda = 2$ and $\lambda = 1$, each PEC has its own cluster, while for $\lambda = 0.5$, there is only one cluster for both PEC, rendering a non-vanishing repulsion at such large distances. It is also important to note that in all three cases as distance l/σ increases, depletion forces raises with an exponential behaviour $\langle F_x \rangle / F_0 \propto -\exp^{-l/\xi}$, where ξ can be understood as the range of the force, in agreement with previous works [198, 199, 200].

4.3.6 Depletion forces for vertical-horizontal PECs

In the previous sections, we showed that forces on horizontal and vertical PECs behave differently as functions of λ, ϕ and l. In this section we provide an analysis of the mean depletion forces between PECs, where the left one is vertical and the right one is horizontal. We study the cases where the vertical PEC have $\lambda = 1.4, 1.6, 2.0$ and the

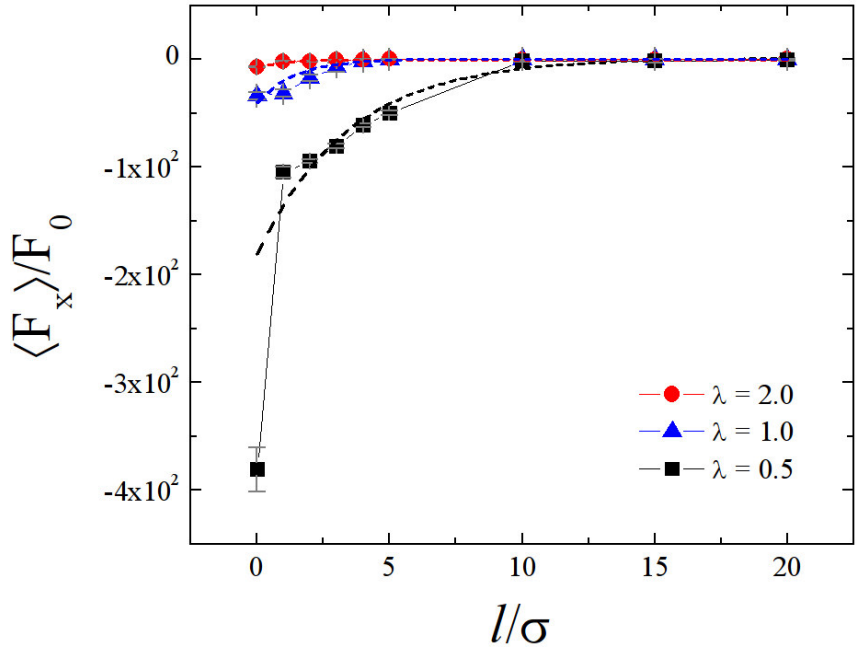

Figure 4.8: The average force $\langle F_x \rangle$ as a function of the distance l/σ for $\phi = 0.1$ and $\eta = 10^{-4}$. Black squares indicates $\lambda = 0.5$, blue triangles indicates $\lambda = 1.0$ and red circles indicates $\lambda = 2.0$. Dashed curves are the exponential fit for $\lambda = 2$ (red) where $\xi \approx 0.89$, $\lambda = 1$ (blue) where $\xi \approx 1.39$ and $\lambda = 0.5$ where $\xi \approx 3.45$ (black).

horizontal PEC have $\lambda = 0.714, 0.625, 0.5$, respectively, such as the product of vertical and horizontal λ is always equal to 1. The depletion force as a function of l/σ (varying from 0 to 1) is shown in Fig. 5.8. The results are qualitatively similar to those observed previously when the obstacles are both horizontal or vertical (Fig. 4.2), i.e, there is a strong increase in magnitude of the repulsive force right below $l = 1.0$, and a subsequent decrease of this magnitude as we bring the PECs closer to each other. The main difference between Figs. 4.2 and 5.8 is that the absolute value of the force in Fig. 5.8 is between the values of those curves in Fig. 4.2 for PECs at the same λ; although they are closer to those values observed for horizontal PEC in Fig. 4.2. Moreover, we found that the force is the same on both PECs.

We should expect that this should occur because none of the ellipses break the symmetry of the system, i.e., there is no induced motion (as would happen if one of those happened to be a half-ellipse). Therefore, the force is equal in both obstacles. Also, the magnitude of this force comes from the aggregate of SPP in between the PECs; now, as we saw in Figs. 4.3, 4.7, and 5.7, this aggregate depends on the shape of the PEC, but as we bring them closer, they merge and form a single structure, exerting the same force in both PECs. From this, we will have an aggregate formed from the cluster of the vertical and the horizontal PEC; and it will be smaller (larger) than between two horizontal (vertical) PEC, and will yield a weaker (stronger) repulsive force.

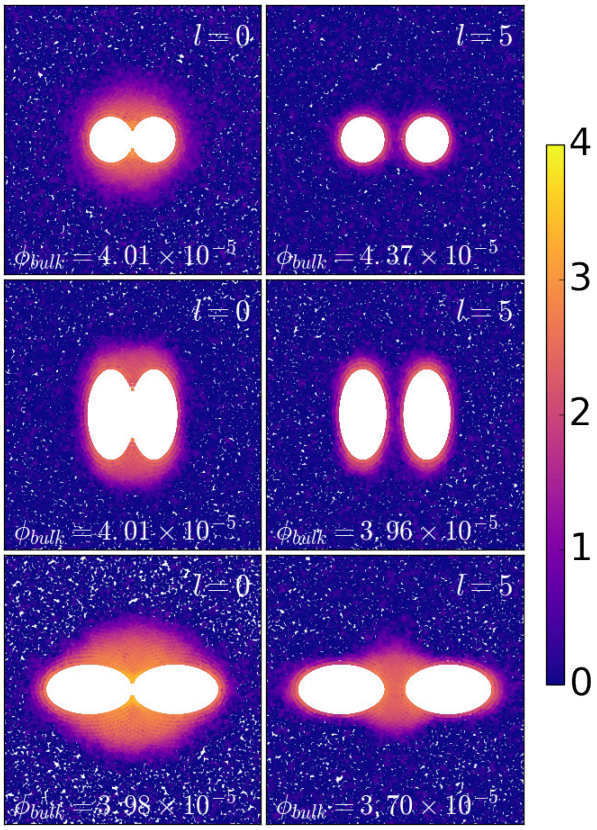

Figure 4.9: The reduced area fraction distribution for different distances between the PEC. The area fraction of the SPP is the same for all the presented cases ($\phi = 0.1$). The passive colloids in the top panels have the parameter $\lambda = 1$. The passive colloids in the middle panels have the parameter $\lambda = 2$, and the passive colloids in the bottom panels have the parameter $\lambda = 0.5$. We consider a logarithmic plasma color code.

4.4 Appendix A

The contact SPP-PEC can be modeled as follows: in order to write the overlap, α, as a function of SPP coordinates, we consider that SPP interacts with a new PEC (PEC') such that its semi-axis are $\sigma/2$ bigger than the original one. So $\alpha = r_{ij}^{(1')} + r_{ij}^{(2')} - 2z'$, where $z' = a'$ for horizontal PEC' and $z' = b'$ for vertical PEC'. Apostrophe ($'$) means the PEC' variables. Equation for $r_{ij}^{(1')}$ and $r_{ij}^{(2')}$ can be written as

$$r_{ij}^{(1')} = \sqrt{(x_i - x'_{f1})^2 + (y_i - y'_{f1})^2} \tag{4.7}$$

$$r_{ij}^{(2')} = \sqrt{(x_i - x'_{f2})^2 + (y_i - y'_{f2})^2} \tag{4.8}$$

where x_i and y_i are SPP coordinates, x_j and y_j are PEC coordinates and x'_{f1} and x'_{f2} are PEC' focus coordinates.

Supposing, at first, a horizontal PEC placed on x-axis, it is important to note that, in this case:
(i) ellipse focus coordinates are $(-e'a', 0)$ and $(e'a', 0)$ (focus 1 and 2, respectively), where

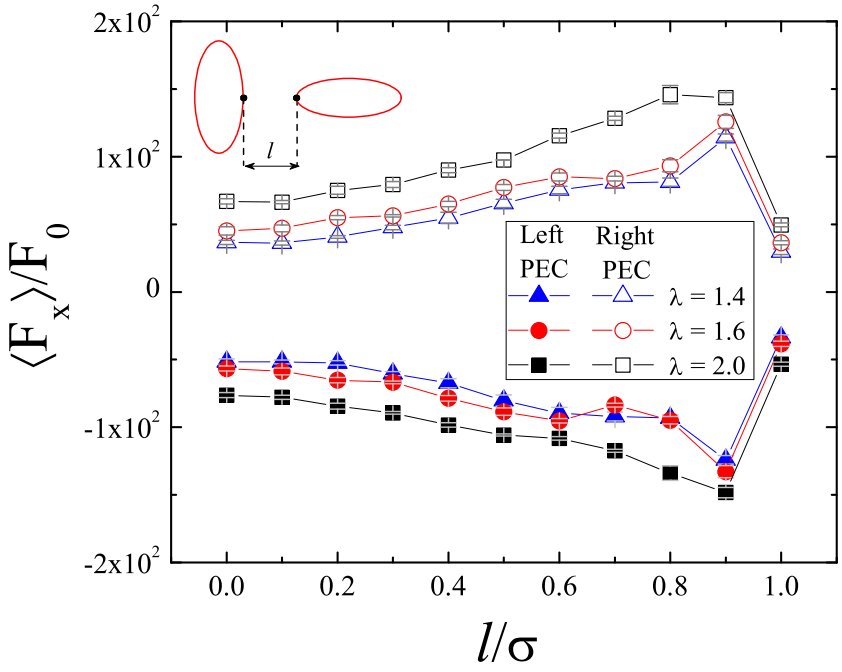

Figure 4.10: Average force $\langle F_x \rangle$ as a function of the distance l/σ for $\phi = 0.1$ and $\eta = 10^{-4}$. $\langle F_x \rangle$ on the left PEC is described by full symbols, while for the right PEC, $\langle F_x \rangle$ are described by empty symbols. Black squares indicates $\lambda = 0.5$, blue triangles indicates $\lambda = 1.0$ and red circles indicates $\lambda = 2.0$.

e' is the eccentricity of PEC'
(ii) $e' = \sqrt{a'^2 - b'^2}/a'$, then $x_{f1} = x_j - \sqrt{(a'^2 - b'^2)}$ and $x_{f2} = x_j + \sqrt{(a'^2 - b'^2)}$ and
(iii) $a^{'} = a + \frac{\sigma}{2}$ and $b^{'} = b + \frac{\sigma}{2}$, so that equations (7) and (8) can be rewritten as

$$r_{ij}^{(1)} = \sqrt{\left(x_i - \left(x_j - \sqrt{\left(a + \frac{\sigma}{2}\right)^2 - \left(b + \frac{\sigma}{2}\right)^2}\right)\right)^2 + y_i^2} \tag{4.9}$$

$$r_{ij}^{(2)} = \sqrt{\left(x_i - \left(x_j + \sqrt{\left(a + \frac{\sigma}{2}\right)^2 - \left(b + \frac{\sigma}{2}\right)^2}\right)\right)^2 + y_i^2} \tag{4.10}$$

If PEC are vertical, ellipse focus coordinates are $(0, -e'a')$ and $(0, e'a')$ and then

$$r_{ij}^{(1)} = \sqrt{x_i^2 + \left(y_i + \sqrt{\left(a + \frac{\sigma}{2}\right)^2 - \left(b + \frac{\sigma}{2}\right)^2}\right)^2} \tag{4.11}$$

$$r_{ij}^{(2)} = \sqrt{x_i^2 + \left(y_i - \sqrt{\left(a + \frac{\sigma}{2}\right)^2 - \left(b + \frac{\sigma}{2}\right)^2}\right)^2} \tag{4.12}$$

5 Depletion forces for different passive objects geometry in a bath of passive particles

5.1 Motivation

When colloidal particles are immersed in a bath of passive particles an attractive depletion force arises between the colloidal particles [194, 228, 249, 250]. This force arises due to the superposition of the excluded volume around the suspended particles, increasing the volume accessible to the particles of the medium, and therefore increasing the entropy of the system. This phenomenon has been studied considerably over the last years through theory of perturbation [191, 251], DFT [252, 253] as well as mean field calculations [254]. A plenty of applications can be mentioned such as its influence on the stability of colloidal suspensions [255, 256, 257, 258, 259], direct self-assembly [260, 261, 262, 263, 264, 265], nonadsorbing polymer solutions [257, 266], phase behavior [267, 268, 269, 270, 271, 272, 273] and biological systems [274, 275].

In 1954, Asakura and Oosawa showed how the depletion forces acts on a system of (i) two-parallel and large plates and (ii) two spherical bodies in a solution of rigid spherical macromolecules, obtaining that for both cases depletion forces induce attraction between the suspended particles [228]. Recently, many works highlighted how the shape of the passive objects can be influential on the depletion force, but considering that the suspended particles are in a bath of active particles. E.g., Ray *et al.* examined different passive object geometries and found regimes in which there is a crossover from attraction to repulsion between the walls as a function of the wall separation and wall length [198]. Harder *et al.* found that colloidal disks feel a repulsive force that is short-ranged in nature and grows in strength with the size ratio between the colloids and active depletants [199]. Ni *et al.* found that the effective force between two hard walls can be tuned from a long range repulsion into a long range attraction by changing the density of active particles [200]. Similar results were also found by Leite *et al.* which showed that a bath of active particles can induce repulsive or attractive depletion forces, depending on the shape of the passive objects, their relative orientation with respect to each other and density of

the active particles in the bath [276]. It is also important to emphasize that experimental studies have already shown that for a bath of passive colloidal particles, the shape of the passive objects also contribute significantly to changes in depletion forces [201].

In this chapter we analyze via molecular dynamics simulations a two-dimensional (2D) system composed of two big passive particles (objects) immersed in a bath of $N = 2000$ smaller passive particles (solvent), for different temperatures. Depletion forces were analyzed for three different shapes of the big particles: horizontal ellipses, semi-circles and triangles, which were not yet studied in the current literature. Different from what is predicted by the Asakura and Oosawa model, the depletion force between particles suspended in a thermal bath is not always attractive. According to our simulations, in the cases of triangular and elliptical objects we observed only repulsion between the objects. Next we explore how the depletion force is influenced by the size of the passive objects, the area fraction of the medium and the angular variation of the triangular passive objects. Depletion forces were also studied for semi-circular objects in function of the distance L between then.

In Sect. 5.2 we introduce the model system and define the key quantities used to characterize the system. In Sect. 5.3, we present and discuss the numerical results.

5.2 Model System

5.2.1 Details of the numerical simulations

Our system consists of two fixed passive objects passive objects, which we will call henceforth as fixed passive objects (FO) in a 2D bath of $N = 2000$ particles (BP). The particles constituting the bath are modeled as soft disks of diameter σ which interact with each other and with the passive objects through spring-like forces of stiffness κ_{BP} and κ_{FO}, respectively, with $\kappa_{\mathrm{FO}} \gg \kappa_{\mathrm{BP}}$. Bath particles are subject to random fluctuations in translational degree of freedom, proportional to the white noise ξ, such that $\langle \xi_i(t) \rangle = 0$ and $\langle \xi_i(t)\xi_j(t') \rangle = 2\xi\delta_{ij}\delta(t - t')$, where ξ is proportional to the temperature. Therefore the equations of motion for the ith bath particle can be written as

$$\frac{\partial \vec{r}_i}{\partial t} = \mu \vec{F}_i + \vec{\xi}_i(t) \tag{5.1}$$

where μ is the BP motility, $\mathbf{F_i} = \sum_{\mathbf{j}} \mathbf{F_{ij}}$ is the total force on particle i due to others bath particles $j's$ (the sum is over $j \neq i$ and FO). $\mathbf{F}_{ij} = -\kappa\alpha_{ij}\hat{\mathbf{r}}_{ij}$ if $\alpha_{ij} > 0$, where $\alpha_{ij} = \frac{1}{2}(d_i + d_j) - r_{ij}$ is the overlap distance between BP i and pbject (BP or FO) j. Note that $d_i = \sigma$ and $d_j = \sigma$ for BP-BP contact. In the case of BP-FO contact α_{ij} assume a specific value which depends on the shape of the FO (see details in 5.3). If $\alpha_{ij} < 0$ (particles not in contact), then $\mathbf{F_{ij}} = \mathbf{0}$. x_i and y_i are the coordinates of the ith BP, and x_j is the coordinate of the jth FO. The FO are assumed to be always along the x-axis

($y_j = 0$).

In all simulations we employed periodic boundary conditions in both $x-$ and $y-$directions. The equations of motion are integrated using a second order stochastic Runge-Kutta algorithm [247], as described in details in chapter 3. Lengths are given in units of σ, and the unit of force F_0 is such that $\kappa_{\rm BP} = \tilde{\kappa}(\sigma/F_0)$ where $\tilde{\kappa}$ has units of force per distance. The unit of time is $t_0 = \sigma/\mu F_0$. Henceforth, all quantities are dimensionless, unless stated otherwise. We consider $\kappa_{BP} = 50$, $\kappa_{FO} = 1000$ and $\mu = 1$. The equations of motion are integrated using a time step $\Delta t = 10^{-3}$. In all simulations, we run 5×10^6 thermalisation time steps and calculated averages over $5 - 15 \times 10^6$ time steps.

5.2.2 Passive elliptical objects

In the case of elliptical passive objects, we consider α_{ij} in the BP-FO interaction as $\alpha_{ij} = R_{ij} - 2a$, where a is the horizontal semi-major axis and $R_{ij} = r_{ij}^{(1)} + r_{ij}^{(2)}$, where $r_{ij}^{(1)}$ ($r_{ij}^{(2)}$) is the distance between the ith BP and the first (second) focus of the jth ellipse (Fig. 5.1) and given by

$$r_{ij}^{(1)} = \sqrt{\left(x_i - \left(x_j - \sqrt{\left(a + \frac{\sigma}{2}\right)^2 - \left(b + \frac{\sigma}{2}\right)^2}\right)\right)^2 + y_i^2}, \tag{5.2}$$

$$r_{ij}^{(2)} = \sqrt{\left(x_i - \left(x_j + \sqrt{\left(a + \frac{\sigma}{2}\right)^2 - \left(b + \frac{\sigma}{2}\right)^2}\right)\right)^2 + y_i^2}. \tag{5.3}$$

where b (smaller) is the vertical semi-minor axis. This is exactly the same equation of the previous work (Eq.(4.2) and Eq.(4.3)) and it is explained in details on section 4.4.

It is convenient to define a dimensionless parameter $\lambda = a/b$. We always consider the vertical axis of the FO equal to 5.

5.2.3 Passive semi-circular objects

For interaction between BP and the circular surface of the FO, we set $\alpha_{ij} = \sigma_i + \sigma_j - r_{ij}$ as the overlap distance between BP i and FO j, where σ_j is the diameter of FO, and r_{ij} is the distance between i and j and can be written as

$$r_{ij} = \sqrt{(x_i - x_j)^2 + y_i^2} \tag{5.4}$$

with $\mathbf{r_{ij}}$ pointing from j to i. For interaction between BP and the flat surface of the passive object, we set $\alpha_{ij} = \sigma_i - r_{ij}$, where r_{ij} is given by $r_{ij} = |x_i - x_j|$ (Fig. 5.2).

5.2.4 Passive triangular objects

For interaction between BP and FO being triangular passive objects, we consider three situations: (i) if BP interact with the inner canned surface of the passive object, we set

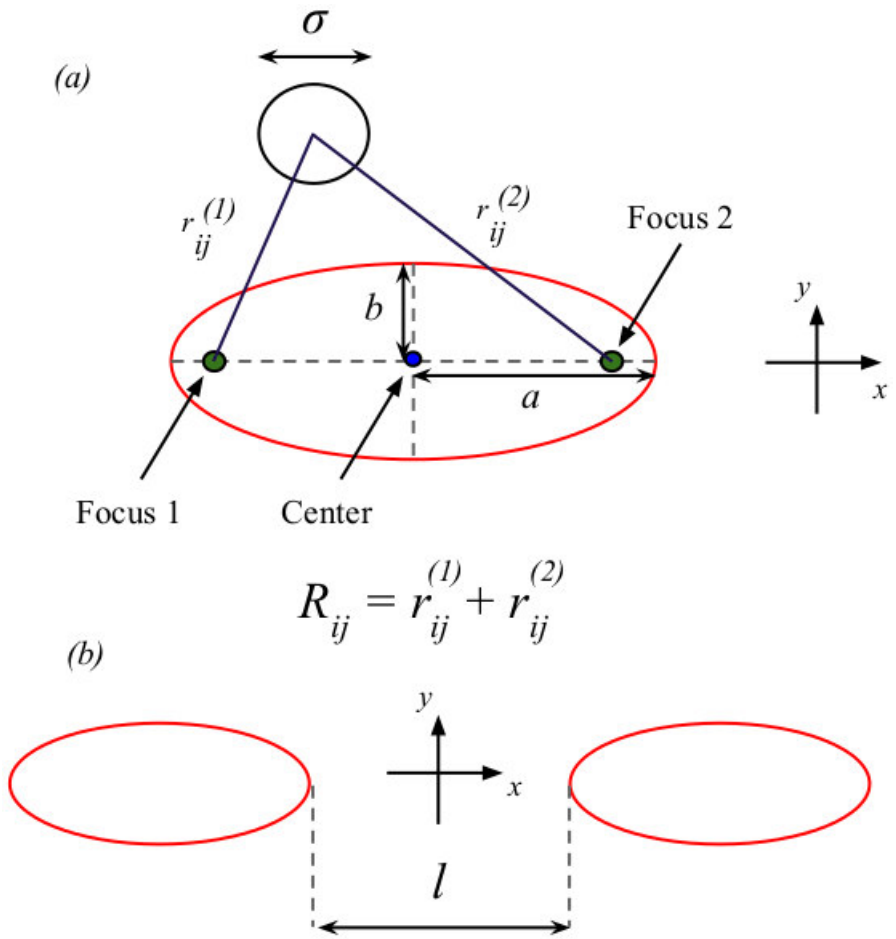

Figure 5.1: (a) Schematic representation of elliptical model system. The black circle represents the BP of diameter σ and red ellipse represents the passive object. $r_{ij}^{(1)}$ ($r_{ij}^{(2)}$) is the distance between the BP and the Focus 1 (Focus 2) of the passive object. a is the size of the horizontal semi-axis and b is the size of the vertical semi-axis. (b) indication of the distance l between the closest points of the passive elliptical colloids.

α_{ij} as

$$\alpha_{ij} = |x_i + k\frac{\sigma}{2}\cos\phi|\sin\phi - |y_i + k'\frac{\sigma}{2}\sin\phi|\cos\phi \tag{5.5}$$

where ϕ is the angle between the y-axis and the 45^o surface line of the passive object, $k = 1(-1)$ if $x_i > 0(< 0)$, and $k' = 1(-1)$ if $y_i < 0(> 0)$. (ii) If BP interact with the outer surface of the passive object, then $\alpha_{ij} = |a + \sigma| - |x_i|$. a is the height of the triangular passive object considering the distance from the vertex that have zero y coordinate, and ϕ is the angle between y semi-axis and the inner flat surface which cross the origin (see Fig. 5.3); and (iii) if BP interact with the corner of the outer surface, then we have that the total force felt by the BP is a combination of (i) and (ii), taking into account the projections of both forces.

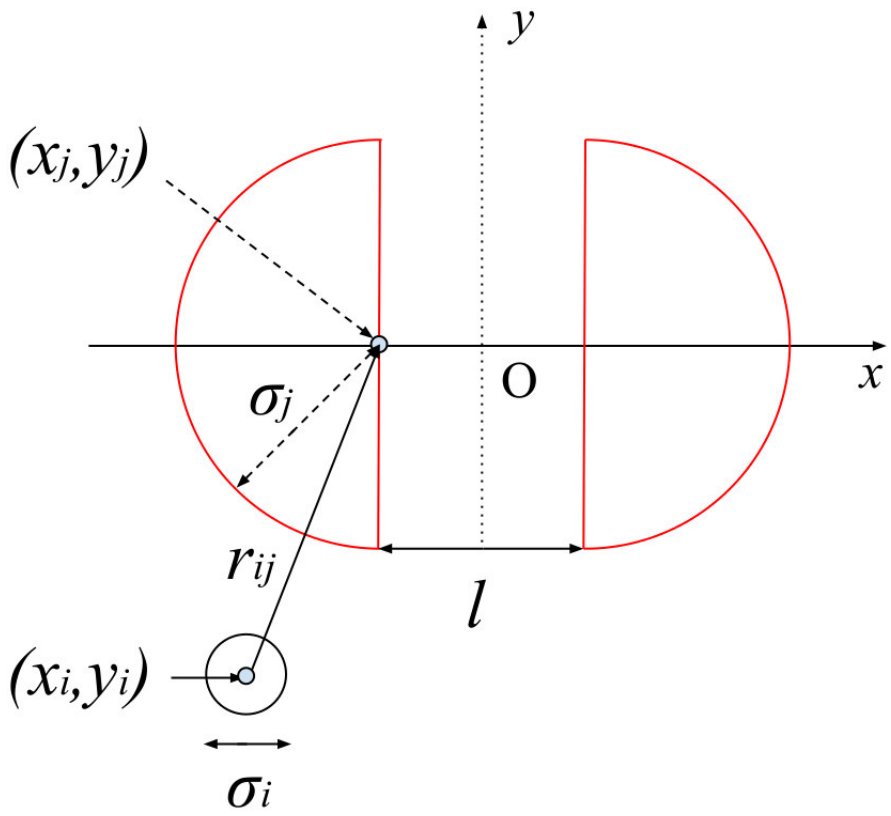

Figure 5.2: (a) Schematic representation of semi-circular model system. (b) The black circle represents the BP diameter σ_i and the red semi-circumferences represents the passive objects. r_{ij} is the distance between BP and FO center. l is the distance between the flat surfaces of the semi-circumferences and σ_j is the radius of the semi-circumference.

5.2.5 Interaction between fixed passive objects

We are interested in the depletion force between FOs in a bath of passive particles subjected only to the thermal fluctuation. We proceed in this way by considering the two FO at fixed separation and by calculating their interaction with the BP. Specifically, we calculate the average force $\langle F_x \rangle$, along the x-direction, exerted on the left passive object by the BP.

As defined in the previous chapter, we will once more consider the area fraction ρ, $\rho = \frac{N\pi}{4(L^2 - S_T)}$, where N is the number of BP, L is the size of the 2D squared simulation box and S_T is the total area occupied by the FO. Note that ρ is related to the density n of BP, i.e. $\rho = \pi n/4$, where n is the BP density.

In order to present how the BP are distributed over the simulation box over time, it is convenient to consider the reduced area fraction distribution, defined as $log_{10}[\rho_i/\rho_{bulk}]$, where ρ_i is the time average area fraction in the i-th sub-box (the total simulation box is split in small sub-boxes) and ρ_{bulk} is the time average area fraction calculated far from the FO. ρ_{bulk} is the average area fraction of the four sub-box located in the corners of the simulation box, which are far enough from the FO in order to "feel" their presence. The

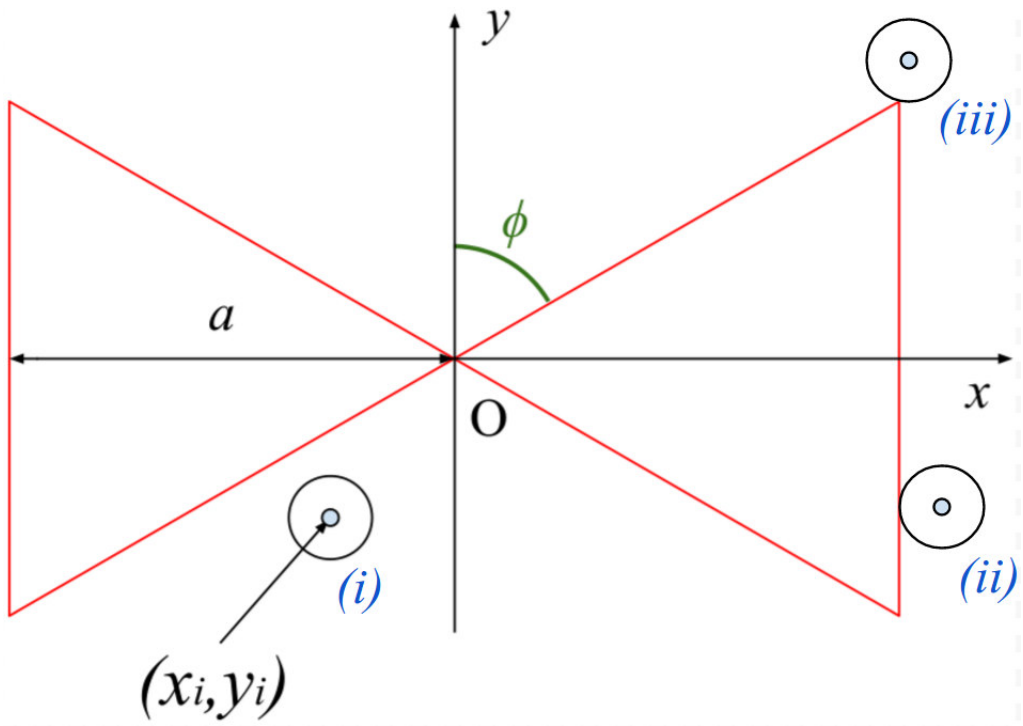

Figure 5.3: Schematic representation of the triangular passive fixed objects (FO). The circle represents the BP of diameter σ and red triangles represent the passive objects. ϕ is the angle between the inner flat surface of the FO and the y-axis. a is the height of the triangular passive object, and (x_i, y_i) are the coordinates of the center of the BP with index i.

reduced area fraction was defined in chapter 4.

5.3 Results and Discussions

5.3.1 Influence of the shape of the passive objects

In this section we analyze the influence of the shape of the FO on the depletion interaction and how such an interaction depends on the temperature. The area fraction is kept constant, with value $\rho = 0.4$. The average force $\langle F_x \rangle$ on the left FO is analyzed as a function of temperature for two different shapes of the passive objects: elliptical and triangular. The results are shown in Fig. 5.4. As can be observed, the average depletion force exhibits negative values in both cases. Our results confirm that the attractive interaction predicted in the Asakura-Oosawa analytical model is not general. Indeed, as pointed out by Dickman *et al.* Therefore, the results shown on Fig. 5.4 allow us to conclude that the resultant direction of depletion forces is sensitive to the shape of the interacting objects and that the results from the Asakura-Oosawa can not be seen as a general rule [191, 192]. A second observation is that the triangular passive objects have

$\langle F_x \rangle$ more intense than the elliptical one. In order to explain such a result, we resort on the distribution density of the BP for three different temperatures ($T = 0.001$, $T = 0.1$ and $T = 10$). The results are shown in Fig. 5.5. We note that although the density distributions lower concentrations around the FO as the temperature is increased, the repulsion between particles increases. This result can be explained by considering that the collisions between BF and FO are more frequent and stronger as temperature is increased; and (ii) elliptical passive object have larger concentrations and lower depletion forces. This leads us to conclude that the main influence on the average forces for different shapes lies on geometric contact between BP and FO more than the BP concentration between passive objects. It is also important to note that as temperature increases depletion forces also increases its magnitude. That is the reason which explain that for triangular passive objects the depletion forces have similar concentrations but induces strongly different intensities.

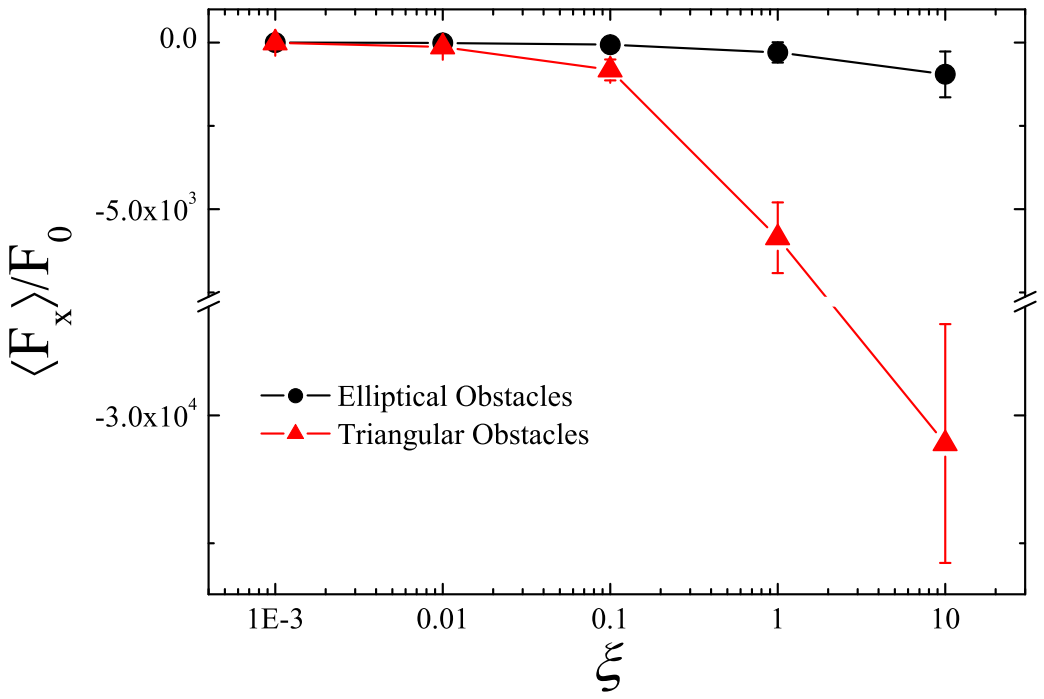

Figure 5.4: The average force $\langle F_x \rangle$ as a function of the temperature ξ for two different shapes of passive objects: (i) ellipsoidal (full black) and (ii) triangular (red). Note that there is a break point ranging from ≈ -8000 to ≈ -28000. The area fraction is $\rho = 0.4$.

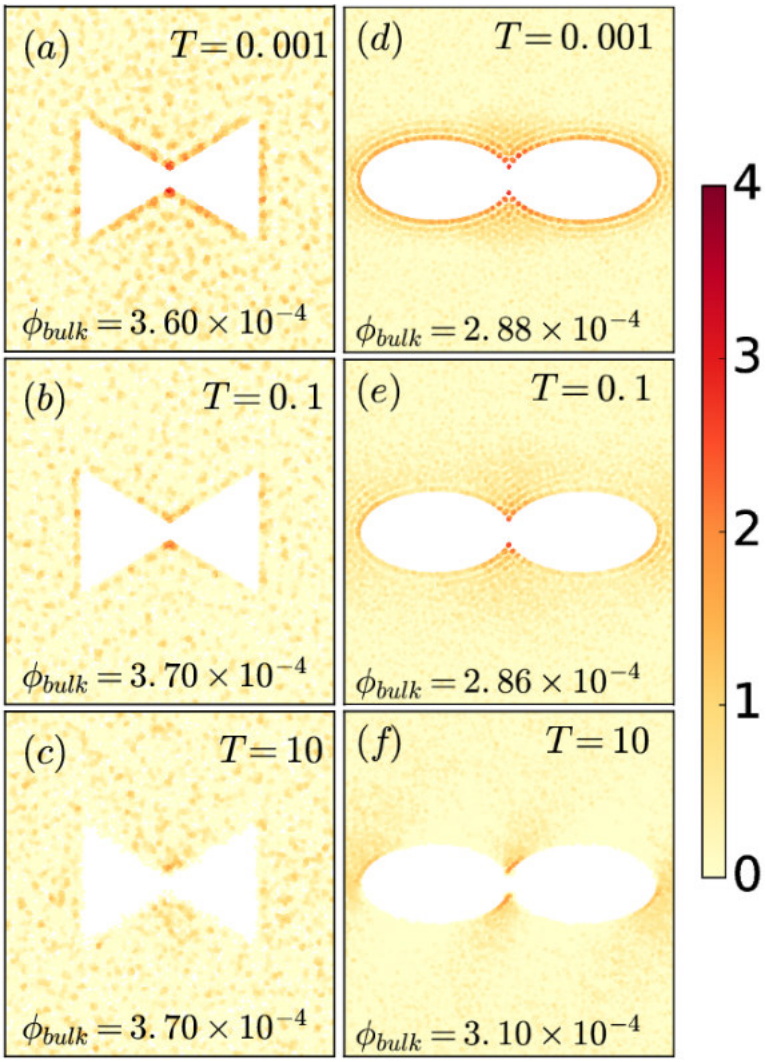

Figure 5.5: Distribution density for two different passive FO. (a-c): triangular and (d-f): elliptical. The area fraction is $\rho = 0.4$.

5.3.2 Influence of the area fraction ρ

In this section we study the dependence of the average force $\langle F_x \rangle$ on the area fraction ρ of the particles. Qualitatively the results are the same for the two shapes presented in Sec. 5.3.1 and are shown in Figs. 5.6.

Fig. 5.6 show that increasing the area fraction implies in increase depletion forces also. Once again, two orders of magnitude on $\langle F_x \rangle$ is observed between the two cases considered. This happens because when area fraction increases, the number of particles on the inner side of passive objects also increases, and hence the BP-FO collisions occur more frequently, for both cases. In other words, increasing area fraction means enhance the difference between inner and outer collisions, inducing depletion forces to increase its intensity, i.e., increase a repulsive behavior.

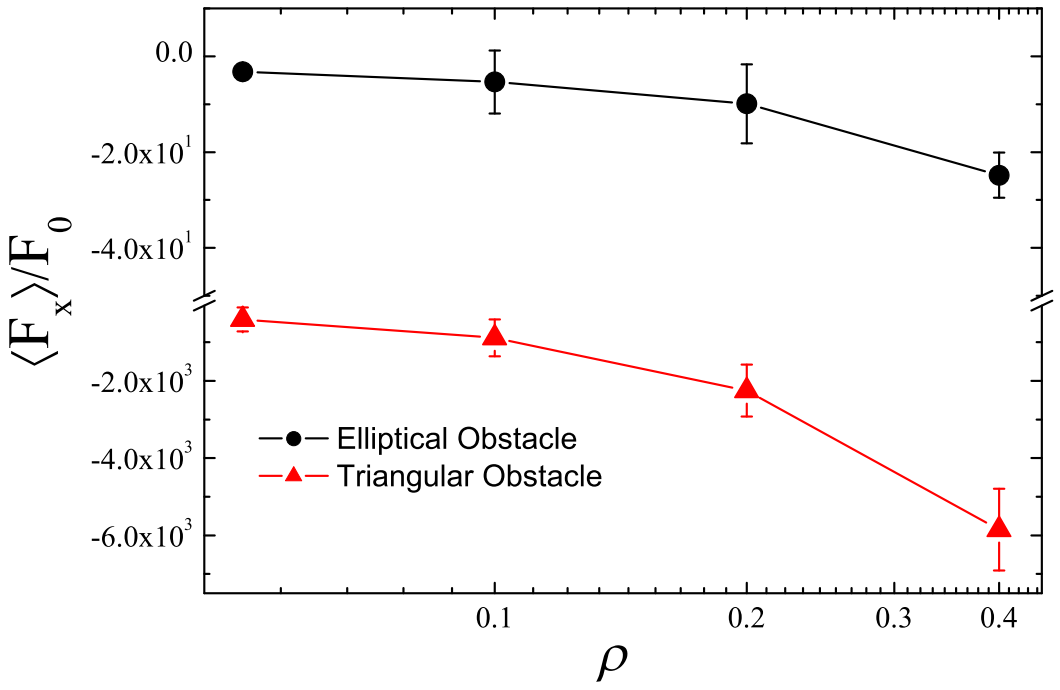

Figure 5.6: The average force $\langle F_x \rangle$ for elliptical (black) and triangular (red) passive FO as a function of the area fraction. The temperature is $\xi = 1$.

5.3.3 Influence of the size

Influence of the size of the FO are studied in this section as a function of temperature ξ, for the two different passive objects shape and simulation results are shown on Fig. 5.7 and 5.8.

For both cases negative repulsive forces still present and are sensitive to temperature, becoming greater as temperature increases. For the elliptical shape, we found that as the ellipse grows thicker, the depletion force is smaller. This can be explained by the fact that thicker ellipses holds more particles in its inner contact region than thinner ellipses, increasing number of collisions and therefore depletion force intensity. As temperature increases, depletion forces increases its intensity for all three values of λ, similar to triangular shape passive objects results.

When triangular passive object shape are investigated, we note that depletion forces for big passive objects are more intense that for small passive objects, i.e., as σ increases, also increases the repulsion induced by the bath. The explanation for that is that when FO are smaller, the number of particles in contact on the inner side of the FO is almost the same for the outer part. As the FO gets bigger then the number of particles on the inner side of the FO becomes greater than the number of particles on the outer side of the FO, induing more repulsion between passive objects.

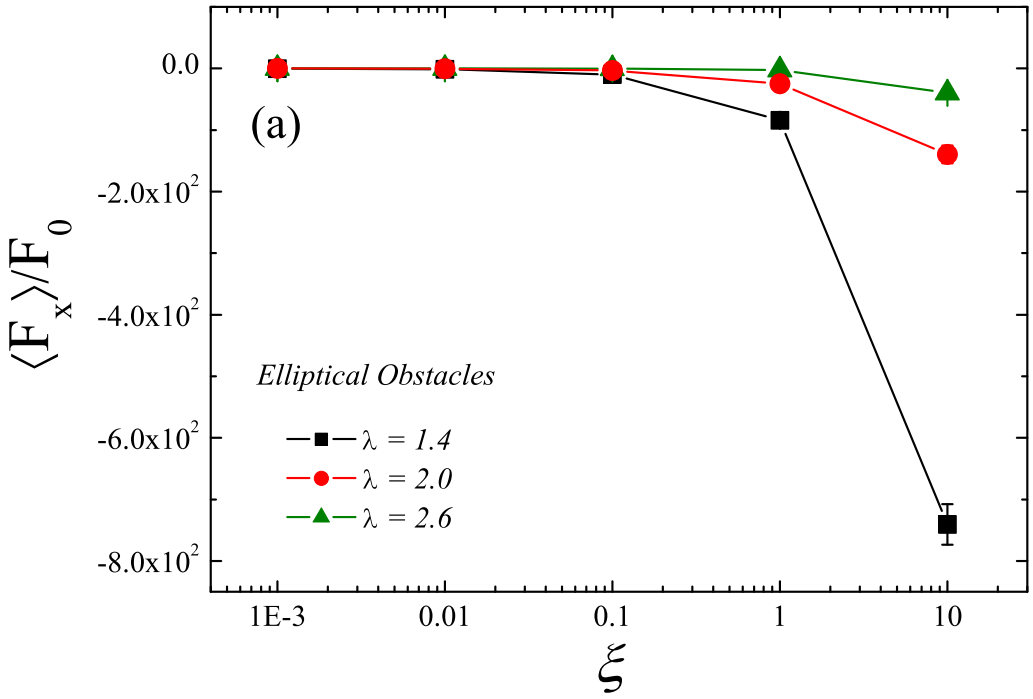

Figure 5.7: The average force $\langle F_x \rangle$ for elliptical passive objects as a function of three different λ: 1.4, 2.0 and 2.6. The area fraction is $\rho = 0.4$.

5.3.4 Influence of the angle ϕ on triangular passive objects

In this section we explore the influence of the angle between the inner flat surfaces of the triangular passive objects on the depletion forces, and its sensitivity to temperature variation. Results are plotted on Fig. 5.9.

Our simulations shown that for $\phi = 60^o$ and $\phi = 75^o$ the average force is repulsive, while for $\phi = 30^o$ and $\phi = 45^o$, the average force is attractive. This happens because as the angle ϕ increases, more particles are allowed to stay in the inner region of FO. This observation lead to conclude that the angle ϕ is a parameter of controlling attraction/repulsion between suspended particles. Another conclusion is that small differences in passive objects shape can lead to huge differences on the resultant force. For example, on Fig. 5.10 it is clear that just by opening the passive object in 15^o, $\langle F_x \rangle / F_0$ varies $\approx 10^4$, for $T = 10$. Another interesting fact is that in our system there is also an optimal angle near $\phi = 45^o$ in which equilibrates BPs and FOs contributions and induces a null resultant average force.

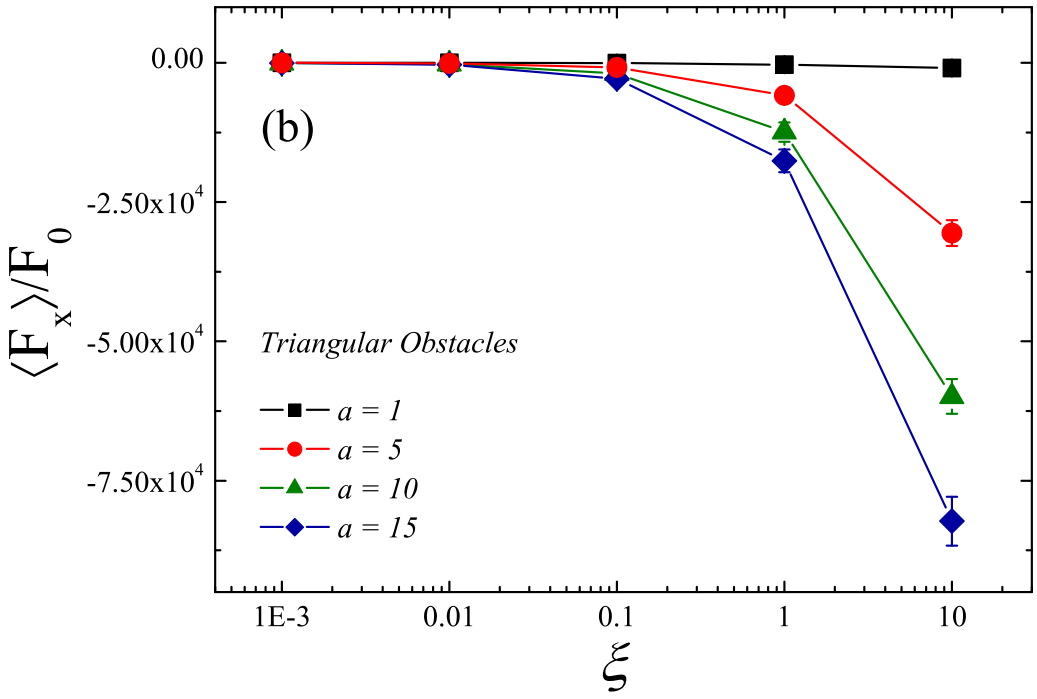

Figure 5.8: The average force $\langle F_x \rangle$ for triangular passive objects as a function of temperature for different sizes of the triangular passive objects. The area fraction is $\rho = 0.4$.

5.3.5 Semi-circular passive objects

In this section we explore semi-circular passive objects where the inner surface is flat and the outer surface is circular, and its dependence on temperature ξ. Results are plotted on Fig. 5.10.

This result show us that it is either possible to have repulsive or attractive forces, which depends on the distance l between the flat surfaces. This result supports previous works [191, 192]. Interesting result are observed when $\xi = 10$, where average force is approximatedly equal in magnitude but in opposite directions, which enphasizes the very sensitive influence of the distance l on the net force between suspended passive objects.

In order to emphasize the sensitivity of depletion forces with the distance l, simulations were performed varying l from 0.1 to 2.0. Results are shown on Fig. 5.11.

We observe that when $l > 0.6$ average forces changes abruptly creating a strong repulsive force between semi-circular passive objects with two orders of magnitude higher. This happens because when $l = 0.7$ particles stay between the passive objects, and by temperature, starts to push passive objects in opposite directions one each other. This result shows that repulsion between flat surfaces is an entirely geometric factor and qualitatively does not depend if the particles are self-propelled or not.

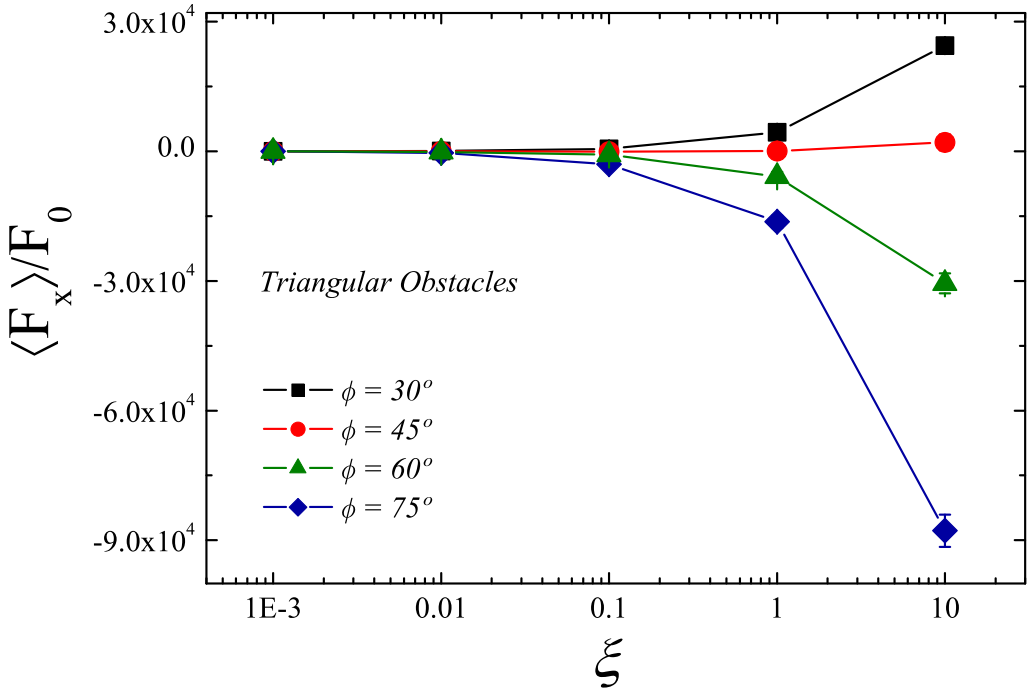

Figure 5.9: The average force $\langle F_x \rangle$ as a function of the temperature for different angles between the triangular passive objects (see Fig. 5.3). Area fraction is $\rho = 0.4$.

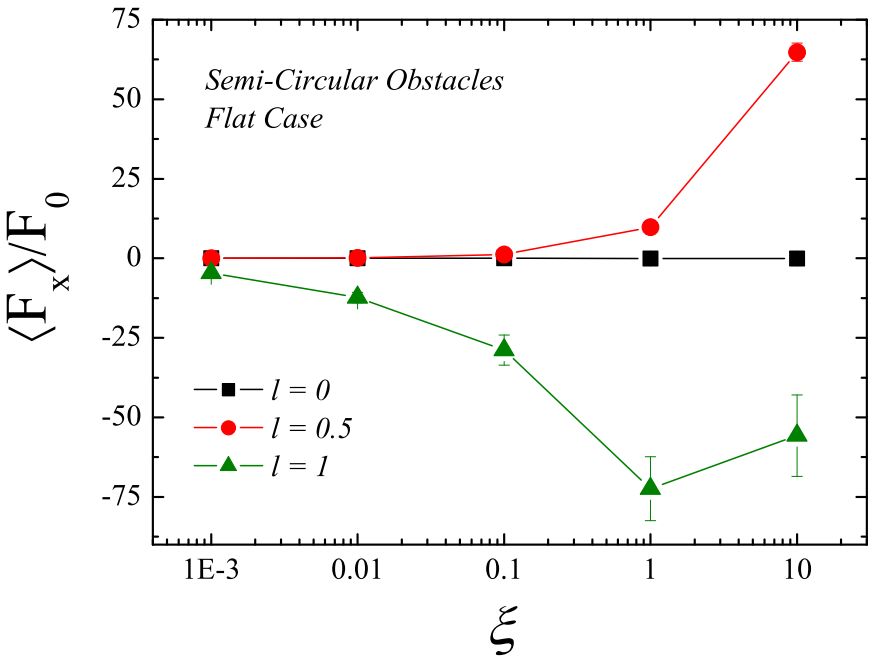

Figure 5.10: The average force $\langle F_x \rangle$ as a function of temperature for different separation between semi-circular passive objects when they are faced to each other trough the flat side. The area fraction is $\rho = 0.4$.

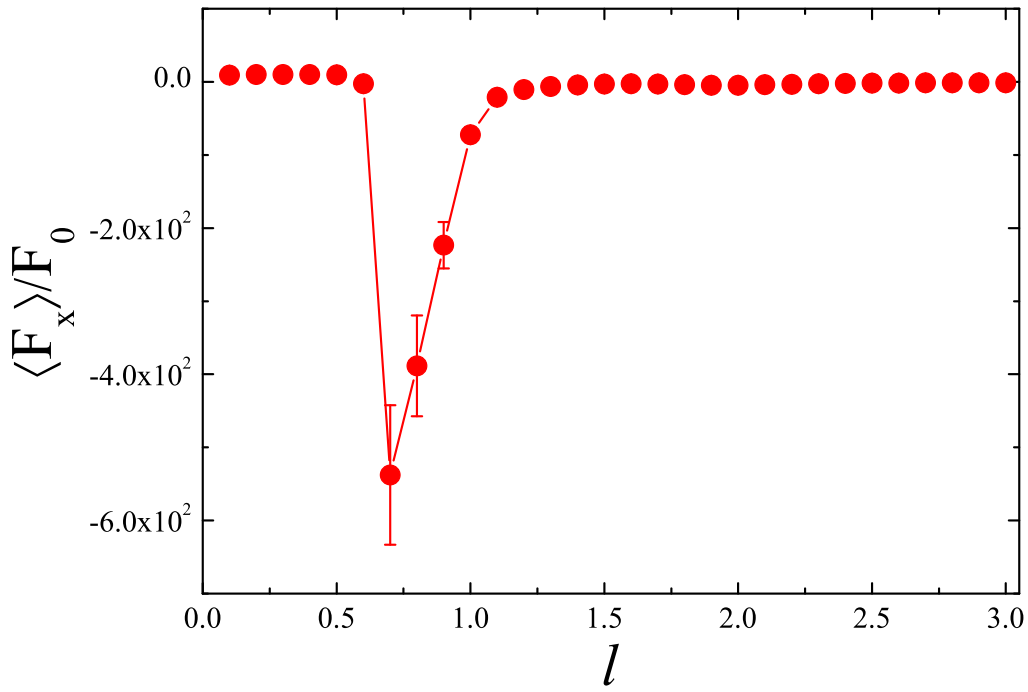

Figure 5.11: The average force $\langle F_x \rangle$ on semi-circular passive objects as a function of the separation l between semi-circular passive objects when they are faced to each other trough the flat side. The area fraction is $\rho = 0.4$. The temperature is $\xi = 1$.

6

Conclusions and Perspectives

On the first part of this thesis, we studied depletion forces on passive elliptical colloids (PEC) immersed in a bath of self propelled particles (SPP). In general, the depletion force is repulsive and depends on the shape (eccentricity) and orientation of the PEC. The dimensionless parameter λ (the ratio between the lengths of the semi-major and semi-minor axis of the ellipse) was defined and used to characterize the shape and orientation of the PEC. Horizontal (along the x-axis) and vertical (along the y-axis) PEC are characterized by $\lambda < 1$ and $\lambda > 1$, respectively. In general, the depletion force observed on horizontal PEC is one order of magnitude larger than that observed on vertical PEC, due to the particular sliding dynamics of active particles in rigid surfaces. We argued that the difference in value of $\langle F_x \rangle$ observed for distinct λ is due to the larger aggregation (the mechanism responsible for repulsion) in between the horizontal PEC as well as the larger horizontal projection of the compressive force between the SPP and PEC for $\lambda < 1.0$. With respect to the separation between the PEC, as the PEC get further away from each other, the magnitude of the depletion force increases until the distance reaches $l = 0.9$, where the force drops sharply, and almost reaches zero. Such a behavior was observed independently of λ. Noise strength has a significant influence on depletion forces, once for the cases studied (circular, vertical and horizontal elliptical objects) the higher the angular noise, the lower the magnitude of the depletion forces. This happens because the clusters around the PEC decrease in size as angular noise raises. By increasing the concentration of active particles (area fraction) we show that it is possible to achieve attractive forces between the PEC for $\lambda \geq 1.0$. High values of the area fraction allow the SPP to coalesce on the outer side of the obstacles, and contribute to lowering the repulsive depletion force. In particular, for $\lambda = 2.0$ (vertical PEC) and $\phi \gtrsim 0.2$, the SPP decrease their presence in the region between the PEC at the same time that they attach to the outer side of the PEC such that the net force becomes attractive. For separation between the PEC $l > 1$, the depletion forces decreases with increasing l but with distinct rates, which depend on the shape of the PEC. E. g., for $l = 5$ and $\lambda = 0.5$ (horizontal PEC), a considerable agglomeration of SPP is still found between the PEC resulting in a non-vanishing repulsive force, distinctly from the cases $\lambda = 1.0$ (circles) and $\lambda = 2.0$

(vertical PEC), where $\langle F_x \rangle \approx 0$. Finally, we studied the depletion force when one horizontal PEC is close to a vertical PEC in a bath of active particles. The depletion force is repulsive, but with an intermediate magnitude compared to those observed in the cases with two horizontal or two vertical PEC.

On the second part of this thesis we analyze via molecular dynamics simulations a two-dimensional system composed of two passive big obstacles immersed in a heat bath of N = 2000 smaller particles. Depletion forces were analyzed for three different shapes of the big objects: horizontal ellipses, triangular and semi-circular, all of them not studied yet in the current literature. We observe that the average depletion force exhibit the expected attractive character for all three shapes studied. Triangular obstacles present the most intense depletion interaction. This lead us to conclude that the main influence on the average forces for different shapes lies on the geometric contact between BP and FO, more than the BP concentration between obstacles. It was also observed that by increasing the area fraction induces depletion forces to increase its intensity. For the elliptical shape, we found that as the ellipse grows thicker, the depletion force is smaller. In this case, as temperature increases, depletion forces increases its intensity. The same behavior was observed for the other two obstacles shapes. When the triangular obstacle shape is investigated, we found that the depletion forces increases with increasing size of the FO (parameter a). We showed that the angle ϕ between triangular obstacles may be considered as a parameter of controlling attraction/repulsion between suspended particles, and a small variation of ϕ can lead to huge differences on the resultant force.

As a perspective, we plan to study the depletion force acting on FO of different shapes immersed in a mixture of passive and active depletants.

We also plan to add complexity in our study by allowing the passive objects to move accordingly in the bath of active and/or passive depletants.

Bibliography

[1] VICSEK, T.; ZAFEIRIS, A. *Phys. Rep.* v.517, p.71, 2012.

[2] JÜLICHER, F. et al. Active behavior of the cytoskeleton. *Phys. Rep.* v.449, p.3, 2007.

[3] SCHALLER, V. et al. Frozen steady states in active systems. *Proc. Natl. Acad. Sci. U. S. A.*, v.108, p.19183–19188, 2011.

[4] ALBERTS, A. et al. *Molecular Biology of the Cell*, 5th ed. Garland Science, New York, 2008.

[5] SUMINO, Y. et al. Large-scale vortex lattice emerging from collectively moving microtubules. *Nature (London)* v.483, p.448, 2012.

[6] DOMBROWSKI, C. et al. Self-concentration and large-scale coherence in bacterial dynamics. *Phys. Rev. Lett.* v.93, p.098103, 2004.

[7] DRESCHER, K. et al. Dancing volvox: hydrodynamic bound states of swimming algae. *Phys. Rev. Lett.* v.102, p.168101, 2009.

[8] DRESCHER, K. et al. Fluid dynamics and noise in bacterial cell–cell and cell–surface scattering. *Proc. Natl. Acad. Sci. U.S.A.* v.108, p.940, 2011.

[9] PERUANI, F. et al. Collective motion and nonequilibrium cluster formation in colonies of gliding bacteria. *Phys. Rev. Lett.* v.108, p.098102, 2012.

[10] POUJADE, M. et al. Collective migration of an epithelial monolayer in response to a model wound. *Proc. Natl. Acad. Sci. U.S.A.* v.104, p.15988, 2007.

[11] FREWEN, T. A. et al. Coarse collective dynamics of animal groups. *Lect. Notes Eng. Comput. Sci.* v.75, p.299, 2011.

[12] CAVAGNA, A. et al. Scale-free correlations in starling flocks. *Proc. Natl. Acad. Sci. U.S.A.* v.107, p.865, 2010.

[13] CAVAGNA, A. Supercooled liquids for pedestrians. *Phys. Rep.* v.476, p.51, 2009.

[14] TREPAT, X. et al. Physical forces during collective cell migration. *Nat. Phys.*, v.5, p.426–430, 2009.

[15] BALLERINI, M. et al. Interaction ruling animal collective behavior depends on topological rather than metric distance: Evidence from a field study. *Proc. Natl. Acad. Sci. U.S.A.*, v.105, p.1232–1237, 2008.

[16] GIBBS, J.; ZHAO, Y. Catalytic nanomotors: fabrication, mechanism, and applications. *Front. Mater. Sci.* v.5, p.25, 2011.

[17] GOLESTANIAN, R.; LIVERPOOL, T. B.; AJDARI, A. Propulsion of a molecular machine by asymmetric distribution of reaction products. *Phys. Rev. Lett.* v.94, p.220801, 2005.

[18] PALACCI, J. et al. Colloidal motility and pattern formation under rectified diffusiophoresis. *Phys. Rev. Lett.* v.104, p.138302, 2010.

[19] PAXTON, W. F. et al. Catalytically induced electrokinetics for motors and micropumps. *J. Am. Chem. Soc.* v.128, p.14881, 2006.

[20] WENSINK, H. H. et al. Mesoscale turbulence in living fluids. *Proc. Natl. Acad. Sci. U.S.A.* v.109, p.14308, 2012.

[21] VICSEK, T. et al. Novel type of phase transition in a system of self-driven particles. *Phys. Rev. Lett.*, v.75, p.1226–1229, 1995.

[22] WENSINK, H. H.; LÖWEN, H. Aggregation of self-propelled colloidal rods near confining walls. *Phys. Rev. E* v.78, p.031409, 2008.

[23] PERUANI, F.; DEUTSCH, A.; BÄR, M. Nonequilibrium clustering of self-propelled rods. *Phys. Rev. E* v.74, p.030904, 2006.

[24] GALADJA, P. et al. A wall of funnels concentrates swimming bacteria. *J. Bacteriol.* v.189, p.8704, 2007.

[25] ANGELANI, L.; DI LEONARDO, R.; RUOCCO, G. Self-starting micromotors in a bacterial bath. *Phys. Rev. Lett.* v.102, p.048104, 2009.

[26] LAMBERT, G.; LIAO, D.; AUSTIN, R. H. Collective escape of chemotactic swimmers through microscopic ratchets. *Phys. Rev. Lett.* v.104, p.168102, 2010.

[27] POTOTSKY, A.; HAHN, A. M.; STARK, H. Rectification of self-propelled particles by symmetric barriers. *Phys. Rev. E* v.87, p.042124, 2013.

[28] SCHWEITZER, F.; SCHIMANSKY-GEIER, L. Clustering of "active" walkers in a two-component system. *Physica (Amsterdam)* v.206A, p.359, 1994.

[29] CATES, M. E. et al. Arrested phase separation in reproducing bacteria creates a generic route to pattern formation. *Proc. Natl. Acad. Sci. U.S.A.* v.107, p.11715, 2010.

[30] THEURKAUFF, I. et al. Dynamic clustering in active colloidal suspensions with chemical signaling. *Phys. Rev. Lett.* v.108, p.268303, 2012.

[31] MCCANDLISH, S. R.; BASKARAN, A.; HAGAN, M. F. Spontaneous segregation of self-propelled particles with different motilities. *Soft Matter* v.8, p.2527, 2012.

[32] FARRELL, F. D. C. et al. Pattern formation in self-propelled particles with density-dependent motility. *Phys. Rev. Lett.* v.108, p.248101, 2012.

[33] REDNER, G. S.; BASKARAN, A.; HAGAN, F. Reentrant phase behavior in active colloids with attraction. *Phys. Rev. E* v.88, p.012305, 2013.

[34] BUTTINONI, I., J. et al. Dynamical clustering and phase separation in suspensions of self-propelled colloidal particles. *Phys. Rev. Lett.* v.110, p.238301, 2013.

[35] JULLIEN, R. et al. *Surface Disordering*, Nova Science, New York, 1992.

[36] KERTESZ, J.; WOLF, D. E. Anomalous roughening in growth processes. *Phys. Rev. Lett.* v.62, p.2571, 1989.

[37] MARTYS, N.; CIELPAK, M.; ROBBINS, M. O. Critical phenomena in fluid invasion of porous media. *Phys. Rev.Lett.* v.66, p.1058, 1991.

[38] CSAHÓK, Z. et al. Dynamics of surface roughening in disordered media. *Physica (Amsterdam)* v.200A, p.136, 1993.

[39] RAMASWAMY, S. The mechanics and statics of active matter. *Ann. Rev. Condens. Matt. Phys.* v.1, p.323–345, 2010.

[40] TONER, J.; TU, Y.; RAMASWAMY, S. Hydrodynamics and phases of flocks. *Ann. Phys. (N.Y.)* 318, 170, 2005.

[41] NARAYAN, V.; RAMASWAMY, S.; MENON, N. Long-lived giant number fluctuations in a swarming granular nematic. *Science* v.317, p.105, 2007.

[42] ZHANG, H. P. et al. Collective motion and density fluctuations in bacterial colonies. *Proc.Natl. Acad. Sci. U.S.A.* v.107, p.13626, 2010.

[43] CORTÉ, L. et al. Random organization in periodically driven systems. *Nat. Phys.* v.4, p.420, 2008.

[44] FRANCESCHINI, A. et al. Transverse alignment of fibers in a periodically sheared suspension: an absorbing phase transition with a slowly varying control parameter. *Phys.Rev. Lett.* v.107, p.250603, 2011.

[45] GOPINATH, A. et al. Dynamical self-regulation in self-propelled particle flows. *Phys. Rev. B* v.85, p.061903, 2012.

[46] GIOMI, L.; LIVERPOOL, T. B.; MARCHETTI, M. C. Sheared active fluids: Thickening, thinning, and vanishing viscosity. *Phys. Rev. E* v.81, p.051908, 2010.

[47] SAINTILLAN, D. Extensional rheology of active suspensions. *Phys. Rev. E* v.81, p.056307, 2010.

[48] CATES, M. E. et al. Shearing active gels close to the isotropic-nematic transition. *Phys. Rev. Lett.* v.101, p.068102, 2008.

[49] DI LEONARDO, R. et al. Bacterial ratchet motors. *Proc. Natl. Acad. Sci. U. S. A.*, v.107, p.9541–9545, 2010.

[50] MARCHETTI, M. C. et al. Hydrodynamics of soft active matter. *Rev. Mod. Phys.* v.85, p.1143–1188, 2013.

[51] TAILLEUR, J.; CATES, M. E. Statistical mechanics of interacting run-and-tumble bacteria. *Phys. Rev. Lett.* v.100, p.218103, 2008.

[52] CATES, M. E.; TAILLEUR, J. When are active Brownian particles and run-and-tumble particles equivalent? Consequences for motility-induced phase separation. *Europhys. Lett.* v.101, p.20010, 2013.

[53] CATES, M. E.; TAILLEUR, J. Motility-induced phase separation. *Annual Review of Condensed Matter Physics* v.6, p.219, 2015.

[54] FILY, Y.; MARCHETTI, M. C. Athermal phase separation of self-propelled particles with no alignment. *Phys. Rev. Lett.* v.108, p.235702, 2012.

[55] REDNER, G. S.; HAGAN, M. F.; BASKARAN, A. Structure and dynamics of a phase-separating active colloidal fluid. *Phys. Rev. Lett.* v.110, p.055701, 2013.

[56] JOANNY, J.-F.; RAMASWAMY, S. Biological physics: Filaments band together. *Nature* v.467, p.33, 2010.

[57] POLIN, M. et al. Chlamydomonas swims with two "gears" in a eukaryotic version of run-and-tumble locomotion*Science* v.325, p.487, 2009.

[58] DREYFUS, R. et al. Microscopic artificial swimmers. *Nature* v.437, p.862–865, 2005

[59] PAXTON, W. F. et al. Catalytic autonomous motion of striped nanorods. *J. Am. Chem. Soc.* v.126, p.13424–13431, 2004.

[60] HOWSE, J. R. et al. Self-motile colloidal particles: From directed propulsion to random walk. *Phys. Rev. Lett.* v.99, p.048102, 2007.

[61] PALACCI, J. et al. Sedimentation and effective temperature of active colloidal suspensions. *Phys.Rev. Lett.* v.105, p.088304, 2010.

[62] SAINTILLAN, D.; SHELLEY, M. J. Instabilities, pattern formation, and mixing in active suspensions. *Phys. Fluids* v.20, p.123304, 2008.

[63] GRÉGOIRE, G.; CHATÉ, H. Onset of collective and cohesive motion. *Phys. Rev. Lett.* v.92, p.025702, 2004.

[64] TIERNO, P. et al. Controlled swimming in confined fluids of magnetically actuated colloidal rotors. *Phys. Rev. Lett.* v.101, p.218304, 2008

[65] SANCHEZ, S. et al. Superfast motion of catalytic microjet engines at physiological temperature. *J. Am. Chem. Soc.* v.133, p.14860–14863, 2001.

[66] LI, J. et al. Water-driven micromotors for rapid photocatalytic degradation of biological and chemical warfare agents. *ACS Nano* v.8, p.11118–11125, 2014.

[67] GHOSH, A.; FISCHER, P. Controlled propulsion of artificial magnetic nanostructured propellers. *Nano Lett.* v.9, p.2243–2245, 2009.

[68] WANG, J. Nano/microscale motors: Biomedical opportunities and challenges. *ACS Nano* v.6, p.5745–5751, 2012.

[69] REYNOLDS, C. W. Flocks, herds and schools: a distributed behavioral model. *ACM Siggraph Computer Graphics* v.21, p.25–34, 1987.

[70] VISWANATHAN, G. M. et al. *The Physics of Foraging: An Introduction to Random Searches and Biological Encounters* (Cambridge University Press, Cambridge, UK). 2011.

[71] HELBING, D. Traffic and related self-driven many-particle systems. *Rev. Mod. Phys.* v.73, p.1067–1141, 2001.

[72] BERG, H. C. *E. coli in Motion* (Springer Verlag, Heidelberg, Germany), 2004.

[73] ABDELMOHSEN, L. K. E. A. et al. Micro- and nano-motors for biomedical applications. *J. Mater. Chem. B* v.2, p.2395–2408, 2014.

[74] GAO, W.; WANG, J. The environmental impact of micro/nanomachines: A review. *ACS Nano* v.8, p.3170–3180, 2014.

[75] NELSON, B. J.; KALIAKATSOS, I. K.; ABBOTT, J. J. Microrobots for minimally invasive medicine. *Annu. Rev.Biomed. Eng.* v.12, p.55–85, 2010.

[76] PATRA, D. S. et al. Intelligent, self-powered, drug delivery systems. *Nanoscale* v.5, p.1273–1283, 2013.

[77] HÄNGGI, P.; MARCHESONI, F. Artificial brownian motors: controlling transport on the nanoscale. *Rev. Mod. Phys.* v.81, p.387–442, 2009.

[78] KOUMAKISM, N. et al. Targeted delivery of colloids by swimming bacteria. *Nat. Commun.* v.4, p.2588, 2013.

[79] SOLOLEV, A. A. et al. Magnetic control of tubular catalytic microbots for the transport, assembly, and delivery of micro-objects. *Adv. Functional Materials* v.20, p.2430–2435, 2010.

[80] SUDIMACK, J.; LEE, R. J. Targeted drug delivery via the folate receptor. *Adv. Drug Delivery Rev.* v. 41, p.147–162, 2000.

[81] STENBERG, P. et al. Theoretical predictions of drug absorption in drug discovery and development. *Clin. Pharmacokinet.* v.41, p.877–899, 2002.

[82] UEKAMA, K. et al. Cyclodextrin drug carrier systems. *Chem. Rev.* v.98, p.2045–2076, 1998.

[83] QIU, Y.; PARK, K. Environment-sensitive hydrogels for drug delivery. *Adv. Drug Delivery Rev.* v.53, p.321–339, 2001.

[84] PANKHURST, Q. A. et al. Applications of magnetic nanoparticles in biomedicine. *J. Phys. D: Appl. Phys.* v.36, p.R167–R181, 2003.

[85] PATRA, D.; SANYAL, A.; ROTELLO, V. M. Colloidal microcapsules: self-assembly of nanoparticles at the liquid–liquid interface. *Chem.–Asian J.* v.5, p.2442–2453, 2010.

[86] KATAOKA, K.; HARADA, A.; NAGASAKI, Y. Block copolymer micelles for drug delivery: design, characterization and biological significance. *Adv. Drug Delivery Rev.* v.47, p.113–131, 2001.

[87] TORCHILIN, V. Recent advances with liposomes as pharmaceutical carriers. *Nat. Rev. Drug Discovery* v.4, p.145–160, 2005.

[88] BURDICK, J. et al. Synthetic nanomotors in microchannel networks: directional microchip motion and controlled manipulation of cargo. *J. Am. Chem. Soc.* v.130, p.8164–8165, 2008.

[89] BARABAN, L., et al. Transport of cargo by catalytic Janus micro-motors, *Soft Matter* v.8, p.48, 2012.

[90] WU, X.; LIBCHABER, A. Particle diffusion in a quasi-two-dimensional bacterial bath. *Phys. Rev. Lett.* v.84, p.3017–3020, 2000.

[91] LEPTOS, K. C. et al. Dynamics of enhanced tracer diffusion in suspensions of swimming eukaryotic microorganisms. *Phys. Rev. Lett.* v.103, p.198103, 2009.

[92] VALERIANI, C. et al. Colloids in a bacterial bath: simulations and experiments. *Soft Matter* v.7, p.5228–5238, 2011.

[93] ANGELANI L. et al. Effective interactions between colloidal particles suspended in a bath of swimming cells. *Phys. Rev. Lett.* v.107, p.138302, 2011.

[94] FRENKEL, D. Entropy-driven phase transitions. *Physica A* v.263, p.26, 1999.

[95] LU, P. J. et al. Gelation of particles with short-range attraction. *Nature* v.453, p.499, 2008

[96] HESS, H.; VOGEL, V. Molecular shuttles based on motor proteins: Active transport in synthetic environments. *Rev. Mol. Biotechnol.* v.82, p.67–85, 2011.

[97] GOEL, A.; VOGEL, V. Harnessing biological motors to engineer systems for nanoscale transport and assembly. *Nat. Nanotechnol.* v.3, p.465–475, 2008.

[98] DARNTON, N. et al. Moving fluid with bacterial carpets. *Biophys. J.* v.86, p.1863–1870, 2004.

[99] MEI, Y. F. et al. Rolled-up nanotech on polymers: from basic perception to self-propelled catalytic microengines. *Chem. Soc. Rev.* v.40, p.2109, 2011.

[100] BALASUBRAMANIAN, S. et al. Micromachineenabled capture and isolation of cancer cells in complex media. *Angew. Chem.*, Int. Ed. v.50, p.4161–4164, 2011.

[101] SANCHEZ, S. et al. Controlled manipulation of multiple cells using catalytic microbots. *Chem. Commun.* v.47, p.698–700, 2011.

[102] WU, J. et al. Motion-based DNA detection using catalytic nanomotors. *Nat. Commun.* v.1, p.1–6, 2010.

[103] WU, J. et al. Ternary surface monolayers for ultrasensitive (zeptomole) amperometric detection of nucleic acid hybridization without signal amplification. *Anal. Chem.* v.82, p.8830–8837, 2010.

[104] GARCIA, M. et al. Micromotor-based lab-on-chip immunoassays. *Nanoscale* v.5, p.1325 – 1331, 2013.

[105] SUNDARARAJAN, S. et al. Catalytic motors for transport of colloidal cargo. *Nano Lett.* v.8, p.1271–1276, 2008.

[106] CAMPUZANO, S. et al. Bacterial isolation by lectin-modified microengines. *Nano Lett.* v.12, p.396–401, 2012.

[107] OROZCO, J. et al. Dynamic isolation and unloading of target proteins by aptamer-modified microtransporters. *Anal. Chem.* v.83, p.7962–7969, 2011.

[108] KAGAN, D. et al. Functionalized micromachines for selective and rapid isolation of nucleic acid targets from complex samples. *Nano Lett.* v.11, p.2083 – 2087, 2011.

[109] SANCHEZ, S. et al. Dynamics of biocatalytic microengines mediated by variable friction control. *J. Am. Chem. Soc.* v.132, p.13144 – 13145, 2010.

[110] GAO, W.; PEI, A.; WANG, J. Water-driven micromotors. *ACS Nano* v.6, p.8432–8438, 2012.

[111] OLSON, E. S. et al. Toward in vivo detection of hydrogen peroxide with ultrasound molecular imaging. *Biomaterials* v.34, p.8918–8924, 2013.

[112] MARTEL, S. et al. Flagellated magnetotactic bacteria as controlled MRI-trackable propulsion and steering systems for medical nanorobots operating in the human microvasculature. *Int. J. Robot. Res.* v.28, p.571– 582, 2009.

[113] ANDREESCU, S. et al. Applications of advanced nanomaterials for environmental monitoring. *J. Environ. Monit.* v.11, p.27–40, 2009.

[114] KARN, B.; KUIKEN, T.; OTTO, M. Nanotechnology and in situ remediation: a review of the benefits and potential risks. *Environ. Health Perspect.* v.117, p.1813–1831, 2009.

[115] ZHANG, W. Nanoscale iron particles for environmental remediation: an overview. *J. Nanopart. Res.* v.5, p.323– 332, 2003.

[116] ARIGA, K. et al. Materials nanoarchitectonics for environmental remediation and sensing. *J. Mater. Chem.* v.22, p.2369–2377, 2012.

[117] OROZCO, J. et al. Micromotor based high-yielding fast oxidative detoxification of chemical threats. *Angew. Chem.*, Int. Ed. v,52, p.13276–13279, 2013.

[118] SOLER, L. et al. Self-propelled micromotors for cleaning polluted water. *ACS Nano* v.7, p.9611–9620, 2013.

[119] OROZCO, J. et al. Artificial enzyme-powered microfish for water quality testing. *ACS Nano* v.7, p.818–824, 2013.

[120] GUIX, M. et al. Superhydrophobic alkanethiol-coated microsubmarines for effective removal of oil. *ACS Nano* v.6, p.4445–4451, 2012.

[121] HANRAHAN, G.; PATIL, D. G.; WANG, J. Electrochemical sensors for environmental monitoring: design, development and applications. *J. Environ. Monit.* v.6, p.657–664, 2004.

[122] FARRÉ, M. et al. Green analytical chemistry in the determination of organic pollutants in the aquatic environment. *Trends Anal. Chem.* v.29, p.1347–1362, 2010.

[123] CAMPUZANO, S. et al. Motion-driven sensing and biosensing using electrochemically propelled nanomotors. *Analyst* v.136, p.4621–4630, 2011.

[124] KAGAN, D. et al. Chemical sensing based on catalytic nanomotors: motion-based detection of trace silver. *J. Am. Chem. Soc.* v.131, p.12082–12083, 2009.

[125] LAGIER, M. et al. An electrochemical RNA hybridization assay for detection of the fecal indicator bacterium escherichia coli. *Mar. Pollut. Bull.* v.50, p.1251–1261, 2005.

[126] WHICKER, F. W. et al. Avoiding destructive remediation at DOE sites. *Science* v.303, p.1615–1616, 2004.

[127] MASQUÉ, N. et al. Synthesis and evaluation of a molecularly imprinted polymer for selective on-line solid-phase extraction of 4-nitrophenol from environmental *Water. Anal. Chem.* 2000, 72, 4122–4126.

[128] OROZCO, J. et al. Molecularly imprinted polymer-based catalytic micromotors for selective protein transport. *J. Am. Chem. Soc.* v.135, p.5336–5339, 2013.

[129] HUANG, C.; SHEN, X. Janus molecularly imprinted polymer particles. *Chem. Commun.* v.50, p.2646–2649, 2014.

[130] KASSIM, I. et al. Locomotion techniques for robotic colonoscopy. *IEEE Eng. Med. Biol. Mag.* v.25, p.49–56, 2006.

[131] BORGES-WALMSLEY, M. I.; WALMSLEY, A. R. The structure and function of drug pumps. *Trends Microbiol.* v.9, p.71–79, 2001.

[132] MURAKAMI, S. et al. Crystal structure of bacterial multidrug efflux transporter AcrB. *Nature* v.419, p.587–593, 2002.

[133] PUTMAN, M.; VEEN, H. W.; KONINGS, W. N. Molecular properties of bacterial multidrug transporters. *Microbiol. Mol. Biol. Rev.* v.64, p.672–693, 2002.

[134] MCKEEGAN, K. S.; BORGES-WALMSLEY, M. I.; WALMSLEY, A. R. The structure and function of drug pumps: an update. *Trends Microbiol.* v.11, p.21–29, 2003.

[135] DEVLIN, P. M. *Brachytherapy: Applications and Techniques.* Philadelphia: Lippincott Williams Wilkins. 448 pp, 2007.

[136] ANDRÄW, N. H. *Magnetism in Medicine: A Handbook.* Weinheim, Germany: Wiley-VCH. 629 pp. 2nd ed., 2007.

[137] ZHANG, H. et al. Microrobotics and MEMS-based fabrication techniques for scaffold-based tissue engineering. *Macromol. Biosci.* v.5, p.477–489, 2005.

[138] PURDY, P. D.; FUJIMOTO, T.; REPLOGLE, R. E. Percutaneous intraspinal navigation for access to the sub- arachnoid space: use of another natural conduit for neurosurgical procedures. *Neurosurg. Focus* v.19, E11, 2005.

[139] GRADY, M. S. et al. Preliminary experimental investigation of in vivo magnetic manipulation: results and potential application in hyperthermia. *Med. Phys.* v.16, p.263–72, 1989.

[140] GRADY, M. S. et al. Nonlinear magnetic stereotaxis: three-dimensional, in vivo remote magnetic manipulation of a small object in canine brain. *Med. Phys.* v.17, p.405–415, 1990.

[141] MCNEIL, R. G. et al. Functional design features and initial performance characteristics of a magnetic-implant guidance system for stereotactic neurosurgery. *IEEE Trans. Biomed. Eng.* v.42, p.793–801, 1995.

[142] KOSA G.; SHOHAM, M. ZAAROOR, M. Propulsion method for swimming microrobots. *IEEE Trans. Robot.* v.23, p.137–150, 2007.

[143] EDD, J. et al. Biomimetic propulsion for a swimming surgical micro-robot. *Proc. IEEE/RSJ Int. Conf. Intell. Robots Syst., Las Vegas, Nev.*, Oct. 27–31, pp. 2583–2588, 2003.

[144] THEOCHARIS, I. P. et al. A two-year prospective study comparing lidocaine 2percent jelly versus peribulbar anaesthesia for 25G and 23G sutureless vitrectomy. *Graefe's Arch. Clin. Exp. Ophthalmol.* v.245, p.1253–1258, 2007.

[145] YESIN, K. B.; VOLLMERS, K.; NELSON, B. J. Modeling and control of untethered biomicrorobots in a fluidic environment using electromagnetic fields. *Int. J. Robot. Res.* v.25, p.527–536, 2006.

[146] ERGENEMAN, O. et al. Functionalizing intraocular microrobots with surface coatings. *Proc. IEEE Int. Conf. Biomed. Robot. Biomechatron., Scottsdale, Ariz.*, Oct. 19–22, pp. 232–237, 2008.

[147] DOGANGIL, G. et al. Toward targeted retinal drug delivery with wireless magnetic microrobots. *Proc. IEEE/RSJ Int. Conf. Intell. Robots Syst., Nice, Fr.*, Sept. 22–26, pp. 1921–26, 2008.

[148] HOLLIGAN, D. L.; GILLIES, G. T.; DAILEY, J. P. Magnetic guidance of ferrofluidic nanoparticles in an in vitro model of intraocular retinal repair. *Nanotechnology* v.14, p.661–66, 2003.

[149] FLAKE, A. W. Surgery in the human fetus: the future. *J. Physiol.* v.547, p.45–51, 2003.

[150] BERRIS, M.; SHOSAN, M. Febotics—a marriage of fetal surgery and robotics. *Comput. Aided Surg.* v.11, p.175–80, 2006.

[151] VOLPE, G.; GIGAN, S.; VOLPE, G. Simulation of the active Brownian motion of a microswimmer. *Am. J. Phys.* v.82, p.659, 2014.

[152] ELGETI, J.; GOMPPER, G. Self-propelled rods near surfaces. *Europhys. Lett.* v.85, p.38002, 2009.

[153] WYSOCKI, A, ; ELGETI, J.; GOMPPER, G. Giant adsorption of microswimmers: Duality of shape asymmetry and wall curvature. *Phys. Rev. E* v.91, p.050302, 2015.

[154] VLADESCU, I. D. et al. Filling an emulsion drop with motile bacteria. *Phys. Rev. Lett.* v.113, p.268101, 2014.

[155] VAN TEEFFELEN, S.; LÖWEN, H. Dynamics of a brownian circle swimmer. *Phys. Rev. E* v.78, p.020101, 2008.

[156] VAN TEEFFELEN, S.; ZIMMERMAN, U.; LÖWEN, H. Clockwise-directional circle swimmer moves counterclock-wise in Petri dish- and ring-like confinements. *Soft Matter* v.5, p.4510, 2009.

[157] SCHNITZER, M. J. Theory of continuum random walks and application to chemotaxis. *Phys. Rev. E* v.48, p.2553, 1993.

[158] TAILLEUR, J.; CATES, M. E. Sedimentation, trapping, and rectification of dilute bacteria. *Europhys. Lett.* v.86, p.60002, 2009.

[159] THURÖFF, F.; WEBER, C. A.; FREY, E. Critical assessment of the Boltzmann approach to active systems. *Phys. Rev. Lett.* v.111, p.190601, 2013.

[160] THURÖFF, F.; WEBER, C. A.; FREY, E. Numerical treatment of the Boltzmann equation for self-propelled particle systems. *Phys. Rev. X* v.4, p.041030, 2014.

[161] MALLORY, S. A. et al. Anomalous thermomechanical properties of a self-propelled colloidal fluid. *Phys. Rev. E* v.89, p.052303, 2014.

[162] SOLON, A. P. et al. Pressure is not a state function for generic active fluids. *Nat. Phys.* v.11, p.673, 2015.

[163] HERNANDEZ-ORTIZ, J. P.; STOLTZ, C. G.; GRAHAM, M. D. Transport and collective dynamics in suspensions of confined swimming particles. *Phys. Rev. Lett.* v.95, p.204501, 2005.

[164] YANG, X.; MANNING, M. L.; MARCHETTI, M. C. Aggregation and segregation of confined active particles. *Soft Matter* v.10, p.6477, 2014.

[165] LUSHI, E.; WIOLAND, H.; GOLDSTEINS, R. E. Fluid flows created by swimming bacteria drive self-organization in confined suspensions. *Proc. Natl. Acad. Sci. U.S.A.* v.111, p.9733, 2014.

[166] WIOLAND, H. et al. Confinement stabilizes a bacterial suspension into a spiral vortex. *Phys. Rev. Lett.* v.110, p. 268102, 2013.

[167] BRICARD, A. et al. Emergent vortices in populations of colloidal rollers. *Nat. Commun.* v.6, p.7470, 2015.

[168] DESEIGNE, J. et al. Vibrated polar disks: Spontaneous motion, binary collisions, and collective dynamics. *Soft Matter* v.8, p.5629, 2012.

[169] KUDROLLI, A. et al. Swarming and swirling in self-propelled polar granular rods. *Phys. Rev. Lett.* v.100, p.058001, 2008.

[170] KAISER, A.; WENSINK, H. H.; LÖWEN, H. How to capture active particles. *Phys. Rev. Lett.* v.108, p.268307, 2012.

[171] KAISER, A. et al. Capturing self-propelled particles in a moving microwedge. *Phys. Rev. E* v.88, p.022311, 2013.

[172] CHEN, Y.-F., et al. Enhancing rectification of a nano-swimmer system by multi-layered asymmetric barriers. *Nanoscale* v.7, p.16451, 2015.

[173] RESTREPO-PÉREZ, L. et al. Trapping self-propelled micromotors with microfabricated chevron and heart-shaped chips. *Lab Chip* v.14, p.1515, 2014.

[174] GUIDOBALDI A. et al. Geometrical guidance and trapping transition of human sperm cells. *Phys. Rev. E* v.89, p.032720, 2014.

[175] WAN, M. B. et al. Rectification of swimming bacteria and self-driven particle systems by arrays of asymmetric barriers. *Phys. Rev. Lett.* v.101, p.018102, 2008.

[176] POTIGUAR, F. Q.; FARIAS G. A.; FERREIRA W. P. Self-propelled particle transport in regular arrays of rigid asymmetric obstacles. *Phys. Rev. E* v.90, p.012307, 2014.

[177] AI, B.-Q.; HE, Y.-F.; ZHONG, W.-R. Entropic ratchet transport of interacting active Brownian particles. *J. Chem. Phys.* v.141, p.194111, 2014.

[178] BERDAKIN, I. et al. Influence of swimming strategy on microorganism separation by asymmetric obstacles. *Phys. Rev. E* v.87, p.052702, 2013.

[179] GHOSH, P. K. et al. Self-propelled Janus particles in a ratchet: Numerical simulations. *Phys. Rev. Lett.* v.110, p.268301, 2013.

[180] REICHHARDT, C.; OLSON REICHHARDT, C. J. Active matter ratchets with an external drift. *Phys. Rev. E* v.88, p.062310, 2013.

[181] MIJALKOV, M.; VOLPE, G. Sorting of chiral microswimmers. *Soft Matter* v.9, p.6376, 2013.

[182] REICHHARDT C.; REICHHARDT, C. J. O. Dynamics and separation of circularly moving particles in asymmetrically patterned arrays. *Phys. Rev. E* v.88, p.042306, 2013.

[183] DROCCO, J. A.; OLSON REICHHARDT, C. J.; REICHHARDT, C. Bidirectional sorting of flocking particles in the presence of asymmetric barriers. *Phys. Rev. E* v.85, p.056102, 2012.

[184] HULME, S. E. et al. Using ratchets and sorters to fractionate motile cells of escherichia coli by length. *Lab Chip* v.8, p.1888, 2008.

[185] OLIVEIRA, C. L. N. et al. Keep-left behavior induced by asymmetrically profiled walls. *Phys. Rev. X* v.6, p.011003, 2016.

[186] MAGGI, C. et al. Self-assembly of micromachining systems powered by Janus micromotors. *Small* v.12, p.446, 2016.

[187] REICHHARDT, C.; OLSON REICHHARDT C. J. Absorbing phase transitions and dynamic freezing in running active matter systems. *Soft Matter* v.10, p.7502, 2014.

[188] CHEPIZHKO, O.; ALTMANN, E. G.; PERUANI, F. Optimal noise maximizes collective motion in heterogeneous media. *Phys. Rev. Lett.* v.110, p.238101, 2013.

[189] CHEPIZHKO, O.; PERUANI, F. Diffusion, subdiffusion, and trapping of active particles in heterogeneous media. *Phys. Rev. Lett.* v.111, p.160604, 2013.

[190] JONES, R. A. L. Soft Condensed Matter. Oxford University Press, Oxford, 2002.

[191] MAO Y.; CATES, M. E.; LEKKERKERKER, H. N. W. Depletion force in colloidal systems. *Physica A* v.222, p.10, 1995.

[192] DICKMAN, R.; ATTARD, P.; SIMONIAN, V. Entropic forces in binary hard sphere mixtures: Theory and simulation. *J. Chem. Phys.* v.107, p.205, 1997.

[193] GOTZELMANN, B.; EVANS, R.; DIETRICH, S. Depletion forces in fluids. *Phys. Rev. E* v.57, p. 6785, 1998.

[194] CASTAÑEDA-PRIEGO, R.; RÓDRIGUEZ-LÓPEZ, A.; MÉNDEZ-ALCARAZ, J. M. Entropic foces in dilute colloidal systems. *Phys. Rev. E* v.73, p.051404, 2006.

[195] MARENDUZZO, D.; FINAN, K.; COOK, PETER R. The depletion attraction: an underappreciated force driving cellular organization. *The Journal of Cell Biology* v.175, p.681, 2006.

[196] BUZZACCARO, S. et al. Critical Depletion. *Phys. Rev. Lett.* v.105, p.198301, 2010.

[197] PARRA-ROJAS, C.; SOTO, R. Casimir effect in swimmer suspensions. *Phys. Rev. E* v.90, p.013024, 2014.

[198] RAY, D.; REICHHARDT, C.; REICHHARDT, C. J. OLSON. Casimir effect in active matter systems. *Phys. Rev. E* v.90, p.013019, 2014.

[199] HARDER, J. et al. The role of particle shape in active depletion. *J. Chem. Phys.* v.141, p.194901, 2014.

[200] NI, R.; STUART A. C.; BOLHUIS P. G. Tunable long range forces mediated by self-propelled colloidal hard spheres. *Phys. Rev. Lett.* v.114, p.018302, 2015.

[201] GRATALE, M. D. et al. Tunable depletion potentials driven by shape variation of surfactant micelles. *Phys. Rev. E* v.93, p.050601(R), 2016.

[202] EINSTEIN, A. Investigations on the Theory of the Brownian Movement. *Ann. Phys. (Berlin)* v.322, p.549, 1905.

[203] CZIRÓK, A.; BARABÁSI, A. L.; VICSEK, T. Collective motion of self-propelled particles: kinetic phase transition in one dimension. *Phys. Rev. Lett.*, v.82, p.209–212, 1999.

[204] COUZIN, I. D. et al. Collective memory and spatial sorting in animal groups. *J. Theor. Biol.*, v.218, p.1–11, 2002.

[205] CUCKER, F.; SMALE, S. Emergent behavior in flocks. *IEEE. T. Automat. Contr.*, v.52, p.852–862, 2007.

[206] COUZIN, I. D. et al. Effective leadership and decision-making in animal groups on the move. *Nature*, v.433, p.513–516, 2005.

[207] JADBABAIE, A.; LIN, J.; MORSE, A. S. Coordination of groups of mobile autonomous agents using nearest neighbor rules. *IEEE. T. Automat. Contr.*, v.48, p.988–1001, 2003.

[208] SHEN, J. Cucker-Smale flocking under hierarchical leadership. *SIAM J. Appl. Math.*, v.68, p.694–719, 2008.

[209] AOKI, I. A simulation study on the schooling mechanism in fish. *Bulletin of the Japanese Society of Scientific Fisheries (Japan)*, 1982.

[210] GAZI, V.; PASSINO, K. M. A class of attractions/repulsion functions for stable swarm aggregations. *Int. J. Control.*, v.77, p.1567–1579, 2004

[211] STRÖMBOM, D. Collective motion from local attraction. *Journal of Theoretical Biology*, v.283, p.145, 2011.

[212] GROSSMAN, D.; ARANSON, I. S.; BEN-JACOB, E. Emergence of agent swarm migration and vortex formations through inelastic collisions. *New Journal of Physics*, v.10, p.023036, 2008.

[213] CHATÉ, H. et al. Modeling collective motion: variations on the Vicsek model. *The European Physical Journal B*, v.64, p.451, 2008.

[214] BECHINGER, C. et al. Active particles in complex and crowded environments. *Rev. of Mod. Phys.*, v. 88, p.045006, 2016.

[215] CHEN, H.-Y.; LEUNG, K.-T. Rotating states of self-propelling particles in two dimensions. *Phys. Rev. E* v.73, p.056107, 2006.

[216] LI, Y.-X.; LUKEMAN, R.; EDELSTEINS-KESHET, L. Minimal mechanisms for school formation in self-propelled particles. *Physica D* v.237, p.699, 2008.

[217] MEHANDIA, V.; PRABUH, R. N. The collective dynamics of self-propelled particles. *J. Fluid Mech.* v.595, p.239, 2008.

[218] TEN HAGEN, B.; WITTKOWSKI, R.; LÖWEN, H. Brownian dynamics of a self-propelled particle in shear flow. *Phys. Rev. E* v.84, p.031105, 2011.

[219] ANGELANI, L.; COSTANZO, A.; DI LEONARDO, R. Active ratchets. *EPL (Europhys. Lett.)* v.96, p.68002, 2011.

[220] YANG, W. et al. Using self-driven microswimmers for particle separation. *Soft Matter* v.8, p.5175, 2012.

[221] WITTKOWSKI, R.; LÖWEN H. Self-propelled brownian spinning top: Dynamics of a biaxial swimmer at low Reynolds numbers. *Phys. Rev. E* v.85, p.021406, 2012.

[222] BIALKÉ, J.; SPECK, T.; LÖWEN, H. Crystallization in a dense suspension of self-propelled particles. *Phys. Rev. Lett.* v.108, p.168301, 2012.

[223] ELGETI, J.; GOMPPER, G. Wall accumulation of self-propelled spheres. *EPL (Europhys. Lett.)* v.101, p.48003, 2013.

[224] FILY, Y.; HENKES, S.; MARCHETTI, M. C. Freezing and phase separation of self-propelled disks. *Soft Matter* v.10, p.2132, 2014.

[225] COSTANZO, A. et al. Motility-sorting of self-propelled particles in microchannels. *EPL (Europhys. Lett.)* v.107, p.36003, 2014.

[226] WANG, Z. et al. Diffusion, sedimentation equilibrium, and harmonic trapping of run-and-tumble nanoswimmers. *Soft Matter* v.10, p.3209, 2014.

[227] CATES, M. E. Diffusive transport without detailed balance in motile bacteria: does microbiology need statistical physics? *Rep. Prog. Phys.* v.75, p.042601, 2012.

[228] ASAKURA, S.; OOSAWA, F. On interaction between two bodies immersed in a solution of macromolecules. *J. of Chem. Phys* v.22, p.7, 1954.

[229] ISRAELACHVILI, J. N. Intermolecular Surface Forces. 3rd ed. Academic Press, London, 1992.

[230] BIBEN, T.; BLADON, P.; FRENKEL, D. Depletion effects in binary hard-sphere fluids. *J. Phys. Condens. Matter* v.8, p.10799, 1996.

[231] CHU, X. L.; NIKOLOV, A. D.; WASAN, D. T. Effects of particle size and polydispersity on the depletion and structural forces in colloidal dispersions. *Langmuir* v.12, p.5004, 1996.

[232] CROCKER, J. C. et al. Entropic attraction and repulsion in binary colloids probed with a line optical tweezer. *Phys. Rev. Lett.* v.82, p.4352, 1999.

[233] OHSHIMA, Y. N. et al. Direct measurement of infinitesimal depletion force in a colloid-polymer mixture by laser radiation pressure. *Phys. Rev. Lett.* v.78, p.3963, 1997.

[234] KNOBEN, W.; BESSELING, N. A. M.; COHEN STUART, M. A. Direct Measurement of Depletion and Hydrodynamic Forces in Solutions of a Reversible Supramolecular Polymer. *Langmuir* v.23, p.6095, 2007.

[235] ALDER, B. J.; WAINWRIGHT, T. E. Phase transition for a hard sphere system. *The Journal of Chemical Physics* v.27, p.1208, 1957.

[236] RAHMAN, A. Correlations in the motion of atoms in liquid argon. *Physical Review* v.136, p.A405, 1964.

[237] VOLPE, G. et al. Microswimmers in patterned environments. *Soft Matter* v.7, p.8810, 2011.

[238] SUEUR, C.; PETIT O. Organization of group members at departure is driven by social structure in Macaca. *Int. Jour. of Primatology* v.29, p.1085, 2008.

[239] KING, A. J. et al. Dominance and affiliation mediate despotism in a social primate. *Curr. Biology* v.18, p.1833, 2008.

[240] FARIA, J. J. et al. Leadership and social information use in human crowds. *Animal Behaviour* v.79, p.895, 2010.

[241] HELBING, D.; FARKAS, I.; VICSEK, T. Simulating dynamical features of escape panic. *Nature* v.407, p.487, 2000.

[242] MOUSSAÏD, M.; HELBING, D.; THERAULAZ, G. How simple rules determine pedestrian behavior and crowd disasters. *Proc. Natl. Acad. Sci. U.S.A.* v.108, p.6884, 2011.

[243] EBBENS, S.; HOWSE, In pursuit of propulsion at the nanoscale, J. *Soft Matter* v.6, p.726, 2010.

[244] PALACCI, J. et al. Light-activated self-propelled colloids. *Phil. Trans. R. Soc. A* v.372, p.20130372, 2014.

[245] BROWN, A.; POON, W. Ionic effects in self-propelled Pt-coated Janus swimmers. *Soft Matter* v.10, p.4016, 2014.

[246] ERBE, A. et al. Various driving mechanisms for generating motion of colloidal particles. *J. Phys. Condens. Matter* v.20, p.404215, 2008.

[247] HONEYCUTT, R. L. Stochastic Runge-Kutta algorithms. I. white noise. *Phys. Rev. A* v.45, p.600, 1992.

[248] STENHAMMAR, J. R. et al. Activity-induced phase separation and self-assembly in mixtures of active and passive particles. *Phys. Rev. Lett.* 114, 018301, 2015.

[249] ASAKURA, S.; OOSAWA, F. Interaction between particles suspended in solutions of macromolecules. *Polym. Sci.* v.33, p.183, 1958.

[250] VRIJ, A. Polymers at interfaces and the interactions in colloidal suspensions. *Pure Appl. Chem.* v.48, p.471, 1976.

[251] LEKKERKERKER, H. N. W.; STROOBANTS, A. On the spinodal instability of highly asymmetric hard sphere suspensions. *Physica A* v.195, p.387, 1993.

[252] ROSENFELD, Y. Phase separation of asymmetric binary hard-sphere fluids: Self-consistent density functional theory. *Phys. Rev. Lett.* v.72, p.3831, 1994.

[253] ROTH, R.; EVANS, R.; DIETRICH, S. Depletion potential in hard-sphere mixtures:Theory and applications. *Phys. Rev. E* v.62, p.5360, 2000.

[254] SCHAINK, H. M.; SMIT, J. A. M. Mean field calculation of polymer segment depletion and depletion induced demixing in ternary systems of globular proteins and flexible polymers in a common solvent. *J. Chem. Phys.* v.107, p.1004, 1997.

[255] RICHETTI, P.; KÉKICHEFF, P. Direct measurement of depletion and structural forces in a micellar system. *Phys. Rev. Lett.* v.68, p.1951, 1992.

[256] LIN, K.-H. et al. Colloidal interactions in suspensions of rods. *Phys. Rev. Lett.* v.87, p.088301, 2001.

[257] TUINIER, R.; RIEGER, J.; DE KRUIF, C. G. Depletion-induced phase separation in colloid–polymer mixtures. *Adv. Colloid Interface Sci.* v.103, p.1, 2003.

[258] VERMA, R. et al. Attractions between hard colloidal spheres in semiflexible polymer solutions. *Macromolecules* v.33, p.177, 2000.

[259] EDWARDS, T. D.; BEVAN, M. A. Polymer mediated depletion attraction and interfacial colloidal phase behavior. *Macromolecules* v.45, p.585, 2012.

[260] KAPLAN, P. D. et al. Entropically driven surface phase separation in binary colloidal mixtures. *Phys. Rev. Lett.* v.72, p.582, 1994.

[261] ZHAO, K.; MASON, T. G. Suppressing and enhancing depletion attractions between surfaces roughened by asperities. *Phys. Rev. Lett.* v.101, p.148301, 2008.

[262] SACANNA, S. et al. Lock and key colloids. *Nature (London)* v.464, p.575, 2010.

[263] ROSSI, L. et al. Cubic crystals from cubic colloids. *Soft Matter* v.7, p.4139, 2011.

[264] KRAFT, D. J. et al. Surface roughness directed self-assembly of patchy particles into colloidal micelles. *Proc. Natl. Acad. Sci. USA* v.109, p.10787, 2012.

[265] GIBAUD, T. et al. Reconfigurable self-assembly through chiral control of interfacial tension. *Nature (London)* v.481, p.348, 2012.

[266] JENKINS, P.; SNOWDEN, M. Depletion flocculation in colloidal dispersions. *Adv. Colloid Interface Sci.* v.68, p.57, 1996.

[267] ADAMS, M. et al. Entropically driven microphase transitions in mixtures of colloidal rods and spheres. *Nature (London)* v.393, p.349, 1998.

[268] STRADNER, A. et al. Equilibrium cluster formation in concentrated protein solutions and colloids. *Nature (London)* v.432, p.492, 2004.

[269] PHAM, K. N. et al. Glasses in hard spheres with short-range attraction. *Phys. Rev. E* v.69, p.011503, 2004.

[270] SAVAGE, J. R. et al. Imaging the sublimation dynamics of colloidal crystallites. *Science* v.314, p.795, 2006.

[271] SIMEONOVA, N. B. et al. Devitrification of colloidal glasses in real space. *Phys. Rev. E* v.73, p.041401, 2006.

[272] NOUMAKIS, N.; PETEKIDIS, G. Two step yielding in attractive colloids: transition from gels to attractive glasses. *Soft Matter* v.7, p.2456, 2011.

[273] TAYLOR, S. L; EVANS, R.; ROYALL, C. P. Temperature as an external field for colloid–polymer mixtures:'quenching'by heating and 'melting'by cooling. *J. Phys.: Condens. Matter* v.24, p.464128, 2012.

[274] ZIMMERMAN, S. B.; MINTON, A. P. Macromolecular crowding: biochemical, biophysical, and physiological consequences. *Annu. Rev. Biophys. Biomol. Struct.* v.22, p.27, 1993.

[275] MINTON, A. P. Implications of macromolecular crowding for protein assembly. *Curr. Opin. Struct. Biol.* v.10, p.34, 2000.

[276] LEITE, L. R. et al. Depletion forces on circular and elliptical obstacles induced by active matter. *Phys. Rev. E* v.94, p.062602, 2016.